University of Nevada, Reno

Structural Controls of the Neal Hot Springs Geothermal System, Eastern Oregon

A thesis submitted in partial fulfillment of the requirements for the degree of Master of Science in Geology

By

Joel H. Edwards

Dr. James E. Faulds/Thesis Advisor

May, 2013

ProQuest LLC.
789 East Eisenhower Parkway
P.O. Box 1346
Ann Arbor, MI 48106 - 1346

University of Nevada, Reno
Statewide • Worldwide

THE GRADUATE SCHOOL

We recommend that the thesis
prepared under our supervision by

JOEL H. EDWARDS

entitled

Structural Controls of the Neal Hot Springs Geothermal System, Eastern Oregon

be accepted in partial fulfillment of the
requirements for the degree of

MASTER OF SCIENCE

James E. Faulds, Ph.D., Advisor

John Louie, Ph.D., Committee Member

David Bennum, Graduate School Representative

Marsha H. Read, Ph. D., Dean, Graduate School

May, 2013

Abstract

Detailed geologic mapping (1:24,000 scale), structural and geochemical analyses, and integration of available geophysical and well-field data were utilized to assess the structural controls of the Neal Hot Springs geothermal field in eastern Oregon. The geothermal field lies within the intersection of two regional grabens, the middle-late Miocene, north-trending, Oregon-Idaho graben and younger late Miocene to Holocene, northwest-trending, western Snake River Plain graben. It is marked by Neal Hot Springs, which effuse from opaline sinter mounds just north of Bully Creek. Production and injection wells, with temperatures up to 142°C, intersect the Neal fault zone at depths of 680-1900 m and subsidiary faults within a relay ramp or step-over within the fault zone.

The stratigraphy at Neal correlates with four regional packages. Basement rocks, discovered in one well, are granite, tentatively correlated with Jurassic Olds Ferry-Izee terrane. Nonconformably above is a thick package of middle Miocene Columbia River Basalt Group lavas, regionally known as the basalt of Malheur Gorge. Conformably above are middle to late Miocene Oregon-Idaho graben lavas, volcaniclastics, fluvial and lacustrine rocks. Overlying are the youngest rocks at Neal, which are late Miocene to Pliocene, western Snake River Plain lacustrine, fluvial, and volcaniclastic rocks.

The structural framework at Neal is characterized by northerly to northwest-striking normal faults, including the geothermally related Neal fault zone. Stress inversion of kinematic data reveal an extensional stress regime, including an interpreted younger, southwest-trending (~243°), least principal stress and an older, west-trending (~265°) least principal stress.

The geothermal field is bounded on the east by the Neal fault, a major, west-dipping, north-northwest-striking, steeply dipping normal to oblique-slip fault, along which geothermal fluids ascend, and on the west by the concealed north-northwest-striking, west-dipping Sugarloaf Butte fault. The Neal fault zone can be modeled into two structural settings: an interpreted older, left-stepping, normal-slip fault zone and a younger, oblique sinistral-normal zone, suggested by the earlier west-trending and later southwest-trending extensional stress regimes. Recent sinistral-normal displacement may have generated a small pull-apart basin in the Neal area and facilitated development of the geothermal system. 'Hard-linkage' between the Neal and Sugarloaf Butte faults occurs through concealed, west-northwest-striking faults, including the Cottonwood Creek subvertical fault, along which lateral fluid-flow is likely. An inferred north-plunging fault intersection at the Neal Hot Springs likely controls the location of the hot springs and sinter terraces.

Young structural features are evident at Neal. The Neal fault zone cuts Quaternary fans and late Miocene lower and upper Bully Creek Formation sedimentary rocks. In addition, the geothermal field is 4 km west of the active, north- to northwest-striking, normal-slip Cottonwood Mountain fault. Furthermore, the field is within several kilometers of recently detected seismicity. This, coupled with its active hot springs (~90°C), opaline sinter mounds, and geothermal fluid flow, suggest that the geothermal field lies within an active (Quaternary), southward-terminating, left-stepping fault zone, which locally acts as a pull-apart basin with sinistral- and normal-slip components.

Acknowledgments

I want to thank my advisor, Dr. James Faulds, for his patience and guidance given to this project and to me personally. I also want to thank Nick Hinz for his constant help with software and data, and for his support and helpful discussions concerning all things geology. I also thank Clinton Colwell, Dr. Mila Adam, and Carl Hoiland, for access to geophysical datasets and their contribution to the structural model at Neal. Thank you to Ian Warren of U.S. Geothermal for providing access to data and for helpful discussions. I'd also like to thank Mark Ferns and Jason McClaughry for their visits in the field and helpful email correspondence concerning Oregon geology. Thank you to James Evans for providing his mapping efforts and thoughts on the geology at Neal. Thanks to Dr. Michael Cosca at the U.S. Geological Survey lab in Denver, Colorado for $^{40}Ar/^{39}Ar$ age dates. I thank my committee members, Dr. John Louie and Dr. David Bennum, for their willingness to meet and provide general advice. I also acknowledge the assistance of Dr. Martin Streck, Spencer Wood, and Matthew Richardson. This work was funded primarily by the U.S. Department of Energy (DE-EE 0002748) and partly by the EERE National Geothermal Student Competition, Geological Society of America, and Nevada Petroleum and Geothermal Society. I also want to thank my friends at UNR, including Ryan Anderson, Greg Dering, and Brett Mayhew for fruitful discussions on this work and on geothermal systems in general. Thank you to Kate and Scott Lamb for providing me a place to stay, food to eat, and engaging discussions during fieldwork. I must thank my family for their support throughout the project.

Table of Contents

List of Figures

1. Introduction

2. Geologic Setting

3. Stratigraphic Framework

4. Structural Framework

5. Discussion

1. Introduction

With global energy demands rising, more viable and economical resources of renewable energy are needed. The science of geology already plays a crucial role in the discovery and production of resources that power the world (e.g., petroleum, uranium, coal). However, further investment, study, and discovery of new resources are needed to keep up with increasing energy consumption demands.

Geothermal resources have provided renewable, baseload electricity in the U.S. for over 50 years. However, the geologic framework and favorable settings of geothermal sites remains poorly understood, and models that accurately predict the location of permeable zones of high-temperature upflow are in incipient stages. Thus, exploration, more specifically drilling, remains a high-risk venture, keeping new development and production growth low and ephemeral.

Previous work done on the structure of geothermal systems illuminates a direct relationship between permeability-temperature and structure (Blackwell, 1983; Barton et al., 1995; Curewitz and Karson, 1997; Faulds et al., 2004, 2006, 2011; Lowell and Rona, 2005; Bell and Ramelli, 2007). Structural pathways provide the necessary permeability for rapid ascent of geothermal fluids. Detailed structural studies of geothermal systems have occurred across much of the Basin and Range, including the Roosevelt, Soda Lake, Salt Wells, Brady's, Desert Peak, Steamboat, Lee-Allen, Dixie Valley, Beowawe, and San Emidio fields (e.g., Edmiston and Benoit, 1984; Layman, 1984; McNitt, 1990; Moore and Nielson, 1994; Blackwell et al., 1999; Blackwell et al., 2002; Faulds et al., 2003, 2006, 2010; Hinz et al., 2008; Rhodes, 2011). Among these systems and others in

the Basin and Range, normal faulting is a generally ubiquitous structural characteristic. Normal faults oriented favorably for dilation and therefore permeability generally strike perpendicular to the least principal stress direction (Barton et al., 1995; Faulds et al., 2006). However, not every favorably oriented fault in the Basin and Range affords permeability and therefore geothermal fluid flow.

Among the optimally oriented faults and fault zones, specific structural settings, with high fracture densities, are known to be conducive for fluid flow. Preliminary results from a recent survey (Faulds et al., 2011) of structural settings of geothermal systems in the Great Basin indicate the relative proportions of these settings among known geothermal fields. The major settings include: 1) step-overs or relay ramps in normal fault zones (Figure 1A) at 32% of known fields; 2) intersections between normal faults and/or transversely oriented strike-slip or oblique-slip faults (Figure 1D) at 22%; 2A) a subset of fault intersections known as displacement transfer zones (i.e. dilational intersections between strike-slip and normal faults); (Figure 1D) at 5%; 3) normal fault terminations or tip-lines (Figure 1B) at 22%; 4) accommodation zones with belts of intermeshing, oppositely dipping normal faults (Figure 1C) at 8%; and 5) transtensional pull-apart zones at 4% (Figure 1) (Faulds et al., 2006, 2011). Other less notable structural settings for geothermal systems are major range front faults at 3% and ‘salients or major bends’ in major normal faults at 3% (Faulds et al., 2011).

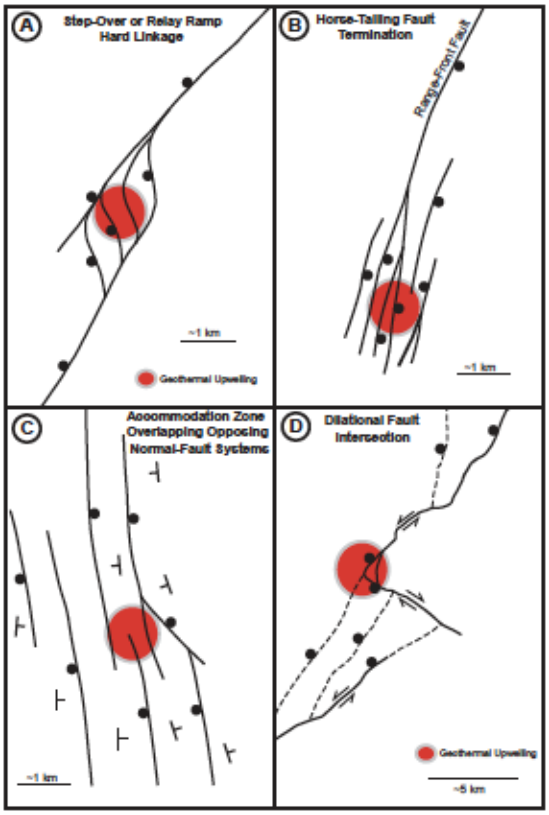

Figure 1.1 - Generalized favorable structural settings for geothermal systems in the Great Basin (from Faulds et al., 2006).

The above-mentioned settings are commonly associated with subvertical conduits of densely fractured rocks proximal to or within Quaternary fault zones (Faulds et al., 2011). These structures can be represented topographically as 1) major steps in range-fronts, 2) interbasinal highs, 3) ranges consisting of low discontinuous ridges, and 4) lateral terminations of ranges (Faulds et al., 2006, 2011). Many systems exhibit a combination of structural settings.

As part of this broader study, the Neal Hot Springs geothermal field in eastern Oregon provides an opportunity to study the structural controls of a producing (as of Fall, 2012) geothermal field. The field lies north of the Great Basin and therefore north of the more well studied systems. Furthermore, it lies at the intersection or overlap zone

between two dominant structural grains, the northerly trending Basin and Range normal fault systems, represented by the Oregon-Idaho graben, and the northwest-trending Vale fault zone (considered in this study as an extension of the western Snake River Plain). Thus, the results of this study likely extend structural models of geothermal systems in the Basin and Range northward to eastern Oregon and the western Snake River Plain, which has high heat flow (> 80 mW/m^2) and a high geothermal gradient (~90 C°/km) (Idaho National Laboratory, 2006).

The main goals of this study were to: 1) regionally correlate and establish stratigraphy in the Neal area, 2) elucidate ages of faulting and estimate offset on major faults, 3) define the geometry and kinematics of fault systems, 4) provide an estimate of the local stress field and least principal stress direction, 5) understand the evolution of the geothermal system, 6) incorporate geologic, geochemical, well field, and geophysical datasets into a structural model of the geothermal system, and 7) augment geothermal exploratory models for both the Basin and Range and western Snake River Plain provinces.

This study included a detailed analysis of the Neal Hot Springs geothermal field and surrounding areas. Methods employed included: 1) detailed geologic mapping of ~90 km^2 at 1:24,000 scale to define the stratigraphic and structural framework (Appendix A) (Plate 1), 2) petrographic analysis of hand samples and 57 thin sections for unit correlation, 3) sampling of 111 surface and down-well lavas for bulk-rock XRF analyses to both chemically identify and correlate discontinuous volcanic rocks (Appendix B), 4) petrographic and geochemical study of the well-field (24 total wells) for reassignment of down-well lithologies, from original U.S. Geothermal logging efforts, into correlated

(from mapping) stratigraphy, 5) structural analysis to delineate the geometry and kinematics of faults and procure the local stress field, 6) integration of seismic reflection, gravity, and well data to constrain the geometry and offset along fault zones in the subsurface, and 7) GIS compilation of the geologic map and available datasets for interpretation of structural controls of the geothermal field.

2. Geologic Setting

REGIONAL STRATIGRAPHY

The stratigraphy at Neal consists of a basement of accreted terrane and intrusive Jurassic granite, as exposed to the north in the Blue Mountains (Figure 2.1). Zircons obtained from granite in NHS-11 yielded preliminary Jurassic ages (Hoiland pers. comm., 2012), constraining the granite to the Jurassic Olds Ferry-Izee terrane (Ferns and McClaughry, 2011), older than the Cretaceous Idaho Batholith. Unconformably overlying the granite are rocks from three major depositional sequences: 1) the middle Miocene Columbia River Basalt Group (regionally known as the Malheur Gorge basalts) (Camp et al., 2003), 2) middle Miocene Oregon-Idaho graben silicic and icelanditic lavas and volcaniclastic rocks (Cummings et al., 2000), and 3) the late Miocene-Pliocene western Snake River Plain calc-alkaline lavas, lacustrine, fluvial, and volcaniclastic rocks (Figure 2.1) (Wood and Clemens, 2002).

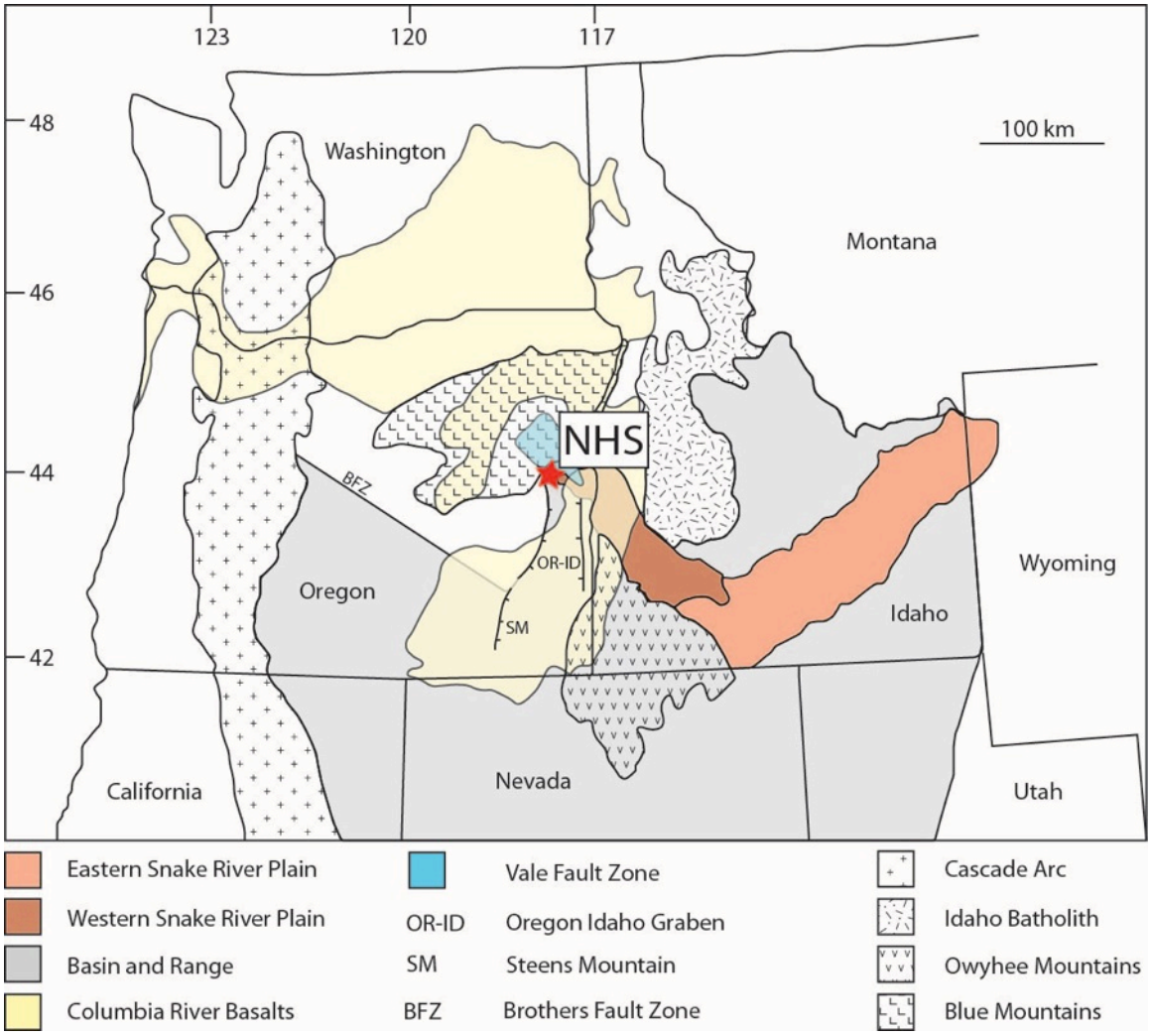

Figure 2.1 –Magmatic and tectonic provinces of the northwestern USA and their geographic relation to the study area. Neal Hot Springs (NHS) is shown by the red star. Modified from Lees (1994).

REGIONAL STRUCTURE

Three regional structural grains are found in eastern Oregon and southern Idaho (Figures 2.1 and 2.2): 1) middle Miocene to present, northeast-trending Yellowstone hot spot track and eastern Snake River Plain, 2) middle Miocene to present northerly trending Basin and Range, and 3) late Miocene to present northwest-trending western Snake River Plain, including the Vale fault zone. The Neal Hot Springs geothermal field is located near the intersection or overlap of the late Miocene-Quaternary, northwest-trending

western Snake River Plain (as considered linked to the Vale fault zone in this study) and the middle Miocene Basin and Range extensional faulting, as expressed by the north-trending, 15.5-10.5 Ma Oregon-Idaho graben (Figures 2.1 and 2.2) (Cummings et al., 2000; Wood and Clemens, 2002).

Figure 2.2 - Digital elevation model showing major tectonic features in the northwestern USA. BFZ: Brothers fault zone, BG: Baker graben, EDFZ: Eugene-Denio fault zone, KMH: Kuna-Mountain Home volcanic rift, LG: LeGrande graben, LVFS: Long Valley Fault System, MFZ: McLoughlin fault zone, OR-ID: Oregon-Idaho, PV: Pine Valley, WSRP:Western Snake River Plain, SMFZ: Steens Mountain fault zone, SPV: Shoe Peg

Valley, VFZ: Vale fault zone. The inset shows a National Agriculture Imagery Program (NAIP) image of the study area.

GPS geodetic data suggest ongoing clockwise rotation of the Pacific northwest U.S., including Oregon, Washington, Idaho, and both northern Utah and Nevada (Figure 2.3) (McCaffrey et al., 2007; Payne et al., 2012). However, residual horizontal velocities, following removal of rotational components, are low for both eastern Oregon and the western Snake River Plain, with calculated extensional strain rates indistinguishable from zero (Payne et al., 2012). These extensional strain rates are an order of magnitude lower than in the

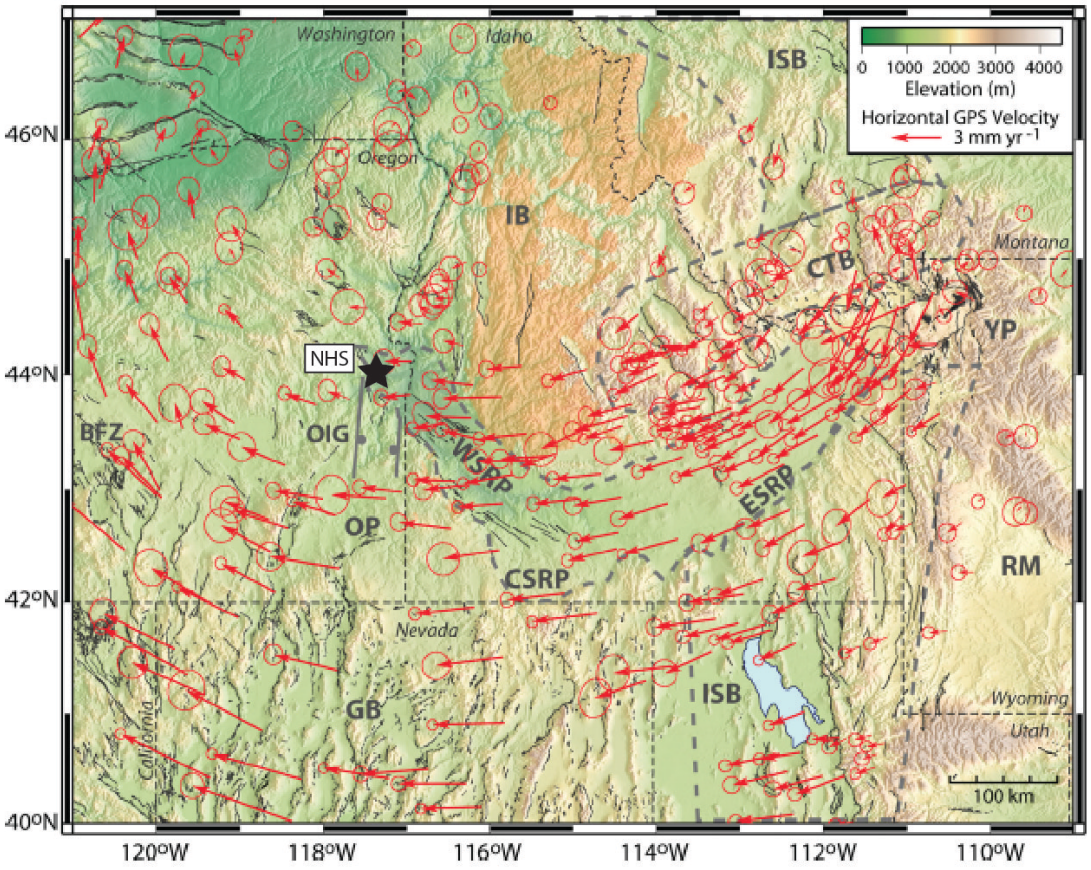

Figure 2.3 – Shaded relief map showing observed horizontal 1994-2010 (red vectors) and uncertainties (at 70% confidence ellipses) in the stable North American reference frame

(SNARF) (Payne et al., 2012). BFZ: Brothers fault zone, CSRP: central Snake River Plain, CTB: Centennial tectonic belt, ESRP: eastern Snake River Plain, GB: Great Basin, IB: Idaho Batholith, ISB: Intermountain seismic belt, OIG: Oregon-Idaho Graben, OP: Owyhee-Oregon Plateau, NHS: Neal Hot Springs (shown by black star), RM: Rocky Mountains, WSRP: western Snake River Plain, YP: Yellowstone Plateau. Modified from Payne et al. (2012).

adjacent Basin and Range region to the south (Payne et al., 2012). Payne et al. (2012) infers right-lateral shear between the rapidly extending Basin and Range and slowly deforming eastern Oregon region, south of Neal and east of the Brothers fault zone (Figure 2.2).

The Oregon-Idaho graben (Figures 2.1, 2.3 & 2.4) is a synvolcanic graben straddling the western margin of the North American craton (Cummings et al., 2000). It evolved as a north-trending middle Miocene rift system incorporating and connecting the northern Nevada rift to the south, Baker and Le Grande grabens to the north, and Columbia River Basalt dike swarms (Cummings et al., 2000). It can be interpreted as a relatively modern structural expression of the Mesozoic cratonic boundary (Cummings et al., 2000).

The extension direction within the Oregon-Idaho graben was generally east-west, as indicated by northerly-striking dikes and normal faults. Initial subsidence and rifting coincided with voluminous silicic and mafic volcanism between 15.5-15.3 Ma (Cummings et al., 2000). Intragraben sub-basin development ensued between 14.3-12.6 Ma, with waning subsidence continuing until cessation near 10.5 Ma (Cummings et al., 2000). Concomitantly, volcaniclastic and lacustrine deposits filled the graben (Cummings et al., 2000).

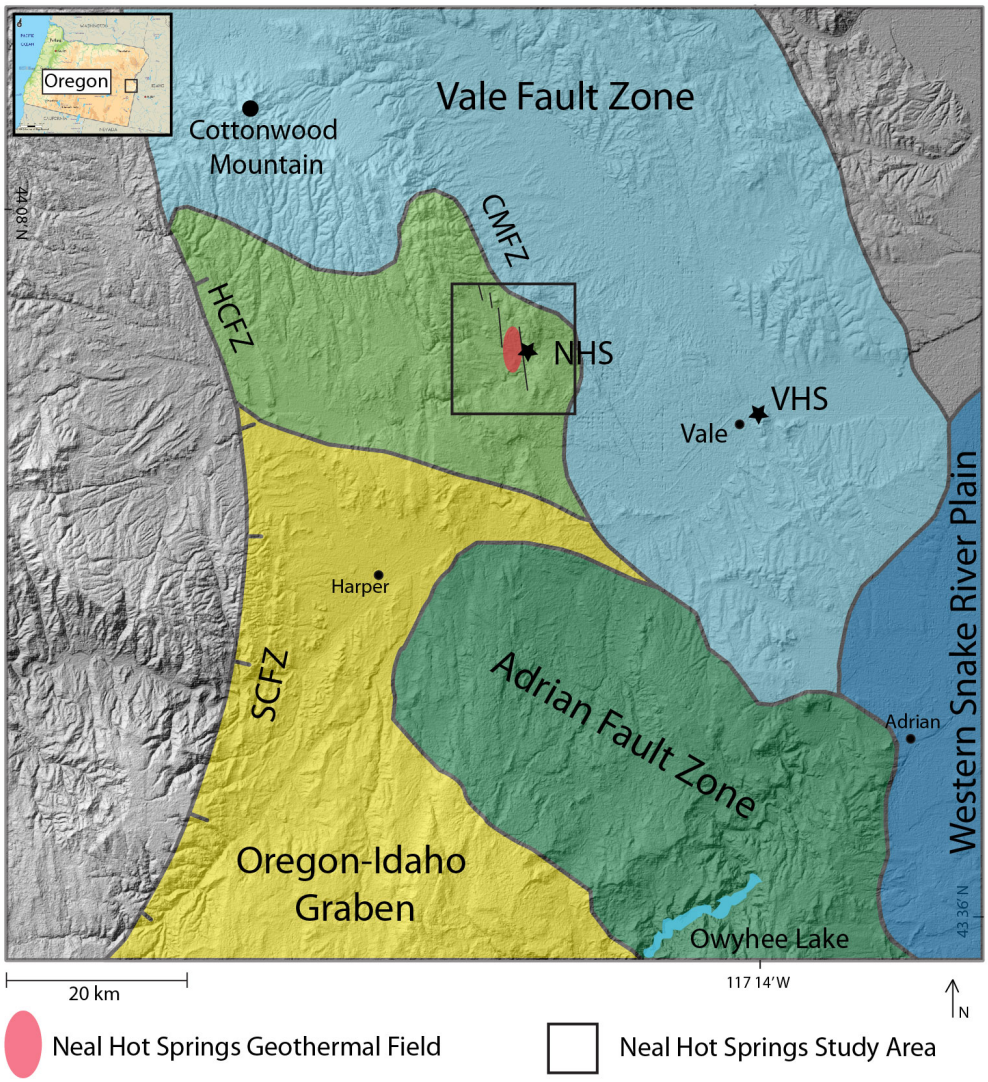

Figure 2.4 – Relationships between Oregon-Idaho graben (yellow), western Snake River Plain (medium blue), Vale fault zone (light blue), and structurally overlapping regions (dark and light green). CMFZ: Cottonwood Mountain fault zone, HCFZ: Hog Creek fault zone, NHS: Neal Hot Springs, SCFZ: Squaw Creek fault zone, VHS: Vale Hot Springs.

Figure 2.4 illustrates the north to north-northeast trend of the Oregon-Idaho graben, with both the cross-cutting Adrian fault zone (western Snake River Plain) and overlapping Vale fault zone (Ferns et al., 1993). Of note is the gradational northward change of the dominant structural grain from north-northeast to north-northwest within

the Oregon-Idaho graben (e.g. compare the Squaw Creek fault zone to the Hog Creek fault zone) (Figure 2.4).

The western Snake River Plain (Figure 2.4) is a late Miocene-Quaternary northwest-trending intracontinental rift basin (Wood and Clemens, 2002). Rifting began ~11 Ma and accommodated over 2 km of offset by 9 Ma (Wood and Clemens, 2002). From 9 Ma to present, long-term average vertical slip rates have been low (0.01 mm/year). Along with active faulting, ~0.3 km of downwarping and compaction of thick sedimentary fill accounts for the conspicuous low topography of the Snake River Plain (Wood and Clemens, 2002). The Kuna-Mountain Home volcanic rift zone is a linear ~N70°W-trending belt of Quaternary basalt vents, marked by shield volcanoes, that are cut by subparallel fissures and faults (Figure 2.2) (Wood and Clemens, 2002). Conner and Conway (2000) demonstrated that trends of magma vents and fissures can reflect the tectonic stress field, with the trend of vents and fissures orthogonal to least principal stress. Assuming such, the active least principal stress across the western Snake River Plain would be southwest-northeast-trending.

The Vale fault zone (Figure 2.4) is a northwest-trending series of lineaments identified by topographic features (Lawrence, 1976). The fault zone is hypothesized to accommodate differential Basin and Range westward extension by right-lateral, strike-slip motion, analogous to the Brothers, Eugene-Denio, and McLoughlin northwest-striking fault zones (Figure 2.2) (Lawrence, 1976). It can also be hypothesized that the Vale fault zone is the northwest extension of the western Snake River Plain as it loses displacement and terminates to the northwest, accommodating mostly normal-slip. Some hypothesize that the Vale fault zone is the southeastern extension of the Olympic-

Wallowa-Lineament (Figure 2.4), similar to the northwest-striking Baker, Crane Creek, and Pine Valley fault zones (Mann and Meyers, 1993). These right-oblique-slip fault zones extend from the north-striking Long Valley Fault System and contain several right steps, producing inferred pull-apart basins forming the Baker, LeGrande, Pine Valley, and Shoe Peg Valley basins (Figure 2.2) (Mann and Meyers, 1993). Historical seismicity is prevalent along the Olympic-Wallowa-Lineament associated fault zones and pull-apart basins (Mann and Meyers, 1993).

The Cottonwood Mountain fault zone (Figure 2.4), part of the Vale fault zone, as defined by Simpson et al. (1993), is a 5 km wide zone of northwest- and northerly-striking normal faults that cut through the northeast corner of the study area, ~4 km northeast of the geothermal field. Knudsen et al. (1995) studied Quaternary faulting along the Cottonwood Mountain fault, a steeply northeast-dipping normal fault. They concluded that scarps and lineaments show evidence for multiple late Quaternary surface faulting events over a rupture length of 36 km. They computed an average dip-slip displacement of 1.2±0.25 m and estimated a range of slip rates from 0.03 to 0.2 mm per year. Because of the strong evidence for late Quaternary faulting, the Cottonwood Mountain fault is considered active (Evans, 1994). Although few historical seismic events have been recorded near Neal Hot Springs, a passive seismic network, constructed in the area by a Boise State University geophysical group in 2011, recently detected <2.0 magnitude earthquakes within ~4 km of Neal (Colwell, pers. comm., 2012).

GEOTHERMAL SYSTEM

The Neal geothermal field lies just west (~0.5 km) of 1) a group of hot springs (approximately 100 m^2 surface area) called Neal Hot Springs that effuse from opaline sinter mounds at high temperatures (~90° C, Warren pers. comm., 2012) and low flow rates, and 2) an ~100 m wide zone of abundantly silicified sediments in the hanging wall of the north- northwest-striking producing fault zone (Figure 2.5).

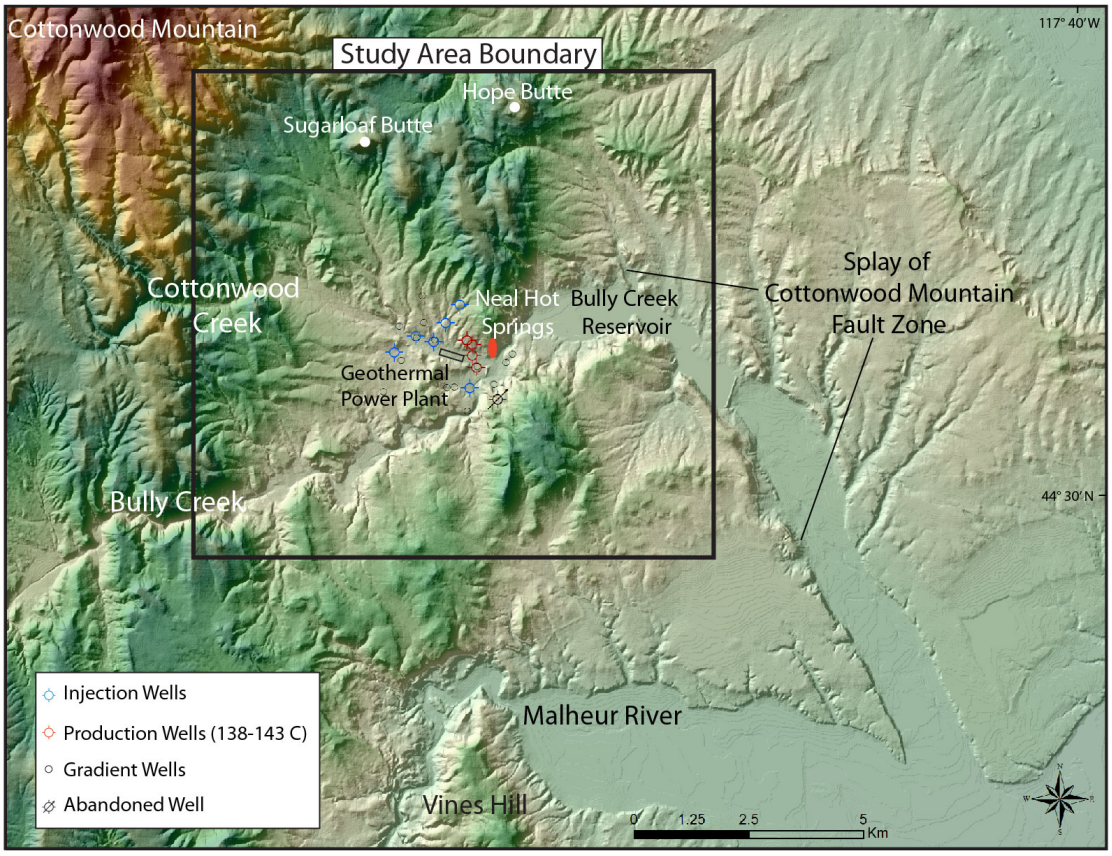

Figure 2.5 – Digital elevation model showing the study area outlined in black, the well field and power plant, and other prominent geographic and topographic features within and surrounding the study area.

The Neal Hot Springs geothermal field is defined by a north-northwest-trending zone of high permeability and high temperature fluids (up to ~142°C) along a steeply west-dipping normal fault. Chevron Minerals originally identified the field during

exploratory natural gas drilling efforts in the late 1970's. Chevron reported a commercial geothermal resource at depths of ~700 m (U.S. Geothermal pers. comm., 2012). In 2006, U.S. Geothermal leased 9.6 square miles of surface rights at Neal Hot Springs and began drilling in 2008.

Pre-drilling, U.S. Geothermal acquired the following datasets: 1) the Chevron Minerals exploratory well and associated data, 2) a detailed gravity survey, and 3) the geometry of a prominent exposed fault, here referred to as the Neal fault. Initial drilling efforts by U.S. Geothermal were successful, with four production wells encountering reservoir temperatures, massive lost circulation, and high flow rates within a fracture zone between 680-1100 m depth. Injection wells have since been drilled north, south, and west of the four production wells with varying success. Geothermometry indicates a higher temperature reservoir at depth, possibly up to ~160°C (U.S. Geothermal pers. comm., 2012).

Construction began on a 23 megawatt, binary cycle power plant in April 2011, with completion in the fourth quarter of 2012. A 25-year Power Purchase Agreement was signed in December, 2009 with Idaho Power Company. Electricity will be sold at $96.00 per megawatt-hour and escalates at a variable percentage annually (U.S. Geothermal pers. comm., 2012).

Regionally, Neal Hot Springs sits within a broad area of high heat flow (>80 mW/m^2) in eastern Oregon (Idaho National Laboratory, 2006). This is likely attributed to an area of anomalously thin continental crust (Eager et al., 2011). The heat flow data illustrate the potential for future geothermal exploration and development in eastern Oregon and along the Snake River Plain (Idaho National Laboratory, 2006).

3. Stratigraphic Framework

The stratigraphic framework at Neal is dominated by a thick section of Miocene-Pliocene volcanic and sedimentary rocks, which overlie Mesozoic granitic and metamorphic basement. Basement rocks include a granite body encountered in well NHS-11 at a depth of 2051 m. Four samples were submitted to Franklin and Marshall X-Ray Laboratory for XRF bulk-rock analysis. Preliminary zircon dates suggest a Jurassic age, which indicates that this granitoid correlates with the accreted Olds Ferry-Izee terrane and its granitic intrusions, part of the Blue Mountains Mesozoic accreted terranes (Hoiland, Stanford SHRIMP Laboratory, pers. comm., 2012). This suggests that Neal lies west of the Mesozoic cratonic margin. The middle Miocene to Pliocene volcanic rocks at Neal generally correlate with strata in the Oregon-Idaho graben to the south (Ferns et al., 1993), the western Snake River Plain to the east (Wood and Clemens, 2002), and more locally in the Vale area, as grouped and defined by Lees (1994) and Hooper et al. (2002a). Correlated volcanic rocks provide stratigraphic markers for both mapping and down-hole correlations. As a part of this study, 111 surface and down-well volcanic rock samples were submitted for XRF bulk-rock analysis to facilitate correlations.

In the Neal area, an ~1.6 km thick package of the middle Miocene basalt of Malheur Gorge (Tbm) nonconformably overlies the Jurassic granite (Camp et al., 2003), (constrained by well NHS-11). Lees (1994) subdivided this package into three chemically distinguishable, yet gradational, tholeiitic packages. Weighted mean $^{40}Ar/^{39}Ar$ ages are: lower Pole Creek basalt at 16.9 ± 0.8 Ma, upper Pole Creek basalt at 16.5 ± 0.3 Ma, and Birch Creek basalt at 15.7 ± 0.01 Ma (Hooper et al., 2002a). Through a comparison of ~700 major and trace element analyses from the Steens basalt, the basalt of Malheur

Gorge, and Columbia River Basalt Group, Binger (1997) concluded that 1) the lower Pole Creek (Tlpc) and Steens basalts are correlative, 2) the upper Pole Creek (Tupc) and Imnaha Basalt (Columbia River Basalt Group) correlate, and 3) the Birch Creek (Tbcr) and Grande Ronde Basalt (Columbia River Basalt Group) are correlative.

The basalt of Malheur Gorge (Tbm, undivided, Plate 1) sequence contains the lower Pole Creek, upper Pole Creek, and Birch Creek basalts. The sequence is poorly exposed in the study area, however, it was intersected in every large-diameter well and a few temperature gradient wells. The sequence was sampled heavily for XRF analysis, and an attempt was made to subdivide the sequence into the three units defined by Hooper et al. (2002a). Mineralogically, the Lower Pole Creek basalts are more plagioclase phyric, with the number of phenocrysts decreasing up-section to the mostly aphyric Birch Creek basalts. However, because of the gradational nature of the sequence, sequence subdivision within well logs was not tenable.

Conformably overlying the basalt of Malheur Gorge sequence is the Hog Creek Formation (Thc, undivided, Plate 1), as defined by Lees (1994). At Neal, the Hog Creek Formation is composed of interlayered Cottonwood Mountain Rhyolite (Trcm) (as named by Evans, 1994), Hunter Creek Basalt (Thb), and volcaniclastic rocks (Thcs, undivided). Field relationships consistently place the Cottonwood Mountain Rhyolite below the Hunter Creek Basalt, with intercalated, discontinuous volcaniclastic sequences. However, well-log studies show a contemporaneous relationship, with multiple packages of basalt throughout the section and thick intercalated volcaniclastic rocks, herein referred to as the Hog Creek sedimentary rocks (Thcs, undivided, Plate 1). Hooper et al. (2002a) obtained

$^{40}Ar/^{39}Ar$ ages of 14.6, 15.7, and 15.5 Ma (± 1.0, ± 0.7, and ± 0.2 Ma, respectively) for the rhyolite and an $^{40}Ar/^{39}Ar$ age of 15.8 ± 0.3 Ma for the basalt.

The Cottonwood Mountain Rhyolite covers much of the northern half of the study area, generally occupying the footwall of northerly-striking, steeply dipping normal faults. Preserved thicknesses of the Cottonwood Mountain Rhyolite reach up to ~200 m but are also as little as ~10 m. Petrographically, the rhyolite varies from vitrophyric and porphyritic to an aphanitic, sugary, lighter variegated groundmass. It contains phenocrysts of plagioclase (~25%), minor quartz (~2%), and sanidine (~1%).

The Hunter Creek Basalt is a dark, dense, sparsely phyric lava, with ~1% plagioclase and olivine phenocrysts. The basalt varies in thicknesses from ~10-100 m. Petrographic analysis shows a groundmass dominated by plagioclase (~70%), with lesser pyroxene (~15%), illite weathering and alteration (~10%), and Fe-oxides (~5%).

Exposures of the Hog Creek Formation in the northern part of the study area are hypothesized to fill a channel or paleovalley, where the Cottonwood Mountain Rhyolite and Hunter Creek Basalt lavas were deposited and eroded coeval to deposition of fluvial sedimentary rocks. Coarse, angular conglomerates and sedimentary breccias cap this sequence in several areas, likely the result of erosional over-steepening and development of talus slopes and small alluvial fans along the margins of the channel.

Conformably overlying the Hog Creek Formation is a package of rocks related to the filling of the middle Miocene Oregon-Idaho graben. In ascending order, this package consists of: 1) a chemically distinct, discontinuous, largely intrusive diabase basalt (Tdb, Plate 1), 2) volcaniclastic, fluvial, and lacustrine Drip Springs Formation (Tds) (Kittleman et al., 1965), 3) local basaltic andesite flows that cap the hillsides south of the

Bully Creek Reservoir and Neal Hot Springs, informally named in this study the Reservoir basaltic andesite (Tbar), and 4) the Vines Hill andesite (Tav) (Brooks, 1991; Brooks and O'Brien, 1992). Deposition likely occurred coeval to the waning subsidence of the Oregon-Idaho graben. $^{40}Ar^{39}Ar$ ages from the Reservoir basaltic andesite are 12.13 ± 0.02 and 12.29 ± 0.09 Ma and from the Vines Hill andesite are 11.46 ± 0.17 and 10.87 ± 0.08 Ma (Cosca written comm., 2013). Hooper et al. (2002a) obtained the youngest $^{40}Ar/^{39}Ar$ age of 10.1 ± 1.4 Ma for the capping Vines Hill andesite, suggesting the Vines Hill andesite filled the upper part of the graben in the Neal area ~10 Ma. Oregon-Idaho graben related rocks crop out throughout the study area, including in the north overlying the Hog Creek Formation, in the southwest along Bully Creek, and in the south and southeast along the Bully Creek Reservoir.

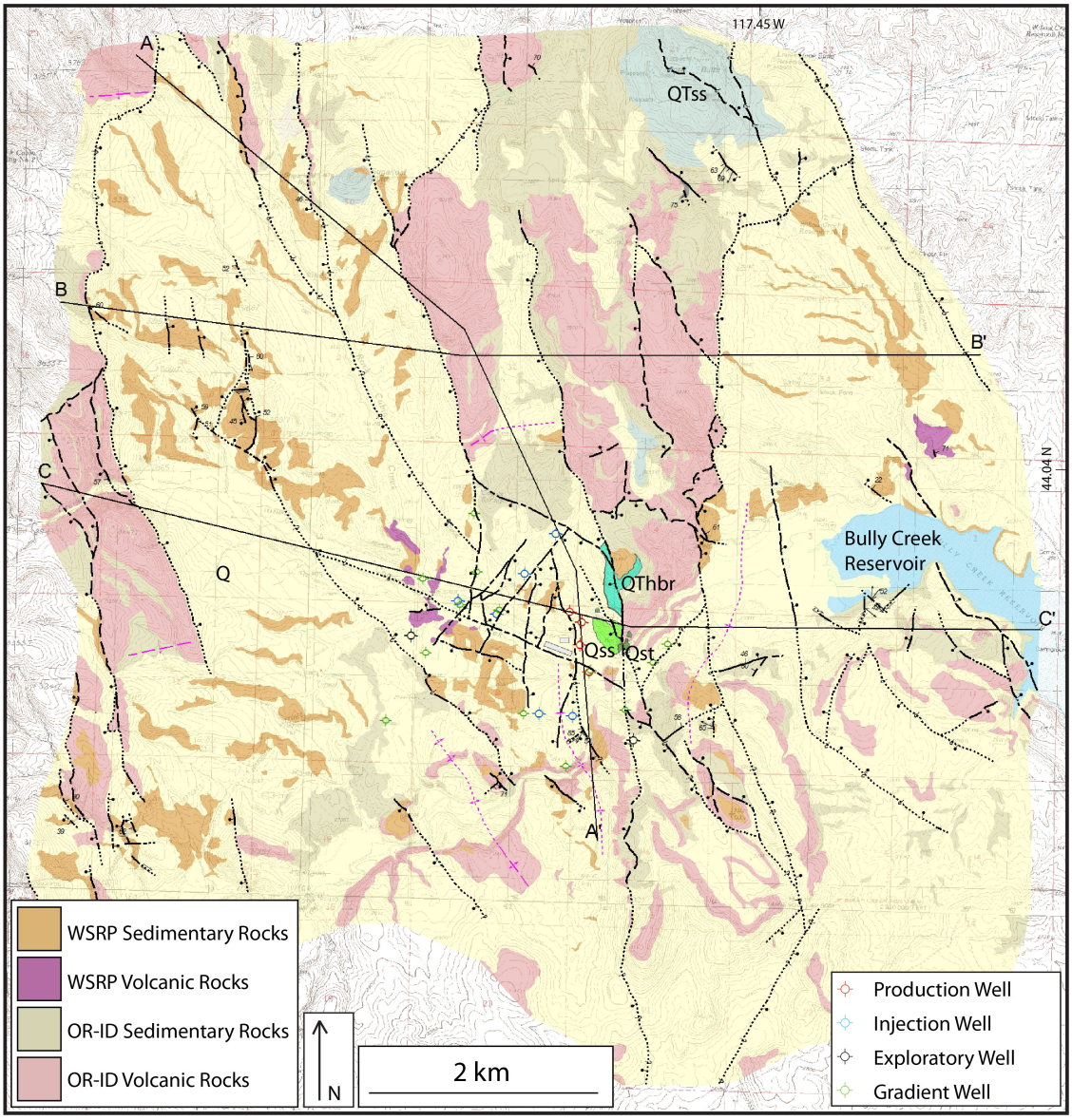

Figure 3.1 - Simplified geologic map of the study area showing well locations and cross section lines. Bar and balls shown on downthrown sides of normal faults. Undivided Quaternary (Q), Silicified sediments (Qss, bright green), opaline sinter (Qst, dark green), silicified sediments (QTss) and hydrothermally altered breccia (QThbr, teal).

Conformably above the Oregon-Idaho graben rocks are the late Miocene – Quaternary western Snake River Plain related rocks. In ascending order, this section consists of: 1) lacustrine and volcaniclastic lower Bully Creek Formation (Tbcl, Plate 1), 2) Neal basalt vent (Tbn, as named in this study), 3) fluvial, volcaniclastic, and lacustrine

upper Bully Creek Formation (Tbcu), and 4) overlying dacite scoria (Tsd). The lower and upper Bully Creek Formation correlates with the lacustrine Chalk Hills Formation of the western Snake River Plain (Malde and Powers, 1962) and the Bully Creek Formation of eastern Oregon (Kittleman et al., 1965). It contains a conspicuous (up to ~10 m thick) aphyric ash-flow tuff, with incorporated, blocks of diatomite. This distinct lithology correlates with the ~8.4 Ma Prater Creek tuff (Ferns, pers. comm., 2012). The Neal basalt is local to the Neal area, venting at the western end of the geothermal field and intercalated with upper Bully Creek Formation rocks. It yielded an $^{40}Ar/^{39}Ar$ age of 8.81 ± 0.05 Ma (Cosca, written comm., 2013). Two younger dacite scorias (Tsd) show similar chemistry to young volcanic rocks grouped by Lees (1994) as the 3-0.8 Ma Kivett sequence and overlie the Neal basalt and upper Bully Creek Formation rocks. These scorias likely represent the youngest volcanic pulses at Neal and are interpreted to be discrete vents, with scatter cone features. Nearby Quaternary volcanism at Malheur Butte, ~25 km east, consists of a small 0.8 ± 0.7 Ma andesitic volcanic vent that intrudes Idaho Group rocks and exhibits a similar geochemical signature to the dacite scorias (Evans, 1994; Hooper et al., 2002a).

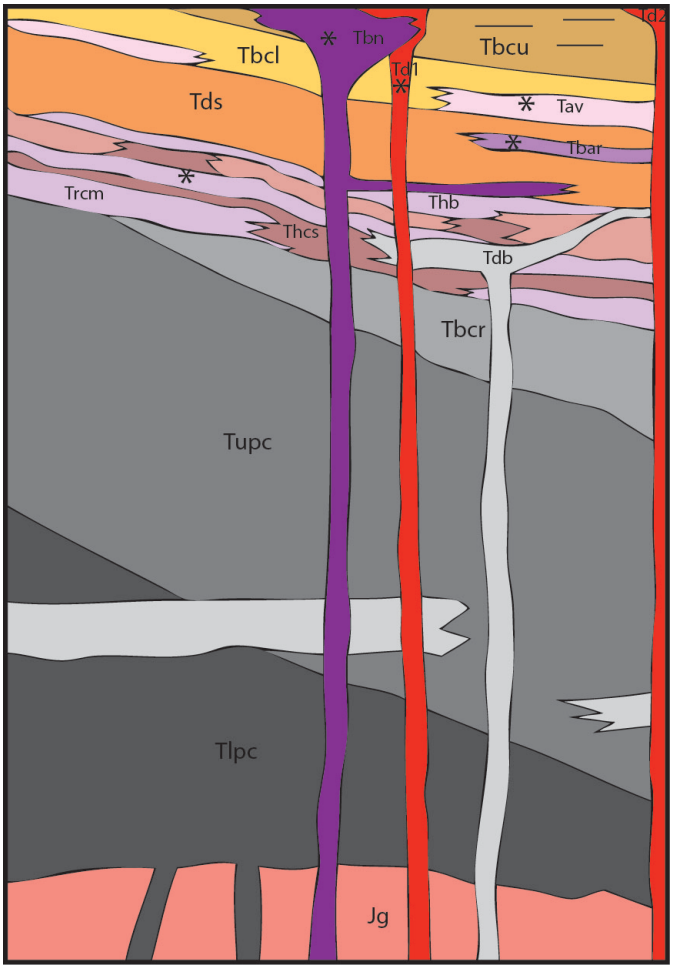

Figure 3.2 – Generalized stratigraphic column of the Neal Hot Springs area showing relative unit thicknesses and approximate degree of tilting. Asterisks denote those rocks submitted for $^{40}Ar/^{39}Ar$ dating. Lithologic units in ascending order: Jg-Olds Ferry-Izee terrane granite; Tlpc-Lower Pole Creek basalt; Tupc-Upper Pole Creek basalt; Tbcr-Birch Creek basalt; Trcm-Cottonwood Mountain Rhyolite; Thcs-Hog Creek volcaniclastics; Thb-Hunter Creek Basalt; Tdb-diabase basalt; Tds-Drip Springs Formation; Tbar-Reservoir basaltic andesite; Tav-Vines Hill andesite; Tbcl-lower Bully Creek Formation; Tcbu-upper Bully Creek Formation; Tbn-Neal basalt; Td1 & Td2-dacite scoria.

BULK-ROCK GEOCHEMISTRY

Boise State University and U.S. Geothermal, along with other grants, contributed toward funding XRF analyses of lavas at Neal. Ian Warren of U.S. Geothermal, Mark Ferns of Eastern Oregon University, and Clinton Colwell of Boise State University all contributed to sample preparation and submittal. Franklin Marshall Laboratory and

Washington State University GeoAnalytical Laboratory performed a total of 111 XRF analyses. Previously analyzed dacite geochemistry was provided by Evans (1994).

Geochemical analyses proved fruitful in this study both for regional and local correlation during both mapping and down-well logging efforts (Appendix B). Appendix B displays the geologic map and geochemical sample locations. Lavas at Neal exhibit a broad compositional range, from mafic basalt through silicic rhyolite (Figure 3.3). The total alkali silica (TAS) diagram proved useful in separating out down-well silicic lavas, namely the Cottonwood Mountain Rhyolite, from mafic lavas, based on their SiO_2 wt% to $Na_2O + K_2O$ wt% ratios. Some mafic lavas cluster coherently in this plot, namely the diabase basalt (Tdb), Neal basalt (Tbn), and lower Pole Creek basalt (Tlpc) units (Figure 3.3). However, the basaltic-andesite through andesite-dacite compositions are too gradational and varied to use the TAS diagram for mafic unit subdivision.

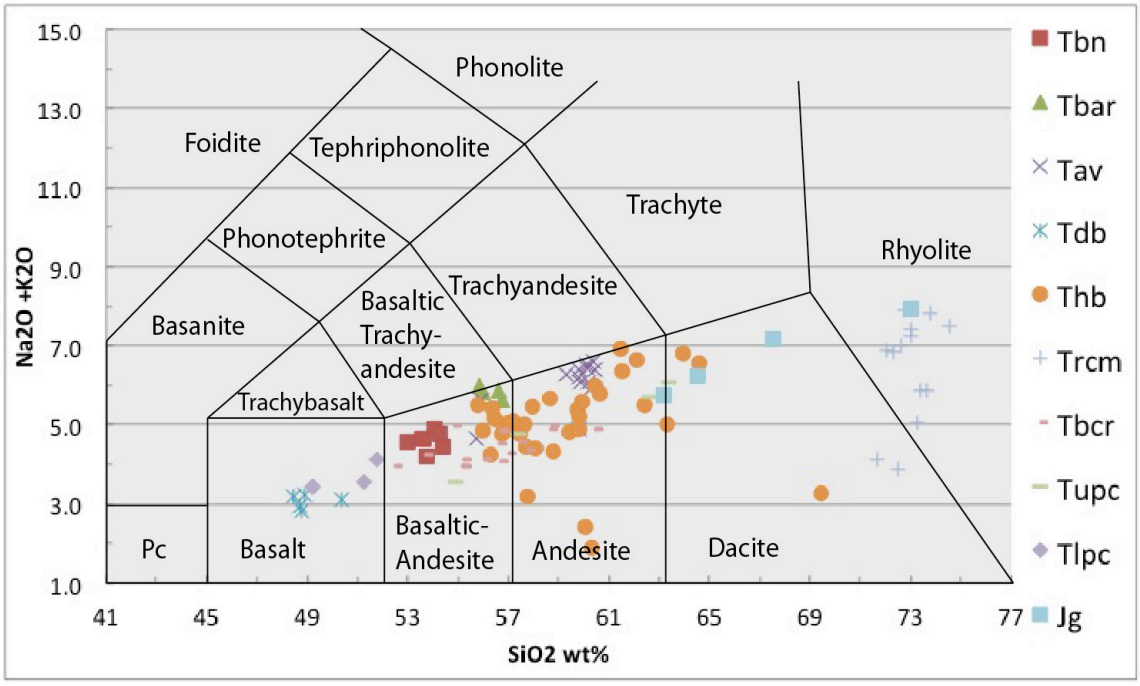

Figure 3.3 – Na_2O+K_2O vs. SiO_2 wt% plots illustrating the compositional range of lavas and an igneous body at Neal. TAS (total alkali silica) diagram with rock names overlain. Lithologic units in ascending order: Jg – Olds Ferry-Izee terrane granite; Tlpc – Lower Pole Creek basalt; Tupc – Upper Pole Creek basalt; Tbcr – Birch Creek basalt; Trcm – Cottonwood Mountain Rhyolite; Thb – Hunter Creek Basalt; Tdb – Diabase basalt; Tbar – Reservoir basaltic andesite; Tav – Vines Hill andesite; Tbn – Neal basalt.

Evolutionary trends of the mafic lavas are clear in Fe/Mg vs. SiO_2 wt% and P_2O_5 vs. TiO_2 wt % plots and provide a method for distinguishing down-well tholeiitic, icelandiitic, and calc-alkalic mafic lavas. Four evolutionary trends are observed at Neal: 1) middle Miocene, large volume tholeiitic lavas, 2) middle Miocene silicic lavas, 3) middle Miocene icelanditic lavas, and 4) late Miocene – Pliocene calc-alkalic lavas (Figure 3.4). Though beyond the scope of this study, the intra-plate extensional corridor of eastern Oregon and the geochemical signatures and evolutionary trends of lavas at Neal can augment our understanding of the evolution of volcanism in intracontinental rift settings.

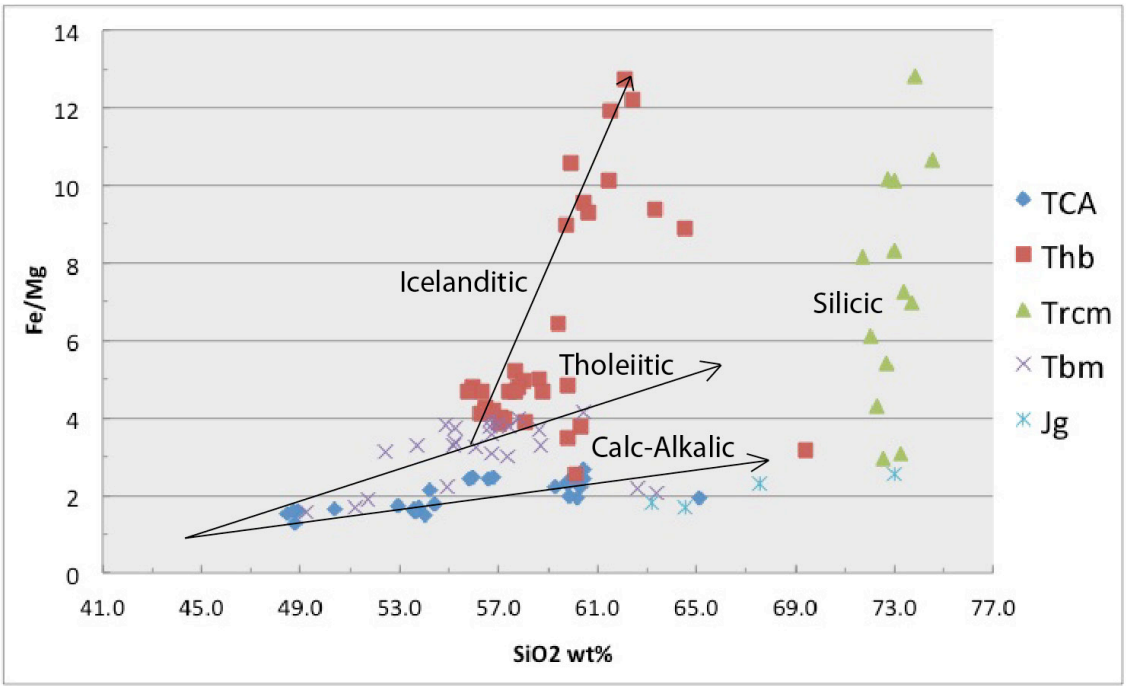

Figure 3.4 – Fe/Mg vs. SiO_2 wt% plot showing four evolutionary trends of volcanism at Neal: tholeiitic, silicic, icelanditic, and calc-alkalic. Lithologic units in ascending order: Jg – Olds Ferry-Izee terrane granite; Tbm – basalt of Malheur Gorge, including units Tlpc, Tupc, Tbcr; Trcm – Cottonwood Mountain Rhyolite; Thb – Hunter Creek Basalt; TCA – all calc-alkaline lavas, including units Tav, Tbar, Tbn, and Tdb.

Trace element studies were helpful for subdivision of calc-alkaline and tholeiitic lavas. Neal lavas exhibit distinct trace element signatures as a result of differentiation processes. Strontium and barium, along with other trace element diagrams not included in this report, provided helpful constraints, when synthesized with major element trends, in recognizing volcanic relationships and mafic unit subdivision. This includes distinguishing between Neal basalt (Tbn), Vines Hill andesite (Tav), Reservoir basaltic andesite (Tbar), Hunter Creek Basalt (Thb), and basalt of Malheur Gorge (Tbm; including Tlpc, Tupc, and Tbc).

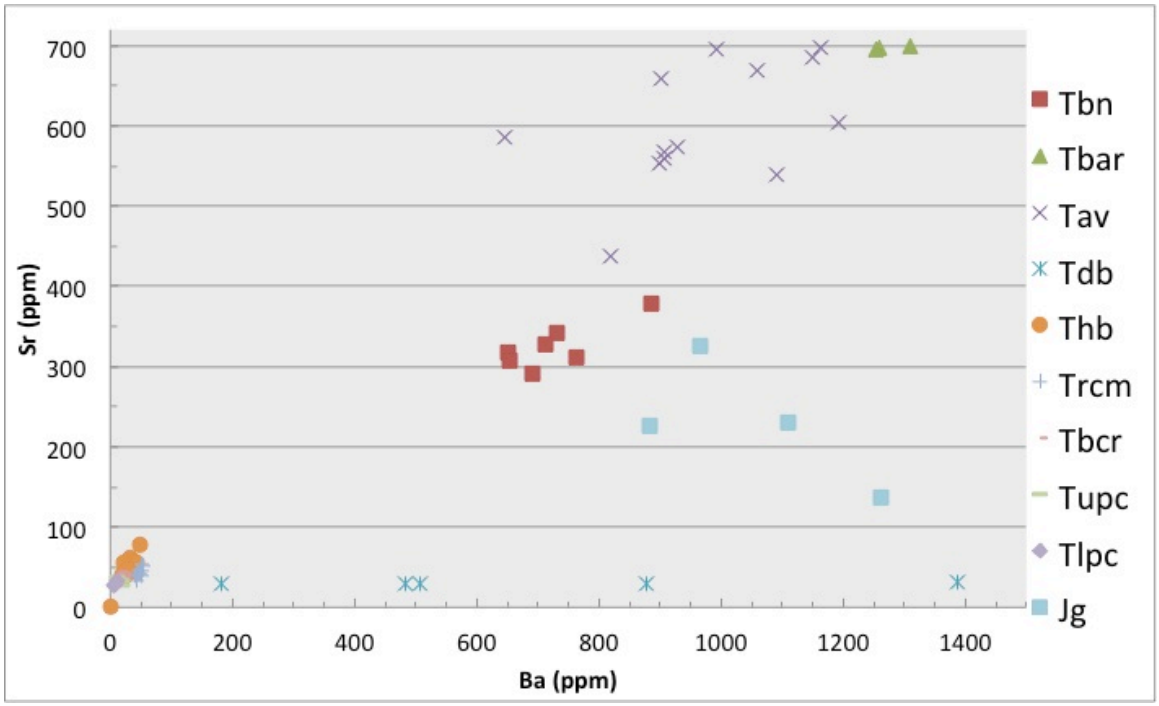

Figure 3.5 – Sr vs. Ba (ppm) plot illustrating trace element differences between mafic lavas. However, this plot is mainly useful for calc-alkaline rocks at this scale. If zoomed into the bottom left corner, trace element differences within tholeiities can be recognized. Lithologic units are the same as in Figure 3.3.

4. Structural Framework

GEOMETRY

The structural framework of the Neal Hot Springs area is characterized by gently, generally east-dipping fault blocks cut by north- to northwest-striking normal faults. Major faults generally dip steeply west and thus accommodated development of east-tilted half grabens. A left-stepping, west-dipping fault system is the most significant fault system in the area. It is directly linked to the geothermal system at Neal Hot Springs and is informally referred to as the Neal fault zone. Lesser north to north-northeast-striking, east- and west-dipping normal faults are also present. Anomalous to the northerly-trending structural grain is the west-northwest-trending Cottonwood Creek, interpreted to

be controlled by a subsidiary fault within the major left-stepping, north-striking fault system.

Tilt attitudes in the Neal Hot Springs area are relatively heterogeneous but can be grouped into several domains (Figure 4.1). The east-central part of the study area, informally labeled here as Domain A, has gently (~5-15°) southward dipping stratigraphy of the upper Bully Creek Formation (Tbcu) (Figures 4.1A and 4.2). These poorly consolidated sediments reflect the most recent episodes of faulting and tilting. Across the central, western, southeastern, and northwestern portions of the study area (labeled here as Domain B), where the basin-fill Bully Creek Formation crops out, the section dips gently eastward (~5-25°) (Figures 4.1B and 4.2). This tilting was likely accommodated by displacement along the Neal fault zone. Tilting in the footwalls of the left-stepping Neal fault zone are also toward the east and northeast (Figure 4.1D). The southeastern portion of the study area, south of the Bully Creek Reservoir, has the most steeply eastward and southeastward tilted rocks, with dips of ~15-35° in the Drip Springs Formation (Figure 4.2). This area is proximal to some landslides and thus the steeper dips could result from local slide blocks. However, the apparent coherent nature of the steeper tilts suggests fault-related tilting. The southwestern and northern portions of the study area (labeled here as Domain C) are dominated by exposures of the sedimentary rocks of the Drip Springs and Hog Creek Formations, with generally subhorizontal attitudes and no dominant tilt direction (Figures 4.1C and 4.2).

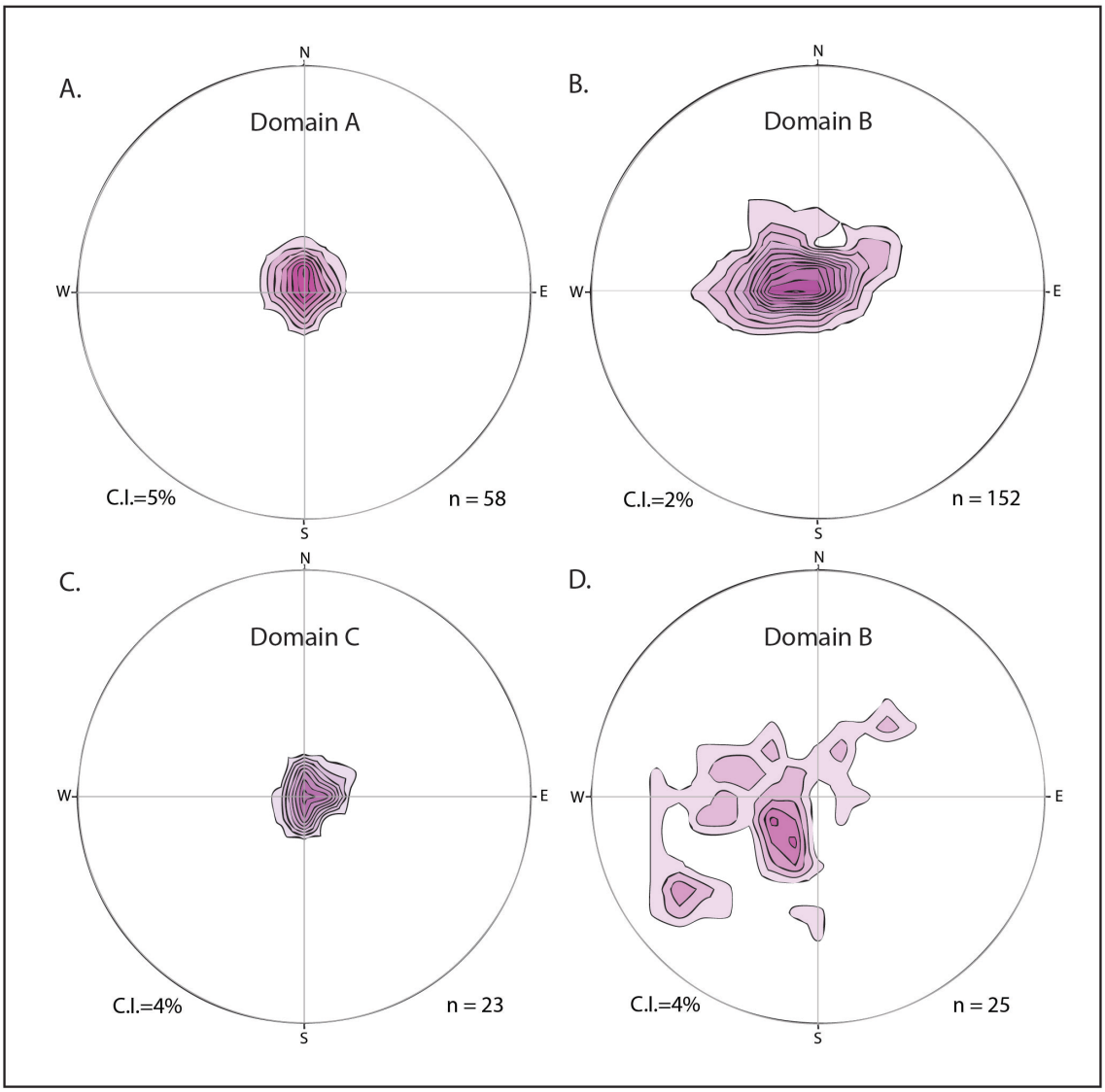

Figure 4.1 – Lower-hemisphere, equal-area stereographic projections of density contour plots of poles to bedding and volcanic flow foliations. Density contour interval equals a percentage (as noted above) of the data per 1% of the area. C.I. = contour interval, n = number of measurements. A. Late Miocene fluvial and pyroclastic rocks, upper Bully Creek Formation (Tbcu); B. Late Miocene lacustrine and pyroclastic rocks, Bully Creek Formation (Tbc); C. Middle Miocene tuffaceous sedimentary rocks, Drip Springs Formation (Tds); D. Middle Miocene flow foliations of volcanic rocks, Cottonwood Mountain rhyolite (Trcm) and Hunter Creek basalt (Thb).

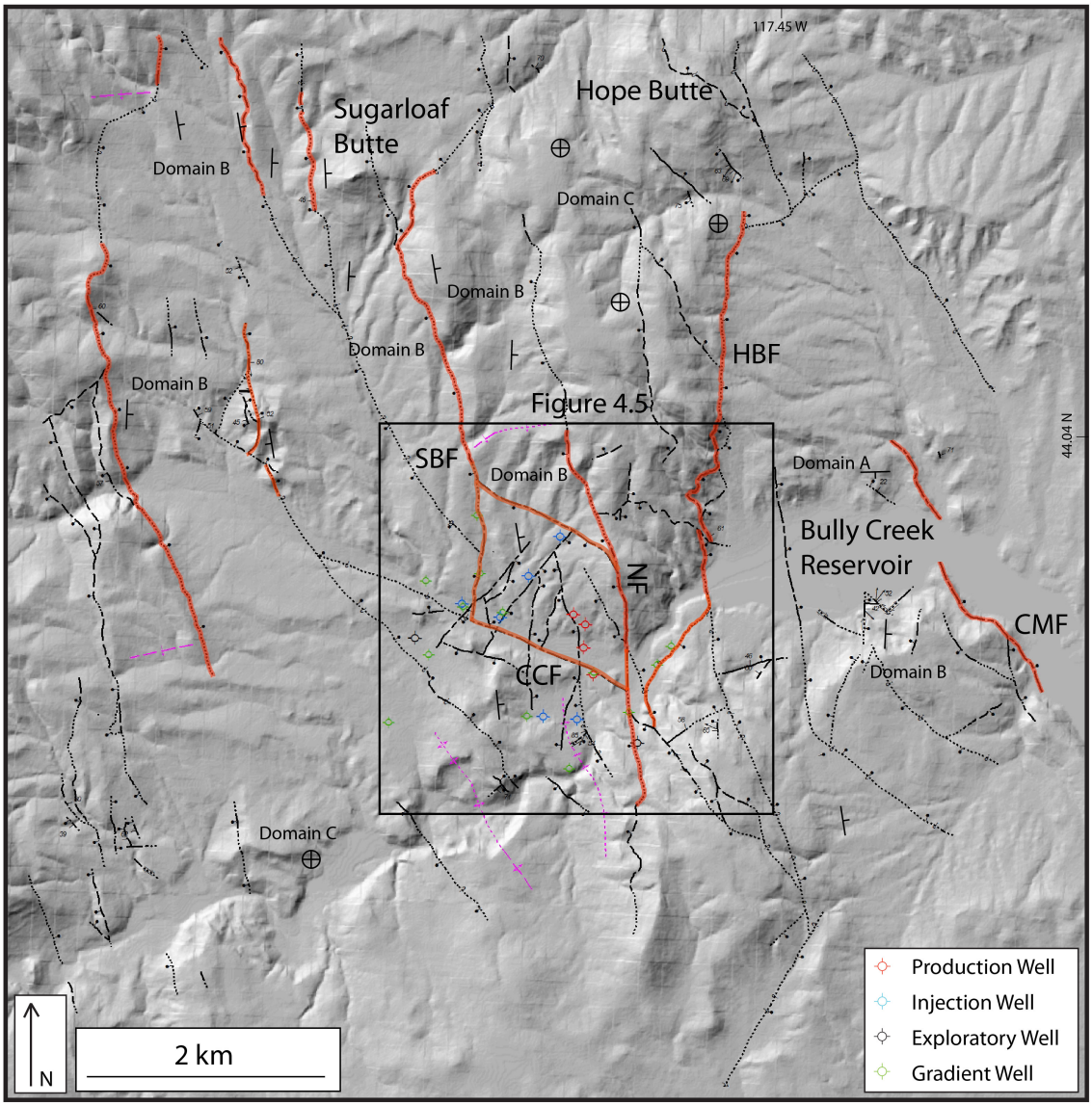

Figure 4.2 – Shaded relief map of the study area showing mapped faults in black; major faults are highlighted in red. Well-field is included. Domains refer to density contour plots of poles to bedding and layering shown in Figure 4.1. CCF, Cottonwood Creek fault; CMF, Cottonwood Mountain fault splay; HBF, Hope Butte fault; NF, Neal fault; SBF, Sugarloaf Butte fault.

The largest displacement and longest faults generally strike north-northwest to north-northeast and dip steeply to both the east and west (Figure 4.2). They accommodated dominantly normal slip, locally with an oblique component. Several faults are informally named in this study: Neal fault (NF), Cottonwood Creek fault (CCF),

Sugarloaf Butte fault (SBF), and Hope Butte fault (HBF) (Figure 4.2). The Neal fault zone includes the Neal, Cottonwood Creek, and Sugarloaf Butte faults, which collectively comprise a left-stepping, steeply west-dipping, southward terminating, north-northwest-striking normal fault system. This fault zone is related to geothermal activity and extends northwestward from the geothermal well-field (Figure 4.2). Vertical throw across these west-dipping faults typically ranges from ~400-800 m (Figure 4.3).

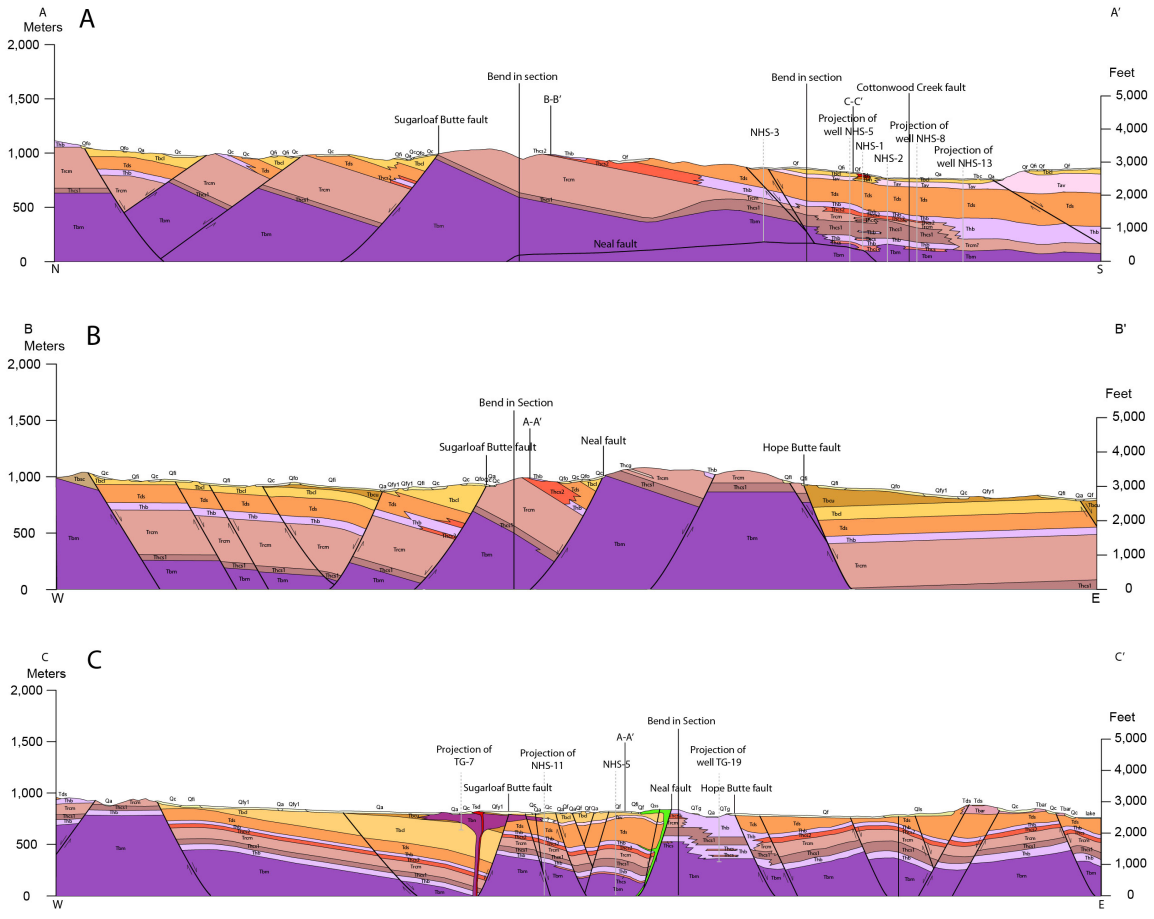

Figure 4.3 – Cross sections of the study area (Plate 1) with no vertical exaggeration. A: Cross-section obliquely cuts across Neal fault zone and extends southward through the well-field. B: Cross-section orthogonal to Neal fault zone, north of well-field. C: Cross-section orthogonal to Neal fault zone through central part of the well-field.

The Neal fault forms the southern and eastern segments of the Neal fault zone (Figures 4.2 and 4.4). It is exposed directly north of the hot springs, with a geometry of

N12°W 57°W, and projects to the western edge of the hot springs and sinter terraces (Figures 4.5 and 4.6), thus suggesting that it channels fluid-flow to the active hot springs. Furthermore, a north-plunging fault intersection between the west-dipping Neal fault and a splay of the east-dipping Hope Butte fault is inferred at the active hot springs. Paleo-sinter drapes silicified Bully Creek Formation rocks ~40 m west of the Neal fault (Figure 4.5E). Abundant silicification and alteration along the Neal fault and proximal to the hot springs provide evidence for the geometry of the Neal fault north and south of its exposure and for its relationship to past and current geothermal flow (Figures 4.5 and 4.6). Chalcedonized Bully Creek Formation rocks exposed across parts of the hillside south and north of the hot springs suggest an older and/or prolonged phase of silicification (Figure 4.6). Epithermal boiling textures, related to an older phase of geothermal activity, are exposed proximal to well pads of NHS-1 and NHS-5, west of the Neal fault and within the step-over (Warren pers. comm., 2013).

The north-northeast-striking, east-dipping Hope Butte fault bounds on the east much of the prominent horst block in the central part of the study area (Figure 4.3B). A relatively deep basin containing upper Bully Creek Formation rocks developed in the hanging wall of the Hope Butte fault. Inferred vertical throw across this fault is ~900 m, with lesser offset to the south (Figures 4.3B,C). The Hope Butte fault is interpreted to splay southward, with the main strand bending southwestward and cutting the horst near Neal Hot Springs (Figure 4.2). East of the Hope Butte fault, broad (~2 km wavelength) anticlinal and synclinal folds suggest a listric geometry to both the Hope Butte and Cottonwood Mountain faults and prominent fault drag along the Hope Butte fault, as evidenced by seismic reflection data and exposed bedding attitudes (Figure 4.3C).

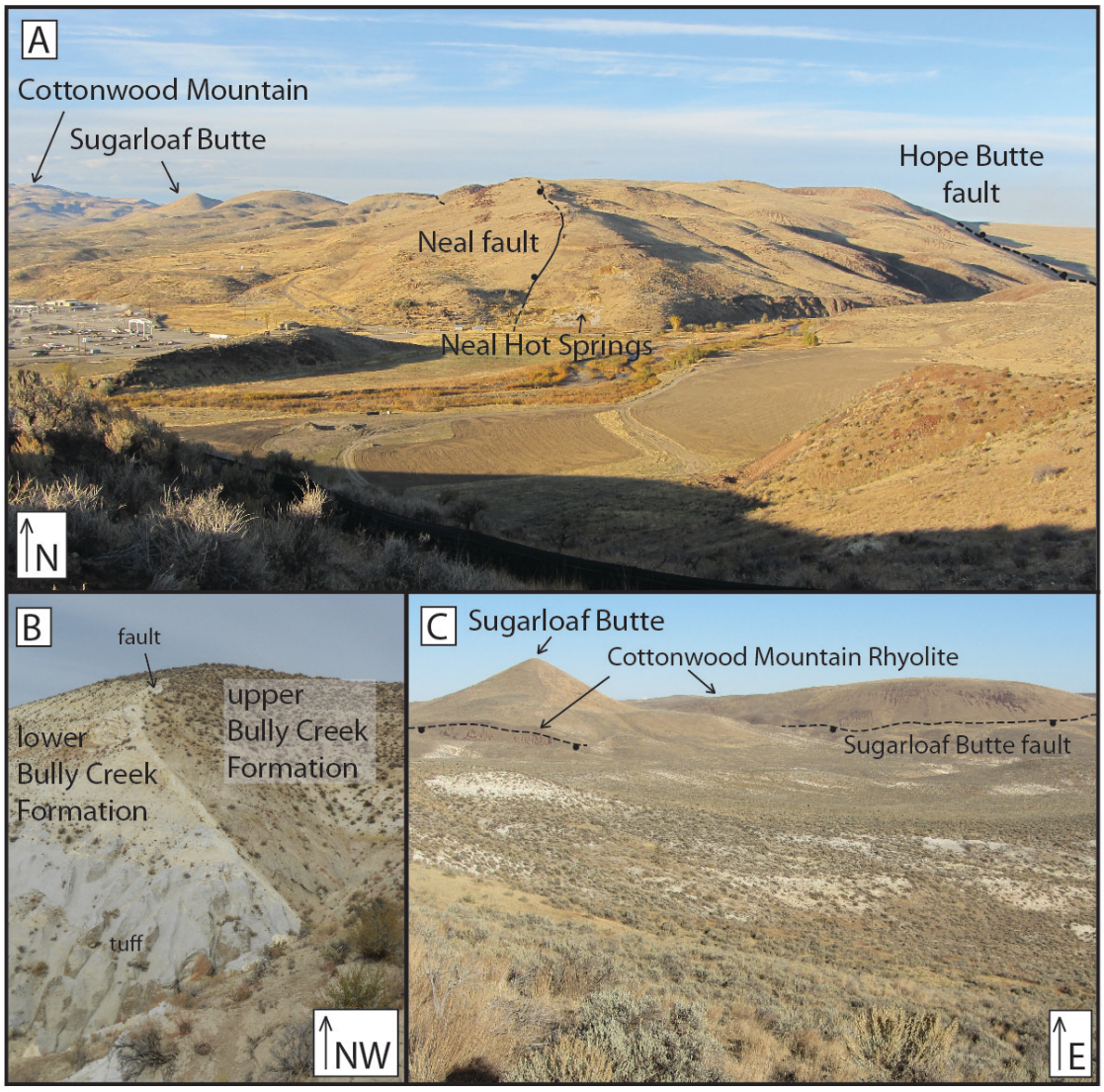

Figure 4.4 – Field photos showing structural and stratigraphic markers. For stratigraphy see Figure 3.2. A) Looking northward at Neal Hot Springs, Neal fault, and Hope Butte fault. B) Major northeast-dipping normal fault juxtaposing lower and upper Bully Creek Formation sedimentary rocks, including a prominent ~10 m thick, gray, aphyric tuff that is conspicuously cut. C) Eastward view of left-stepping Neal fault zone, including the Sugarloaf Butte fault.

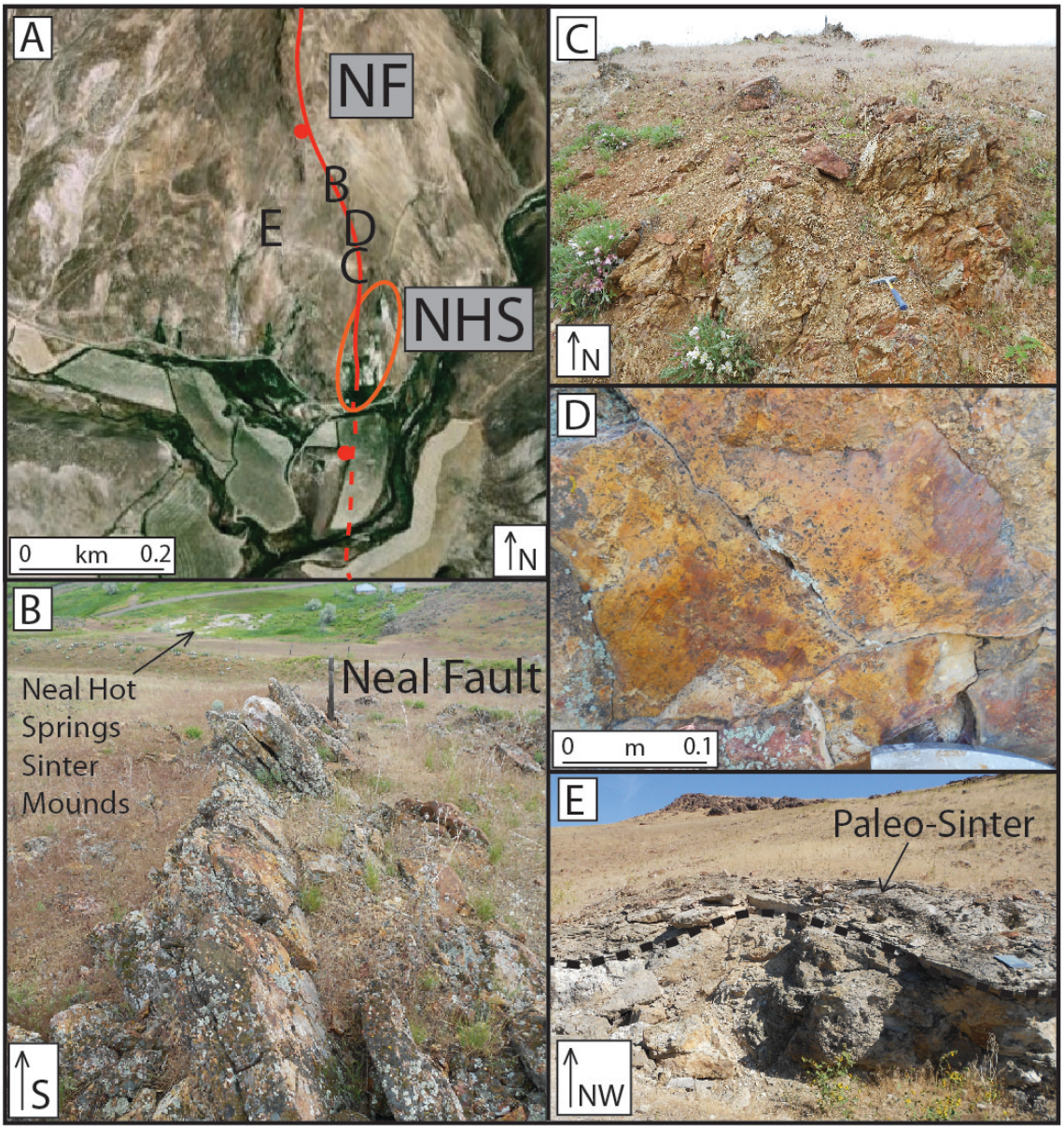

Figure 4.5 – Neal fault and associated geothermal features. A) Google earth image of Neal Hot Springs (NHS-enclosed by red ellipse) and Neal fault (NF-denoted by red line), with letters showing locations of photos. B) Neal fault surface exposure looking southward along strike with hot springs and sinter mounds below. C) Hanging wall damage zone of Neal fault. D) Slickenlines on Neal fault surface. E) Paleo-sinter draping altered and silicified sedimentary rocks of the Bully Creek Formation.

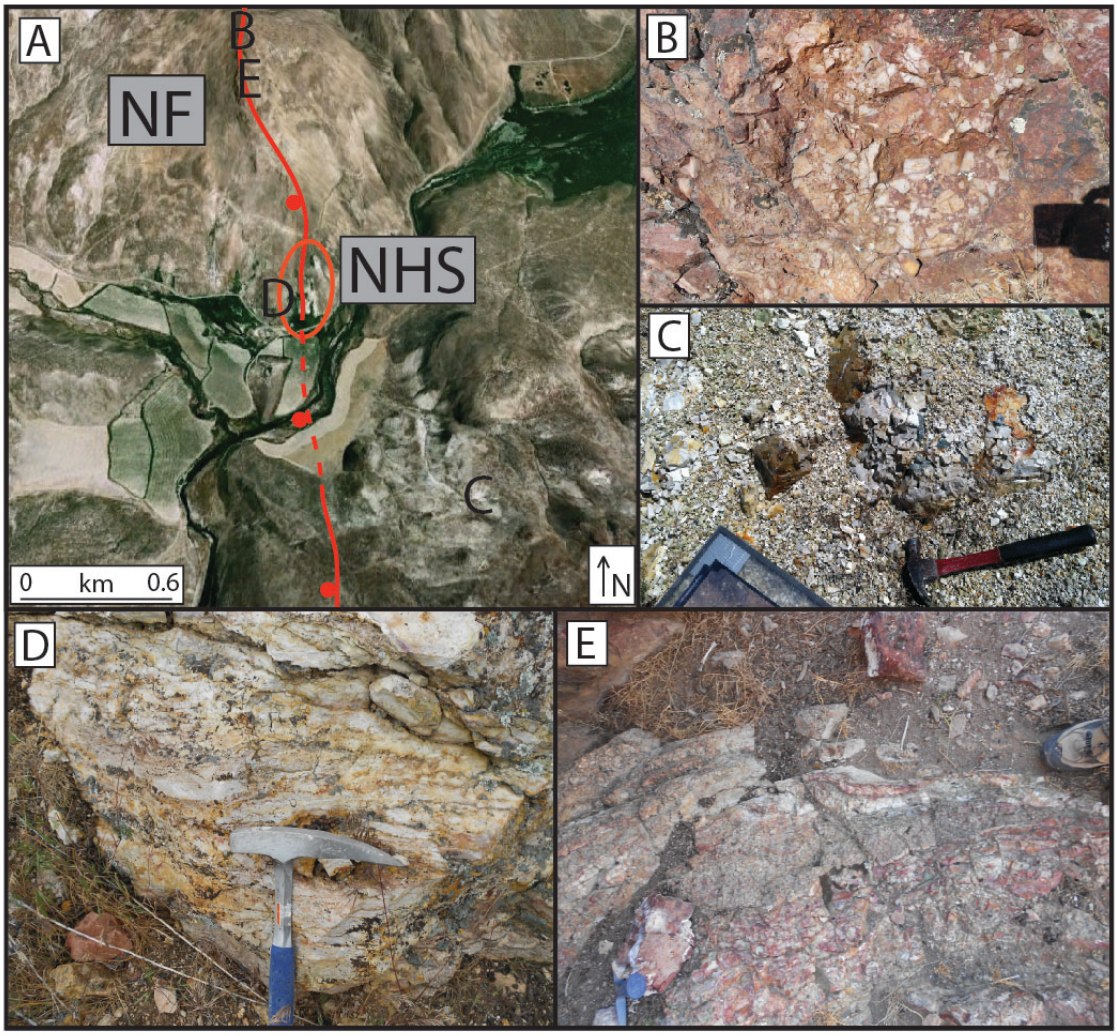

Figure 4.6 – Geothermal features along or proximal to Neal fault and Neal Hot Springs. A) Google earth image of Neal fault (red line) and area near fault, with letters denoting locations of other photos; B) hydrothermally altered breccia, QThbr in Plate 1; C) chalcedony in altered Bully Creek Formation; D) partially silicified sedimentary rocks, with casts of reeds; E) vein of reddish silica.

Much of the 1.5 km wide, main left step-over within the Neal fault zone that includes the well-field is poorly exposed due to Quaternary cover. Geologic mapping, well-field studies (including down-well lithologies, temperature profiles, and lost circulation zones), and integrated geophysical studies (Colwell et al., 2012) helped to infer the overall structural framework and concealed structures in this area. The

temperature anomaly is focused within the step-over and along the Neal fault, as evidenced by a contour plot of down-hole temperature data (Figure 4.7).

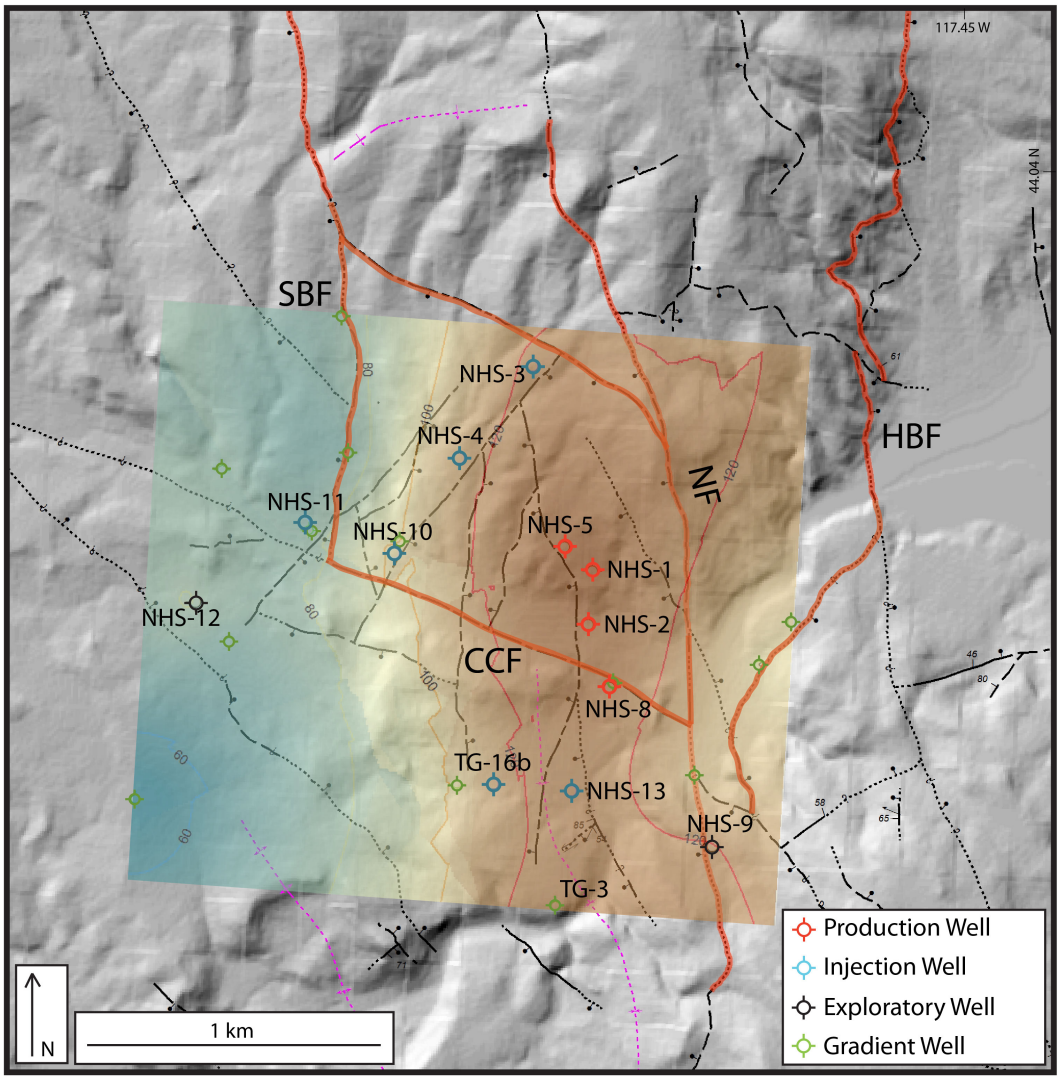

Figure 4.7 – Hillshade digital elevation model of well-field overlain by faults (major faults highlighted in red) and showing maximum down-hole temperatures. Warmer colors represent temperatures up to 142°C and cooler colors down to 80°C (bottom hole temperatures). Production, injection, and exploration wells are labeled.

The main step-over is respectively bounded on its east and west ends by the Neal and Sugarloaf Butte faults, both north- to north-northwest-striking and steeply west-dipping (Figure 4.7). 'Hard-linkage' between these faults is provided by west-northwest-

striking inferred faults, including the Cottonwood Creek fault (Figure 4.7), as evidenced by the linear nature of Cottonwood Creek and gravity modeling (Colwell et al., 2012). Closely spaced, oppositely dipping faults also occupy the step-over and cut across the well field, with interpreted northerly strikes and steep east and west dips (Figure 4.7), as evidenced by seismic reflection and well data. These faults have vertical throw up to 60 m and greater offset down-section. Opposing tilts accommodated by these oppositely dipping faults probably produced the minor synclinal and anticlinal folds within the step-over (Figure 4.3C).

FAULT KINEMATICS

Present-day regional stress field orientations in eastern Oregon are poorly understood, partially due to a dearth of seismologic data, a lack of Holocene fault studies, and limited GPS monitoring. In order to understand the strain history and local stress conditions at Neal, fault geometries and kinematic indicators (slickenlines, rough facets, and Reidel shears) were measured (e.g., Angelier et al., 1985; Gauthier and Angelier, 1985; Petit, 1987). Approximately 49 measurements of 44 faults were acquired, with 19 measurements providing both slip direction and sense-of-slip data (Figure 4.8A). Normal separation characterizes nearly all mapped faults. Kinematic data indicate generally west- and east-trending slip directions on most major and minor northerly-striking faults (Figure 4.8B). However, some north-northwest-striking faults accommodated sinistral-normal slip and north-south- to north-northeast-trending slip directions (Figure 4.8C).

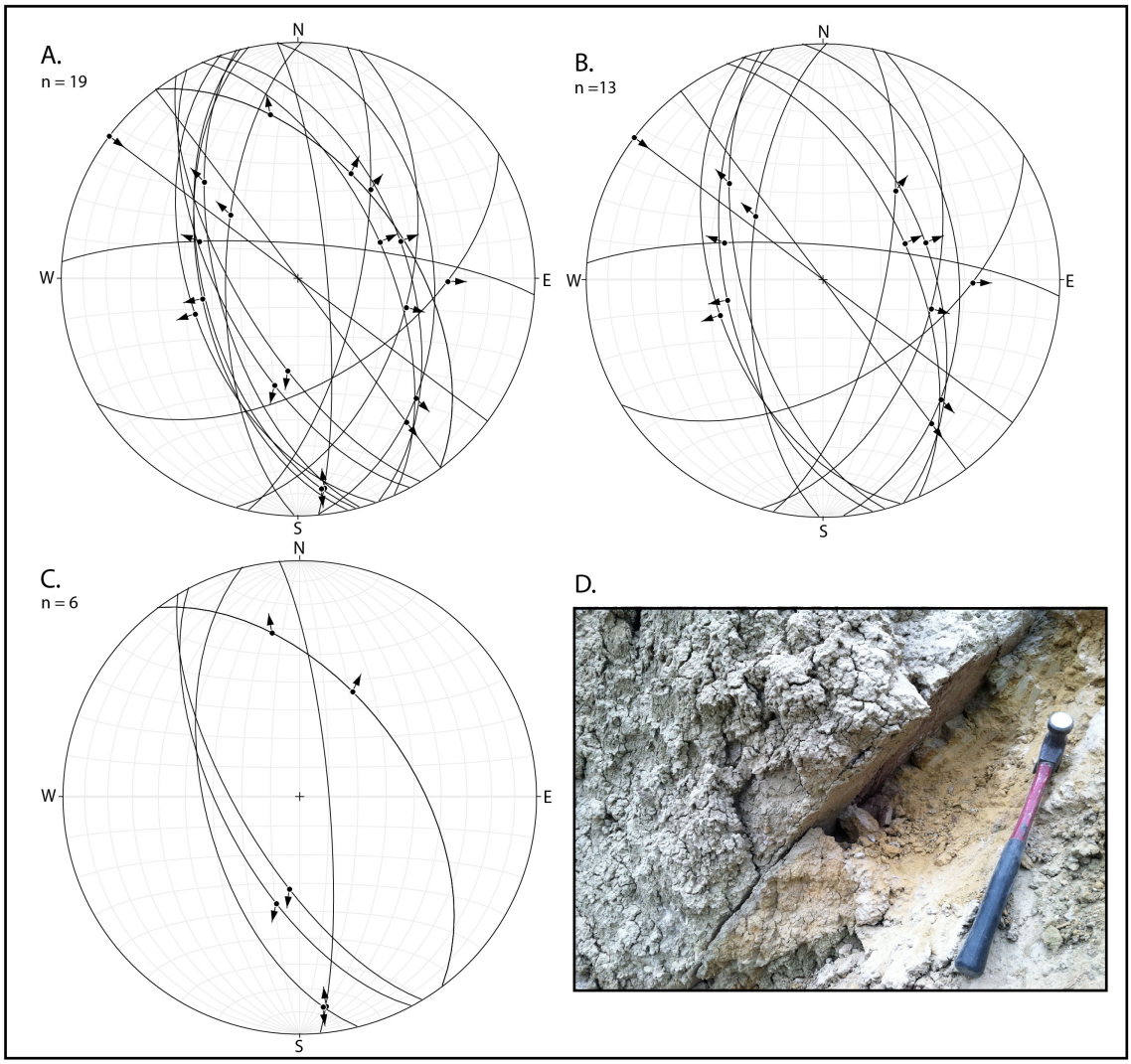

Figure 4.8 – Lower-hemisphere, equal area stereographic projections of fault planes (great circles) and slip vectors (arrows), as measured on exposed fault planes and deduced from kinematic indicators (e.g., slickenlines, rough facets, and Riedel shears). A. All fault measurements. B. Faults indicating west-east-trending slip direction. C. Faults indicating north-south-trending slip direction. D. Representative fault surface. n = number of measurements.

STRAIN AND STRESS FIELD ANALYSIS

Kinematic fault-slip analysis at Neal is contingent upon many factors, including both the quality and accuracy of field measurements and several assumptions regarding local deformation. These assumptions include: 1) fault kinematics are scale-invariant; 2) 2) folding and tilting of strata are syntectonic; 3) faults have not been rotated about a

vertical axis; 4) faults sampled and measured are representative of stress and strain across the study area; and 5) strain is homogeneous across the study area (e.g., Marrett and Allmendinger, 1990). The latter was qualitatively assessed by comparing fault kinematics across different portions of the study area.

Principal extension and shortening axes were determined for each fault to identify kinematic consistencies and heterogeneities within the slip data (e.g., Marrett and Allmendinger, 1990) using the computer program FaultKin 5.6.1 of Allmendinger et al. (2012). Heterogeneous fault sets were separated into homogeneous data (Marrett and Allmendinger, 1990). Linked Bingham statistics of the shortening and extension axes characterize the orientation of the strain ellipse at Neal, with the longest, intermediate, and shortest axes of the strain ellipse displayed and illustrated as epsilon 1, epsilon 2, and epsilon 3 (Figure 4.9) (Allmendinger et al., 2012). Using the computer program Tectonics FP 1.5 of Reiter and Acs (1999), direct inversion (Angelier, 1979) of the kinematic data was performed (Figure 4.9). At Neal, maximum strain (epsilon 1) and least principal stress (sigma 3) are subparallel, suggesting that deformation and the local stress field are directly linked.

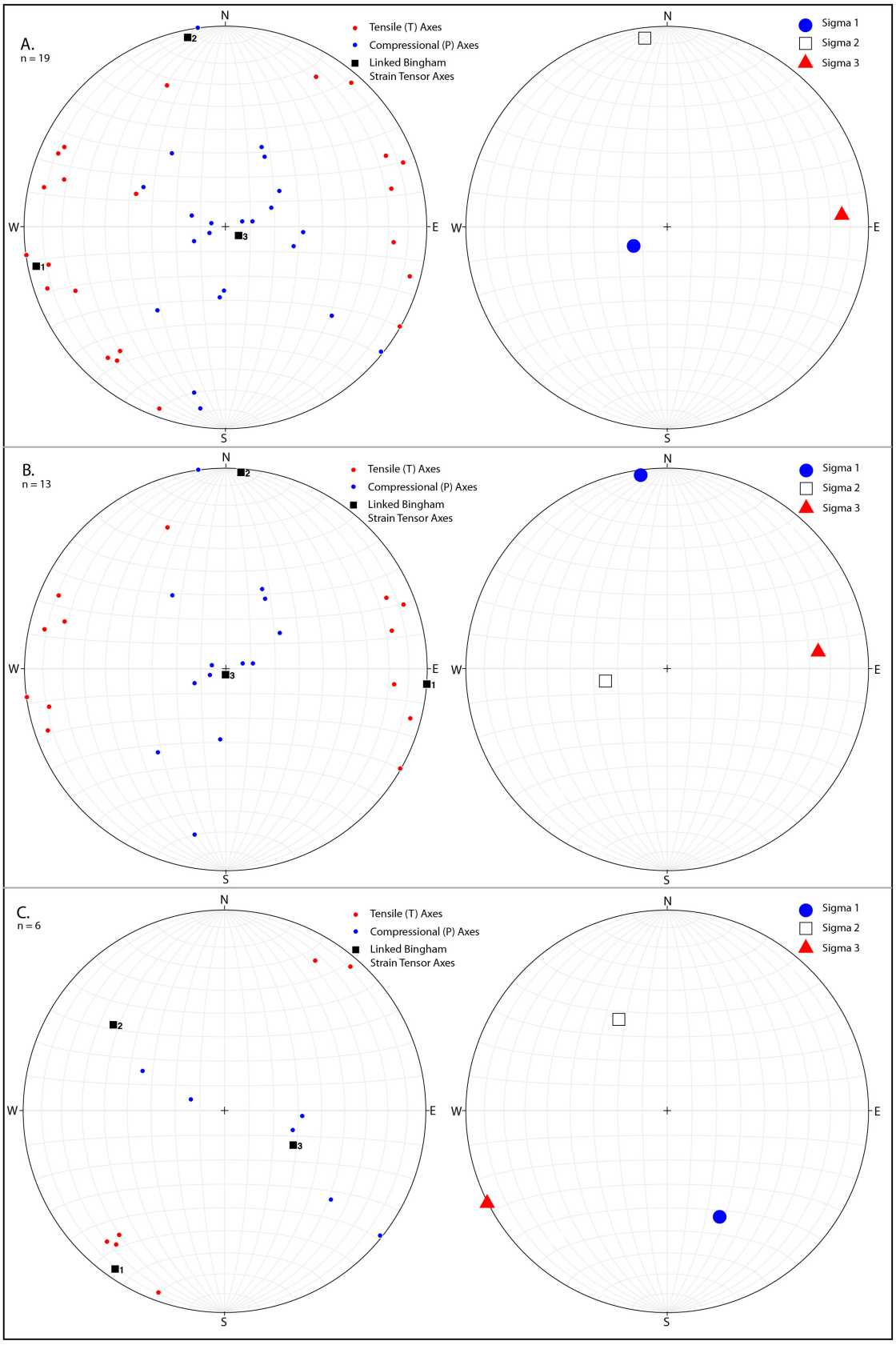
A.
n = 19
Tensile (T) Axes
Compressional (P) Axes
Linked Bingham
Strain Tensor Axes
Sigma 1
Sigma 2
Sigma 3
B.
n = 13
Tensile (T) Axes
Compressional (P) Axes
Linked Bingham
Strain Tensor Axes
Sigma 1
Sigma 2
Sigma 3
C.
n = 6
Tensile (T) Axes
Compressional (P) Axes
Linked Bingham
Strain Tensor Axes
Sigma 1
Sigma 2
Sigma 3
N
S
E
W

Figure 4.9 – Lower-hemisphere, equal area stereographic projections of P-compressional (blue dots) and T-tensile (red dots) axes, calculated linked Bingham strain axes (black squares), and average principal stress orientations (sigma 1: blue circle; sigma 2: square; sigma 3: red triangle) derived from kinematic data. A. All faults indicating west-trending (~260°) extension axis and least principal stress. B. Main fault population indicating west-trending extension axis and least principal stress. C. Fault subpopulation suggesting a southwest-trending extension axis and least principal stress. n = number of measurements.

Kinematic data from the main population of faults indicate an east-west-trending extension axis and a least principal stress orientation of ~085° (Figure 4.9B). This orientation is orthogonal to the northerly-striking faults throughout the study area and suggests primarily normal slip. Kinematic data from a subpopulation of faults suggest a southwest-northeast-trending extension axis, with a least principal stress orientation of ~243° (Figure 4.9C). This orientation is oblique to the northerly-striking faults and north-northwest-striking Neal fault zone, suggesting a sinistral component of deformation on the northerly striking faults. Southwest-directed extension at Neal is subparallel to the interpreted active regional least principal stress of the western Snake River Plain.

Multi-modal distribution of stress-strain axes at Neal can result from several mechanisms, including triaxial deformation, preexisting anisotropies and fault reactivation, strain compatibility, and/or multiple episodes of deformation (Marrett and Allmendinger, 1990). Multiple episodes of deformation and fault reactivation are compatible with the regional framework of eastern Oregon, but full resolution of the distribution of stress-strain axes hinges upon the collection of more fault-slip data.

GEOPHYSICAL CONSTRAINTS

Geophysical investigations by Boise State University at Neal Hot Springs have provided detailed information on fault location and geometry, as well as the presence of geothermal waters (Colwell et al., 2012). Datasets were acquired during the 2011 Neal

Hot Springs geophysics field camp conducted by Boise State University and Colorado School of Mines and as part of the 2012 National Geothermal Student Competition sponsored by the Department of Energy. Data were also collected separately by Clinton Colwell of Boise State University. Previously acquired data at Neal include gravity, as provided by U.S. Geothermal.

Local Gravity

U.S. Geothermal collected local gravity data in a grid with roughly 300 m spacing between stations. They first tied the data to absolute gravity at a nearby benchmark reduced to a Bouguer anomaly with a 2.20 $\frac{\boldsymbol{kg}}{\boldsymbol{m^3}}$ Bouguer slab density and gridded at a 300 m grid-cell size (Colwell et al., 2012). Trials of data reduction using the horizontal gradient method and total gradient method are described by Colwell et al. (2012). If the results from the horizontal and total gradient methods are overlain, dip direction on the faults can be obtained (Figure 4.10) (Sheriff, 2010; Colwell et al., 2012).

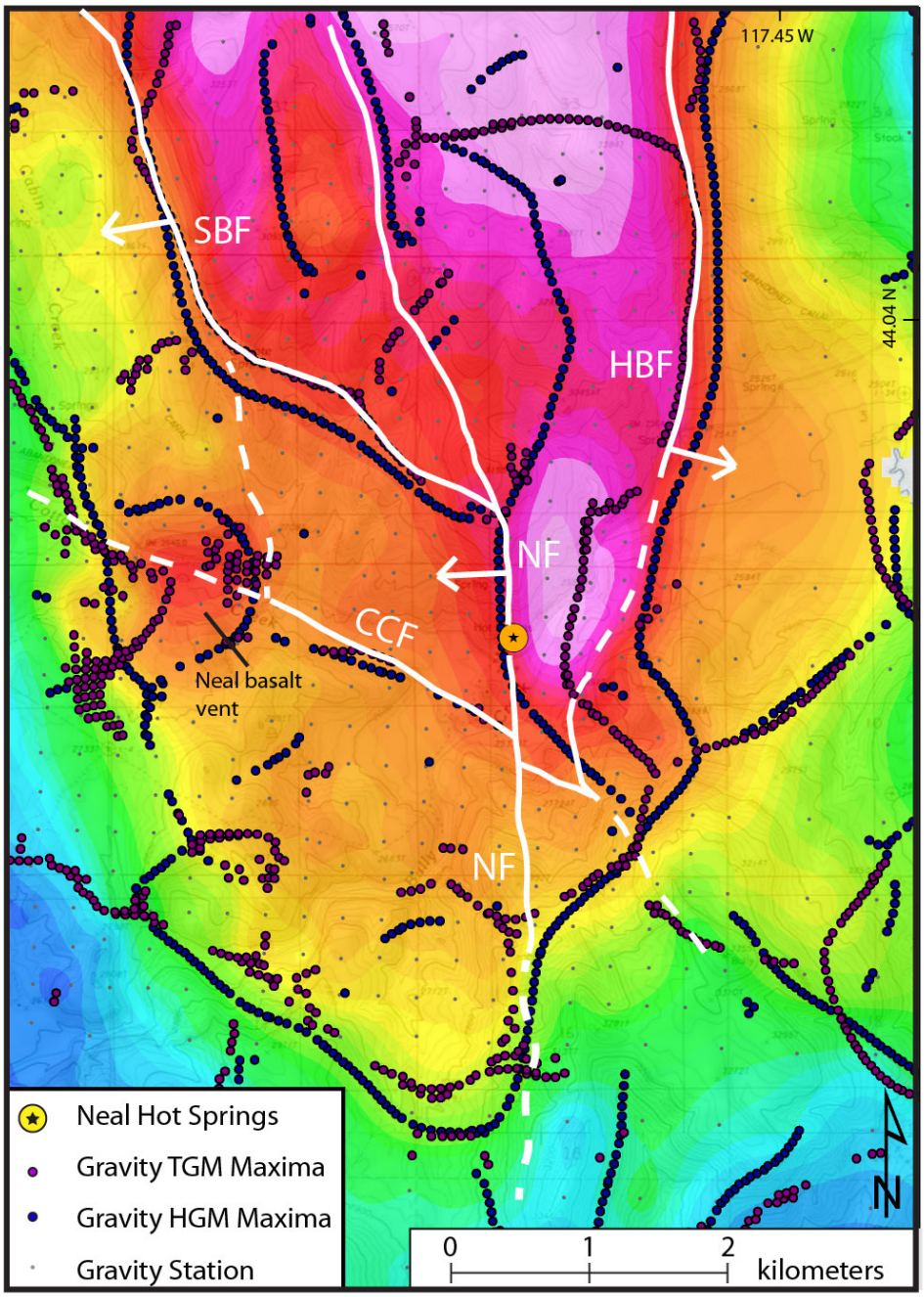

Figure 4.10 - Local gravity map of Neal Hot Springs. Figure modified from Colwell et al. (2012). Faults interpreted from the horizontal gradient method and total gradient method are highlighted (white lines) along with the associated dip direction obtained from assuming that total gradient method maxima lie up dip from horizontal gradient method maxima (white arrows). Fault names same as in Figure 4.2. Warmer colors denote higher gravity anomaly, cooler colors denote lower.

From this analysis, several faults can be interpreted, including the Sugarloaf Butte, Hope Butte, Cottonwood Creek, and Neal faults (Colwell et al., 2012). For example, the Neal fault, which accommodates geothermal production, is shown as a west-dipping, north-northwest striking fault (Colwell et al., 2012). The poorly exposed Cottonwood Creek fault can also be modeled from the gravity data as a west-northwest-striking subvertical fault (Colwell et al., 2012). The well-defined step-over in the gravity data and sharp gravity contrasts across major faults (e.g., Sugarloaf Butte and Hope Butte faults) and Neal basalt vent are noteworthy (Figure 4.10).

Seismic Reflection Imaging

Seismic reflection surveys were conducted during the 2011 summer geophysical field camp by the Colorado School of Mines and Boise State University (Figure 4.11). Seismic velocity and density contrasts at Neal allowed seismic imaging at different scales: vibrator trucks for lower frequencies, and a hammer seismic truck for higher frequencies.

Two 20-ton Veritas Vibroseis© trucks along with a Sercel 120-channel recording system for a cable having a group spacing of 30 m produced an image of the upper 1 km of the subsurface. The line was processed using standard seismic processing flows, including post-stack migration and depth conversion (Colwell et al., 2012).

The vibrator line is a west-east transect across the well-field and eastern portion of the study area. The vibrator line provided useful data for the eastern portion of the study area, crossing and imaging both the Hope Butte and Cottonwood Mountain faults, while the vibrator line west of the Hope Butte fault provided poor data. Reflectors near

major faults reveal prominent drag features. In general, reflectors also have attitudes similar to those of exposed strata at the surface (Figure 4.12).

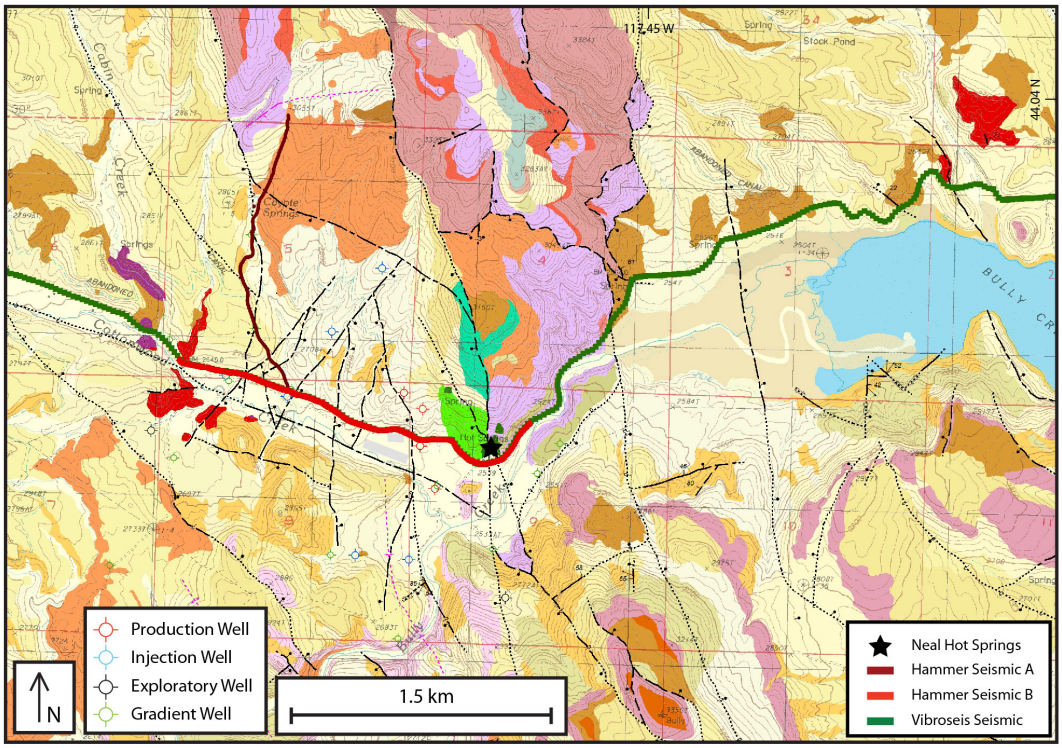

Figure 4.11 – Location map for seismic surveys (Colwell et al., 2012).

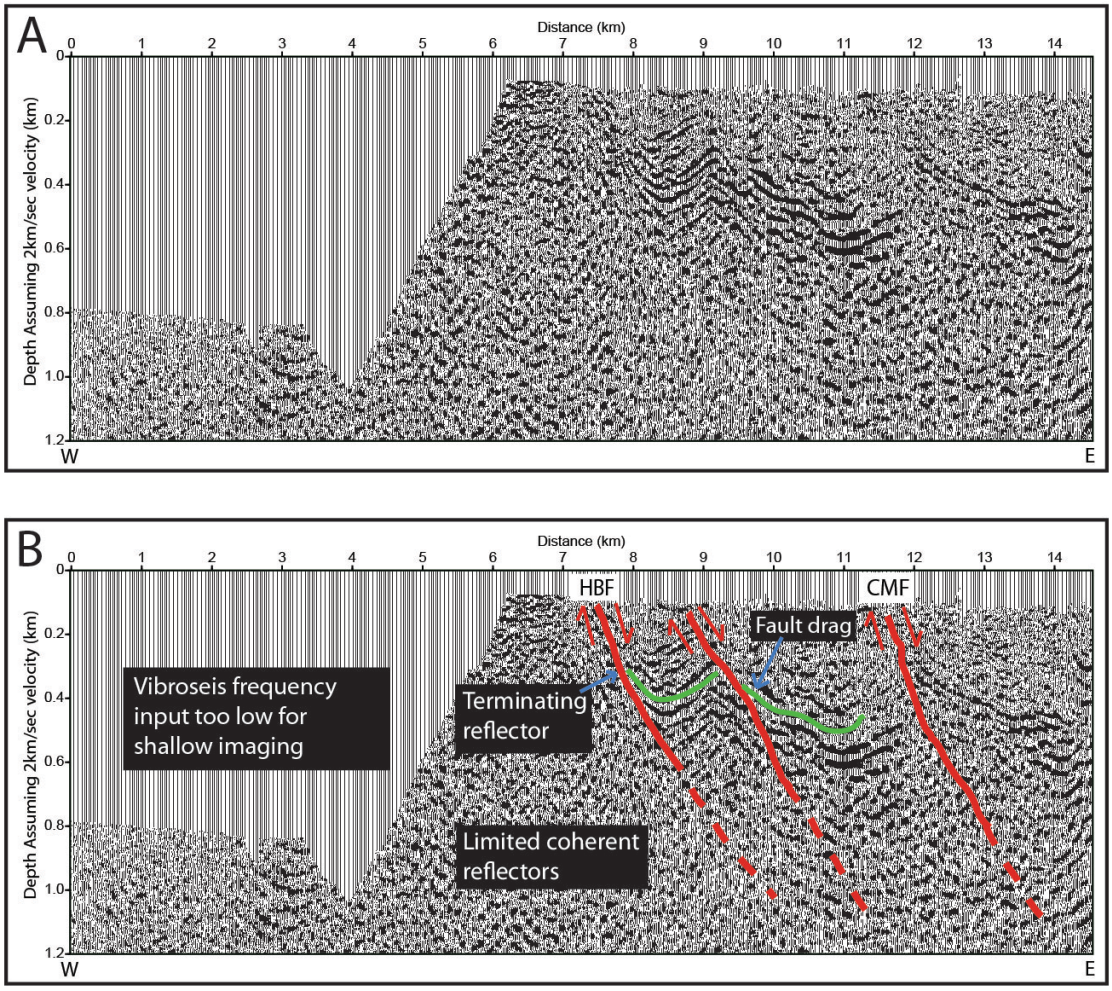

Figure 4.12 – Migrated west-east vibrator section from west of Neal Hot Springs to the eastern end of the study area, crossing both the Hope Butte fault (HBF) and Cottonwood Mountain fault splay (CMF) (see Figure 4.11). Red lines denote interpreted faults. Vertical exaggeration about 8x. Seismic image provided by Colwell et al. (2012). A. Uninterpreted. B. Interpreted.

The resolution of seismic reflection surveys is limited by the frequency input of the seismic impulse. Large vibrator trucks are limited to lower frequencies. A 50 kg hammer seismic source yielded higher frequencies (Figures 4.13 & 4.14). The two higher-resolution, shallow seismic lines were acquired with 96 active channels at a geophone spacing of 5 m, imaging the shallow subsurface west of the Neal fault (Colwell et al., 2012).

Hammer-seismic line A is a north-south transect across the western end of the well-field (Figure 4.13). Coherent southward-dipping reflectors are imaged along with several interpreted faults, including the Sugarloaf Butte fault, in off-line sideswipe or apparent dip. Another possible interpretation is that the southward dipping reflectors result from southward-increasing displacement along the Neal fault.

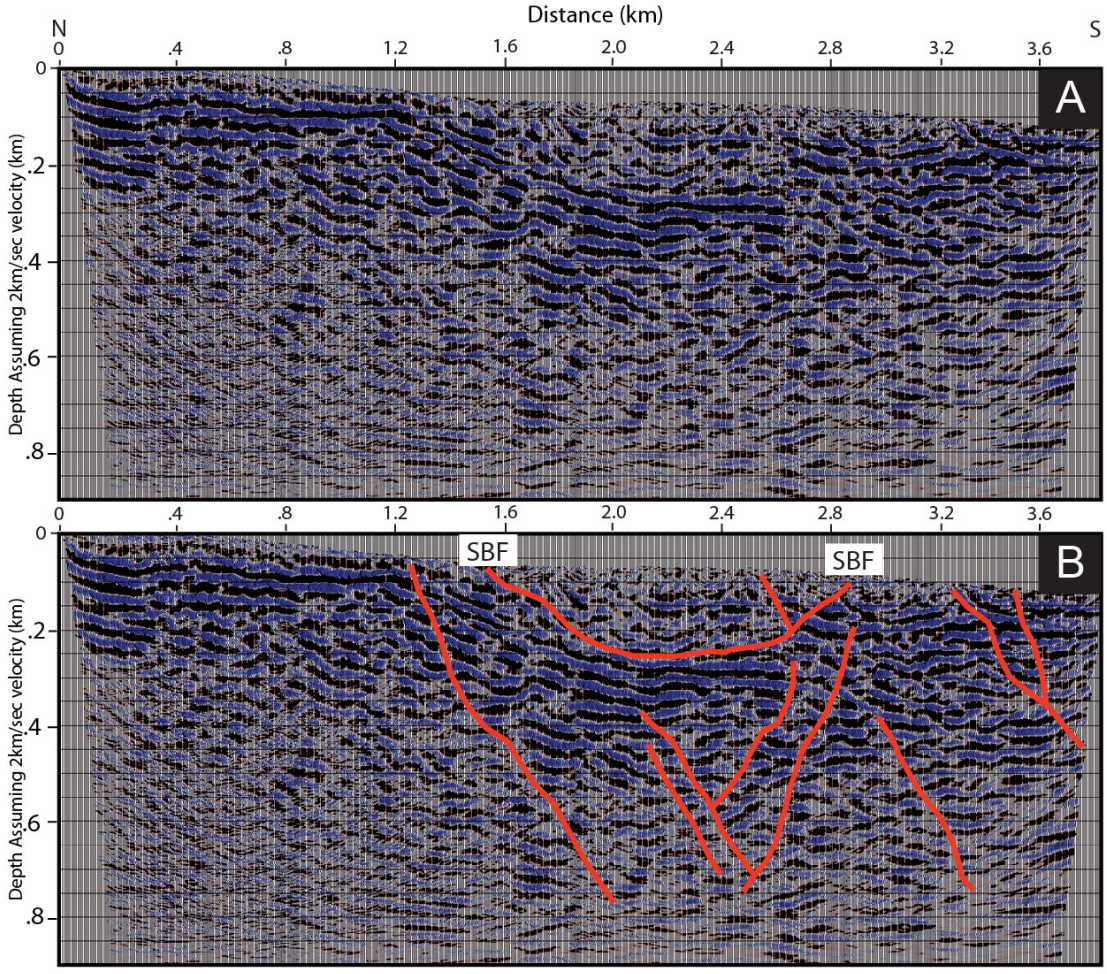

Figure 4.13 – Migrated hammer-seismic section A. A north-south transect across the western end of the well-field (see Figure 4.11). Red lines denote interpreted faults. Sugarloaf Butte fault is SBF. Vertical exaggeration is about 2x. Seismic image provided by Colwell et al. (2012). A. Uninterpreted. B. Interpreted.

Hammer-seismic line B (Figure 4.14) images the Neal fault, dipping ~60° west, and the Sugarloaf Butte fault at the western end of the step-over. More importantly, it

images the subsurface of the largely covered (extensively by fans) step-over and the well field, including a series of closely spaced, east- and west-dipping faults. Wells NHS-10, NHS-11, and TG-16b intersected moderately high permeable zones within this area.

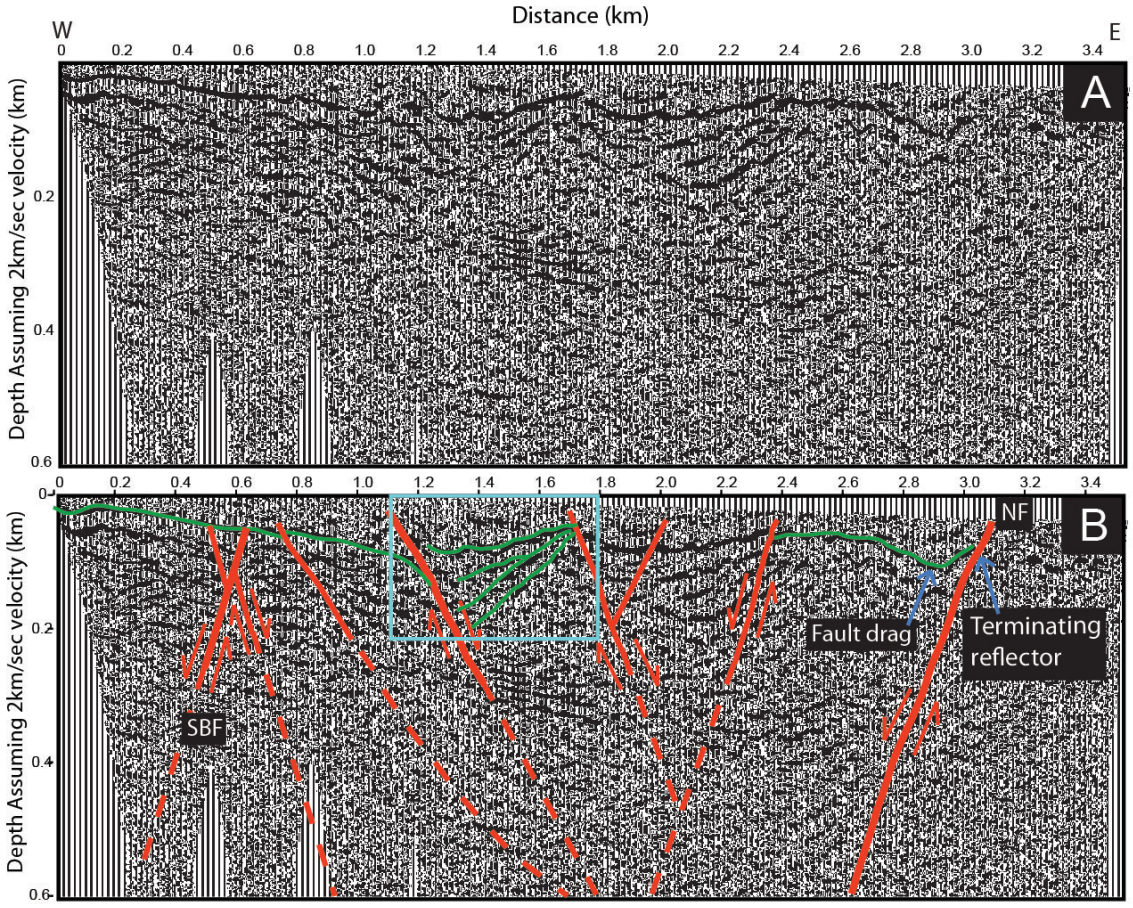

Figure 4.14 – Migrated hammer seismic section B. Hammer seismic section B is a west-east transect across the well-field, from west of Sugarloaf Butte fault (SBF) to east of Neal fault (NF) (see Figure 4.11). Red lines denote interpreted faults. Blue box outlines steepening dips of reflections from basin stratigraphy, highlighted with green lines. Vertical exaggeration about 2x. Seismic image provided by Colwell et al. (2012). A. Uninterpreted. B. Interpreted.

5. Discussion

TIMING OF DEFORMATION

Geochemical and stratigraphic correlations and structural data from this study, as well as existing geochronology in the region (Lees, 1994; Hooper et al., 2002a), place

constraints on the timing of Neogene deformation in the Neal geothermal area. Extension began in the middle Miocene and has continued episodically to the present.

The first major episode of Neogene deformation in the Neal area probably began in the middle Miocene, as evidenced by large thickness variations in the ~15-16 Ma Cottonwood Mountain Rhyolite (Trcm) and ~15.8 Ma Hunter Creek Basalt (Thb). These units vary from tens to >100 m in thickness. Some of the thickness variations probably result from deposition in paleocanyons or paleovalleys or proximity to local volcanic centers, especially for the more viscous rhyolite lavas. However, thickness variations as observed in well logs within the geothermal field demonstrate that both of these volcanic sequences and intercalated volcaniclastic rocks thicken and thin near inferred normal faults. Furthermore, vertical throw across faults increases down-section. These relations suggest that deposition of the Hog Creek Formation was partially fault controlled, and thus extension had begun by ~15-16 Ma in the Neal area.

Middle Miocene extension within eastern Oregon induced development of the Oregon-Idaho graben (Cummings et al., 2000). Northerly-striking faults along the margins of and within the graben controlled thicknesses of coeval rhyolite and basalt (Cummings et al., 2000). Thus, the earliest deformation at Neal, as recorded in the Hog Creek Formation, was probably related to the formation and initial subsidence of the Oregon-Idaho graben.

Thickness variations of the overlying Drip Springs Formation (~15-10 Ma) indicate that extension continued in the Neal area through middle to late Miocene time. The Drip Springs Formation thickens proximal to half-graben bounding and intra-graben faults, including the Sugarloaf Butte, Hope Butte, and Neal faults (Figure 4.3C). Growth

faulting is also evident in the Drip Springs Formation, with steepening seismic reflectors down section proximal to an interpreted east-dipping, intra-graben fault (Figure 4.17). This suggests that deposition of the Drip Springs Formation was coeval with continuing extension at Neal.

Middle to late Miocene extension is documented south of Neal within the Oregon-Idaho graben, where several northerly striking intra-graben fault zones control thicknesses of middle Miocene basin-fill sedimentary rocks (Cummings et al., 2000). Thus, it is hypothesized that middle to late Miocene deformation at Neal represents continued development of the Oregon-Idaho graben.

Deformation continued at Neal, from late Miocene to present, along northerly-striking faults, including the Sugarloaf Butte, Neal, and Hope Butte faults. The Reservoir basaltic andesite (~12 Ma), Vines Hill andesite (~11.5-10 Ma), upper and lower Bully Creek Formation (~10-7 Ma), and Quaternary sediments are faulted and offset across the study area. The Bully Creek Formation thickens proximal to half-graben bounding faults, such as the Sugarloaf Butte and Neal faults, suggesting concurrent extension and deposition (Figure 4.3). Relative tilts lessen up-section, from gentle to moderate tilts in the lower Bully Creek Formation (~5-25°) to consistently gentle tilts in the upper Bully Creek Formation (0-10°) (Figure 4.1). The Sugarloaf Butte, Hope Butte, and Neal faults cut Quaternary fans, and the Neal fault serves as a conduit for geothermal fluid ascent suggesting recent (likely Holocene) deformation. Furthermore, recently detected seismicity (<2.0 magnitude) nearby (<4 km), via a passive seismic network assembled at Neal and monitored by Boise State University (Colwell pers. comm., 2012), suggests proximal Holocene deformation.

Late Miocene to present deformation in the region has been documented within the western Snake River Plain, along the Vale fault zone, and along the Olympic-Wallowa-lineament and its associated fault zones to the east, southeast, and northeast of Neal, respectively. Initial subsidence occurred within the western Snake River Plain ~11 Ma, with continued deformation to the present (Wood and Clemens, 2002). Historical seismicity has occurred along the Olympic-Wallowa-lineament and associated fault zones, including the north-striking Long Valley fault system (Figure 2.2) (Mann and Meyers, 1993). South of Neal, the northwest-striking Adrian fault zone, an extension of the western Snake River Plain, cross-cuts older north-striking faults of the Oregon-Idaho graben (Figure 2.4) (Ferns et al., 1993). The Neal fault zone strikes north-northwest, including the Sugarloaf Butte and Neal faults, and parallels the northwest-striking Vale fault zone (locally the Cottonwood Mountain fault zone) and associated fault zones of the Olympic-Wallowa-lineament, suggesting similar and related recent deformation across the region.

STRUCTURAL CONTROLS ON GEOTHERMAL ACTIVITY

Successful drilling efforts (in terms of permeability and temperature) have all penetrated the Neal fault (four production wells and three injection wells) or been limited to the step-over within the Neal fault zone (three injection wells). Wells drilled west and east of the step-over have also encountered high temperatures but with little to no permeability (preliminary results of flow testing at NHS-9 is needed to confirm this) (U.S. Geothermal, pers. comm., 2013). Thus, the locus of the geothermal system clearly occupies the step-over within the Neal fault zone, particularly the eastern part of the step-

over along the Neal fault. Furthermore, a north-plunging fault intersection between the west-dipping Neal fault and a splay of the east-dipping Hope Butte fault is inferred at Neal Hot Springs, likely controlling the location of the sinter terraces and active hot springs (Figure 5.1).

Surface traces and three point solutions (Warren, pers. comm., 2012) based on lost circulation zones encountered in several wells (NH-3, NHS-4, NHS-1, NHS-5, NHS-2, NHS-8, and NHS-13) indicate that the Neal fault strikes ~N0^{o}-N30^{o}W and dips 57-65^{o}W. It is important to note that the surface trace of the southern part of the fault strikes more northerly (~N0^{o}W) as compared to the fractures accommodating the maximum fluid flow in the area (~N25-30^{o}W). This may indicate that fault splays striking north-northwest are more dilatant and thus more conducive to channeling fluids than more northerly striking fractures within the fault zone.

An important question is how far south does the Neal fault extend. Prominent fault drag, with steeply west-dipping foliations within the Vines Hill andesite, is observed along the western edge of the prominent ridge directly south of the hot springs. However, a high gravity gradient is not observed that far south, but rather ends just south of the confluence of Cottonwood and Bully Creeks (Figure 4.10), suggesting that the Neal fault loses significant displacement in that vicinity. Only low permeability was intersected in TG-3 (Figure 4.5), either because the 1352 m deep well was not drilled deep enough to intersect the Neal fault or the Neal fault does not extend that far south. The Neal fault is likely losing displacement and thus horse-tailing to the south of Bully Creek. The prominent drag-folding observed in this area may be indicative of a southward terminating fault. Multiple splays associated with the horse-tailing southern end of the

Neal fault may increase fracture density and therefore permeability directly south of Bully Creek, which may account for moderately high permeability intersected in TG-16b (Figure 4.5).

Within the step-over production and injection wells intersected low to high permeability at various depths. These lost circulation zones represent permeability hosted in multiple fractured pathways and illustrate the high fracture density within the step-over.

Imaged fractures, including fractures hosting the highest permeability and thus supporting production and injection, in NHS-8 and NHS-13, strike north-northwest (Warren, pers. comm., 2013). Considering that the stress field determinations derived from kinematic data suggest both west-trending (~265^{o}) and southwest-trending (~243^{o}) least principle stresses, the highest permeability along the north-northwest-striking fractures implies that the southwest-trending least principle stress is active today, as it would provide greater dilatency on north-northwest-striking fractures. Furthermore, a north-striking fracture hosting lesser permeability has also been imaged in well NHS-13 (Warren, pers. comm., 2013), suggesting lesser dilatancy along north-striking fractures.

With present-day southwest-directed extension, the left step-over within the north- to north-northwest-striking Neal fault zone can be modeled as a small pull-apart basin. Southwest-directed extension suggests a left-lateral strike-slip component on northerly striking faults. The left step within the northerly striking Neal fault zone would therefore accommodate a greater component of extension and thus serve as small pull-apart zone (Figure 5.1) (Mann et al., 1983). This model would account for greater fluid flow on north-northwest-striking splays of the Neal fault and possibly for good

permeability on the inferred Cottonwood Creek fault. The model is also compatible with surface features observed in the area, including an exposure of the Neal fault, where kinematic indicators suggest both normal and sinistral slip.

Other splays of the Neal fault zone have controlled nearby geothermal and volcanic activity outside of the active geothermal system. Sugarloaf Butte, ~5 km northwest of the geothermal field, is a completely silicified and replaced, erosionally resistant hill with a conspicuous conical shape. This butte was formed as sedimentary rocks in the Bully Creek or Drip Springs Formation were flooded by silica-rich fluids. This butte lies within a prominent left-step of the Neal fault zone (Figures 3.1 and 4.1), suggesting possible southeastward migration of geothermal activity through time. This migration could reflect a southward propagation of the Neal fault zone. Furthermore, both the Neal basalt vent and overlying dacite scoria lie along the concealed southern tip of the Sugarloaf Butte fault at the western end of the left step-over, suggesting fault control of volcanic activity as well.

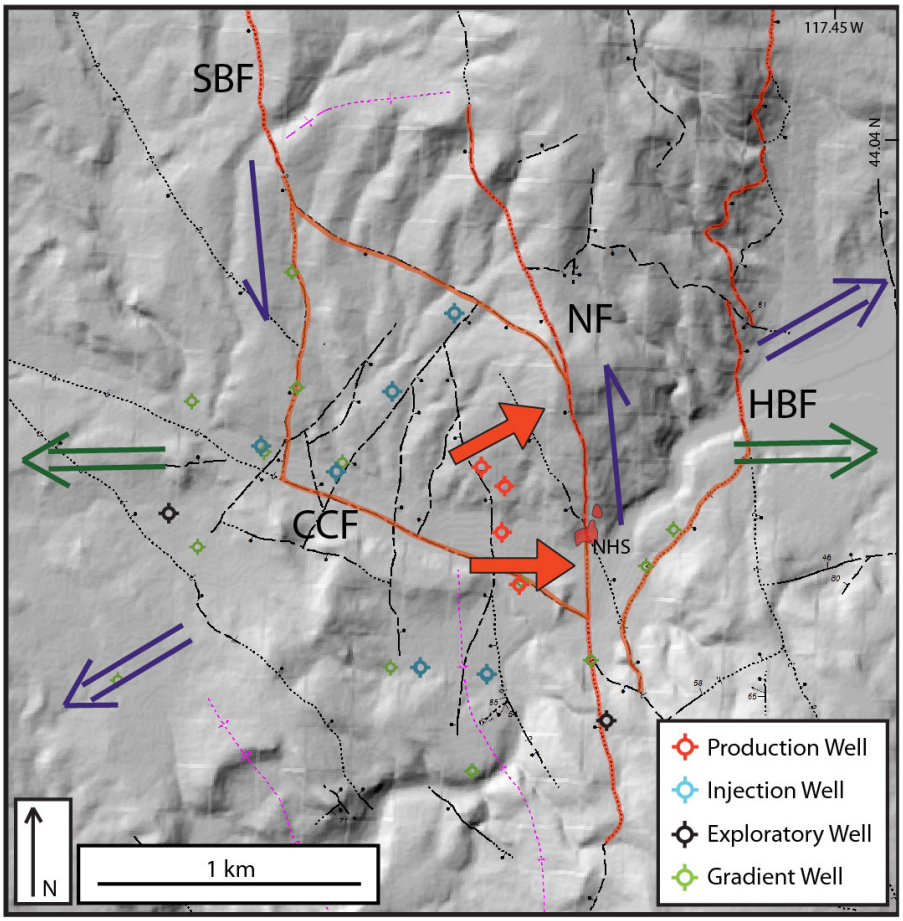

Figure 5.1 – Conceptual structural model of Neal fault zone and geothermal flow. Double lined green arrows represent inferred older, west-northwest directed extension; double lined purple arrows represent inferred younger, southwest directed extension; half purple arrows represent left-lateral motion; red solid arrows represent inferred geothermal upflow. CCF – Cottonwood Creek fault, HBF – Hope Butte fault, NF – Neal fault, NHS – Neal Hot Springs, SBF – Sugarloaf Butte fault.

GEOTHERMAL SYSTEM ANALOGS

Hot-spring type epithermal precious-metal prospects, silica- and carbonate-flooded, erosionally resistant buttes, and active hot springs are prevalent across eastern Oregon. Two broad structural groups can be recognized: 1) those formed along northerly-striking, Oregon-Idaho intra-graben fault zones (e.g., Quartz Mountain) and 2) those found proximal to or along northwest- to north-northwest-striking faults and fault zones,

such as the Adrian and Vale fault zones (e.g., Chalk Butte). Furthermore, two distinct periods of hot-spring activity are recognized: 1) older systems (e.g., Mahogony Mountain), which are hosted by middle Miocene arkosic sandstones and conglomerates (equivalent in age to the Drip Springs Formation), and 2) younger systems (e.g., Shell Rock Butte), which are hosted by upper Miocene-Pliocene tuffaceous siltstones and sandstones (equivalent in age to the Bully Creek Formation and Idaho Group) (Cummings et al., 2000; Gilbert, 1988).

Large geothermal systems developed within the Oregon-Idaho graben during intra-graben subsidence along northerly-striking fault zones, forming hot-spring type epithermal prospects. Bedded sinter, hydrothermal breccias, and exhalative chert indicate either subaerial or subaqueous hot-spring activity (Cummings et al., 2000). The Red Butte, Quartz Mountain, Katie, Grassy Mountain, and Mahogany Mountain precious-metal prospects are all hosted in middle Miocene sedimentary rocks and are related to northerly-striking intra-graben fault zones (Evans, 1986; Gilbert, 1988; Ferns and Ramp, 1989; Ferns et al., 1993; Rytuba and Vander Meulen, 1991).

Following the cessation of the Oregon-Idaho graben, geothermal systems developed within the Adrian and Vale fault zones (Figure 2.4). Prominent buttes mark remnant geothermal activity and are characterized by resistant caps of commonly red- and yellow-weathering, densely indurated sandstone and conglomerate, as at Vale and Rhinehart Buttes (Brown, 1982). The capping sediments were flooded by silica- and/or carbonate-rich fluids and form resistant outcrops that weather into blocky talus (Ferns, 1990). Several of these prominent buttes are gold prospects, including Shell Rock Butte, Chalk Butte, Deer Butte, Mitchell Butte, Sagebrush gulch, and Mahogony Mountain

(Ferns, 1990; Ferns et al., 1993; Ramp and Ferns, 1989), and are hosted in late Miocene to Pliocene sedimentary rocks. Proximal faults strike northwest to north and likely provided pathways for ascending geothermal fluids.

Vale Hot Springs, ~20 km east of Neal Hot Springs, effuse along the Malheur River just east of Vale, Oregon, with temperatures as high as 92.5°C and flow rates of ~20 gallons/minute (Russell, 1903). They have been utilized by man for various purposes, including a sanatorium, swimming pool, slaughterhouse, floral greenhouse, and 180,000 ft^2 mushroom growing plant (Gannett, 1988). The hot springs are the surface expression of a broad hot aquifer between Rhinehart Buttes and the Malheur River, approximately ~0.16 km^2 across, with warm wells up to ~38°C as far away as 1.6 km (Gannett, 1988). The aquifer is hypothesized to be sourced by 'hot, deep circulating regional ground water' within the north-northwest-striking Vale fault zone (Gannett, 1988).

Spatial relationships between young mineralization (late Miocene – Pliocene) and active geothermal systems occur at many localities in both eastern Oregon and in the northern Basin and Range (Cummings 1991a; Cummings et al., 2000; Coolbaugh et al., 2005). The Hope Butte gold project, 5 km north of Neal Hot Springs, has an estimated resource between 5-8 million tons of mineralized material with a grade between 0.91-0.94 grams gold per ton (Kenai Resources, 2013). Estimated mineralization age ranges from 3 to 12 Ma (Ferns pers. comm., 2012; Warren pers. comm., 2013). Its structural and temporal relationship to the Neal Hot Springs geothermal system is unknown, except that the north-northeast-striking Hope Butte fault projects through the prospect.

These relations indicate that geothermal activity has been widespread in eastern Oregon since the middle Miocene. The spatial relations between present-day geothermal systems and older epithermal mineral deposits suggest that favorable structural settings for hydrothermal activity have been maintained in some areas for many millions of years. It is also noteworthy that many of the epithermal mineral deposits are hosted by altered sedimentary rocks that occupy grabens. This further suggests that large amounts of hydrothermal fluids generally flow into permeable layers within the sedimentary basins rather than emanating at the surface. Thus, it is very possible that blind or hidden geothermal systems abound in the region. Similar to that hypothesized for the Great Basin region to the south (e.g., Coolbaugh et al., 2006), most of the hydrothermal fluids may be leaking out into permeable sedimentary layers at depth with no hot springs or fumaroles at the surface. Thus, the geothermal potential of eastern Oregon may be greater than current estimates would predict. Structural settings similar to that at Neal (e.g., step-overs or relay ramps) may be viable targets for blind geothermal systems elsewhere in the region.

6. Conclusions and Implications

The Neal geothermal field lies within the intersection of two regional grabens, the middle-late Miocene, north-trending, Oregon-Idaho graben and younger late Miocene to Holocene, northwest-trending, western Snake River Plain graben. It is marked by Neal Hot Springs, which effuse from opaline sinter mounds just north of Bully Creek. Production and injection wells, with temperatures up to 142°C, intersect the Neal fault

zone at depths of 680-1900 m and subsidiary faults within a relay ramp or step-over within the Neal fault zone.

The stratigraphy at Neal correlates with four regional packages. Basement rocks, discovered in one well, are granite, tentatively correlated with Jurassic Olds Ferry-Izee terrane. Nonconformably above is a thick package of middle Miocene Columbia River Basalt Group lavas, regionally known as the basalt of Malheur Gorge. Conformably above are middle to late Miocene Oregon-Idaho graben lavas, volcaniclastics, fluvial and lacustrine rocks. Overlying are the youngest rocks at Neal, which are late Miocene to Pliocene, western Snake River Plain lacustrine, fluvial, and volcaniclastic rocks.

The structural framework at Neal is characterized by northerly to northwest-striking normal faults, including the geothermally related Neal fault zone. Stress inversion of kinematic data reveal an extensional stress regime, including an interpreted younger, southwest-trending (~243°), least principal stress and an older, west-trending (~265°) least principal stress.

The geothermal system occupies a left step in the northerly striking Neal fault zone. It is bounded on the east by the Neal fault, a major, west-dipping, north-northwest-striking, steeply dipping normal to sinistral-normal fault, along which geothermal fluids ascend, and on the west by the north-northwest-striking, west-dipping, Sugarloaf Butte fault. The Neal fault zone probably evolved through two episodes of deformation: 1) an older, left-stepping, normal-slip fault zone associated with west-trending extension, and 2) a younger, oblique sinistral-normal fault zone related to southwest-trending extension. Recent sinistral-normal displacement may have generated a small pull-apart basin in the Neal area and facilitated development of the geothermal system. 'Hard-linkage' between

the Neal and Sugarloaf Butte faults occurs through concealed, west-northwest-striking faults, including the Cottonwood Creek subvertical fault, along which lateral fluid-flow is likely. An inferred north-plunging fault intersection at the Neal Hot Springs likely controls the location of the hot springs and sinter terraces.

Young structural features are evident at Neal as faults in the Neal fault zone and throughout the study area cut Quaternary fans and lower and upper Bully Creek Formation sedimentary rocks. In addition, the geothermal field is 4 km west of the active, north- to northwest-striking, normal-slip Cottonwood Mountain fault. Recently detected seismicity has also been documented within several kilometers of the geothermal field (Colwell pers. comm., 2012).

Geothermal and volcanic activity related to the Neal fault zone is suggested by the silicified Sugarloaf Butte, Neal basalt vent, and dacite scoria. This coupled with its active hot springs (~90°C), opaline sinter mounds, and geothermal fluid flow suggest that the geothermal field lies within an active (Quaternary), southward-terminating, left-stepping fault zone, which locally acts as a pull-apart basin with sinistral- and normal-slip components.

This study demonstrates the efficacy of using established structural models from the Basin and Range in eastern Oregon and the western Snake River Plain, including the Vale fault zone. Geothermal activity at Neal is demonstrated to be fault controlled and to be related to a known, conducive structural setting, the step-over (or relay ramp). Future geothermal exploration and development in eastern Oregon and western Idaho can be augmented by this approach.

References

Angelier, J., 1979, Determination of the mean principal directions of stresses for a given fault population, Tectonophysics, v. 56, p. 17-26.

Angelier, J., Colletta, B., and Anderson, R.E., 1985, Neogene paleostress changes in the Basin and Range: A case study at Hoover Dam, Nevada-Arizona: Geological Society of America Bulletin, v. 96, p. 347-361.

Allmendinger, R. W., Cardozo, N. C., and Fisher, D., 2012, Structural Geology Algorithms: Vectors & Tensors: Cambridge, England, Cambridge University Press, 289 p.

Barton, C.A., Zoback, D.M., and Moos, D., 1995, Fluid flow along potentially active faults in crystalline rock: Geology, v. 23, no. 8, p. 683-686.

Bell, J.W. and Ramelli, A.R., 2007, Active faults and neotectonics at geothermal sites in the western Basin and Range: Preliminary results: Geothermal Resources Council Transactions, v. 31. p. 375-378.

Blackwell, D.D., 1983, Heat flow in the northern Basin and Range province: Geothermal Resources Council Special Report 13, p. 81-93.

Blackwell, D.D., Wisan, K, Benoit, D. and Gollan, B., 1999, Structure of the Dixie Valley geothermal system, a “typical” Basin and Range geothermal system, from thermal and gravity data: Geothermal Resources Council Transactions, v. 23, p. 525-531.

Blackwell, D.D., Leidig, M., Smith R.P., and Johnson, S.D., 2002, Exploration and development techniques for Basin and Range geothermal systems: Examples from Dixie Valley, Nevada: Geothermal Resources Council Transactions, v. 26, p. 513-518.

Brooks, H.C., 1991, Geology and mineral resources map of the Vines Hill quadrangle, Malheur County, Oregon: Oregon Department of Geology and Mineral Industries Geological Map Series, GMS-63, scale 1:24,000.

Brooks, H.C. and O’Brien, 1992, Geology and mineral resources map of the Little Valley quadrangle, Malheur County, Oregon: Oregon Department of Geology and Mineral Industries Geological Map Series, GMS-72, scale 1:24,000.

Brooks, H.C. and O’Brien, 1992, Geology and mineral resources map of the Westfall quadrangle, Malheur County, Oregon: Oregon Department of Geology and Mineral Industries Geological Map Series, GMS-71, scale 1:24,000.

Brown, D.E., 1982, Geology and mineral resources map of the Vale East quadrangle, Malheur County, Oregon: Oregon Department of Geology and Mineral Industries, scale 1:24,000.

Camp, V.E., Ross, M.E., and Hanson, W.E., 2003, Genesis of flood basalts and Basin and Range volcanic rocks from Steens Mountain to the Malheur River Gorge, Oregon: Geological Society of America Bulletin, v. 115, p. 105-128.

Colwell, C., VanWijk, K., Liberty, L., Warren, I., and Revil, A., 2012, Integrated geophysical exploration of a known geothermal resource: Neal Hot Springs: Society of Exploration Geophysicists Technical Program Expanded Abstracts, p. 1-5.

Coolbaugh, M.F., Arehart, G.B., Faulds, J.E., and Garside, L.J., 2005, Geothermal systems in the Great Basin, western United States: Modern analogues to the roles of magmatism, structure, and regional tectonics in the formation of gold deposits, *in* Rhoden, H.N., Steininger, R.C., and Vikre, P.G., eds., Geological Society of Nevada Symposium: Window to the World, p. 1063–1081.

Conner, C.B., and Conway, M.F., 2000, Basalt volcanic fields, in Sigurdsson, H. ed., Encyclopedia of Volcanoes: Academic Press, New York, p. 331-343.

Cummings, M.L., 1991a, Relations among volcaniclastic sedimentation, volcanism, faulting, and hydrothermal activity west of Lake Owyhee, Malheur County, Oregon, *in* Raines, G., Lisle, R.E., Schafer, R.W., and Wilkinson, W.H., eds., Geology and ore deposits of the Great Basin: Geological Society of Nevada, Symposium Proceedings, v. 1, p. 111 – 132.

Cummings, M.L., Evans, J.G., Ferns, M.L., and Lees, K.R., 2000, Stratigraphic and structural evolution of the middle Miocene synvolcanic Oregon-Idaho graben: Geological Society of America Bulletin, v. 112, p. 668 – 682.

Curewitz, D. and Karson, J.A., 1997, Structural settings of hydrothermal outflow: Fracture permeability maintained by fault propagation and interaction: Journal of Volcanology and Geothermal Research, v. 79, p. 149-168.

Eager, K., Fouch, M., James, D., and Carlson, R., 2011, Crustal structure beneath the High Lava Plains of eastern Oregon and surrounding regions from receiver function analysis: Journal of Geophysical Research: Solid Earth, v. 116, 18 p.

Edmiston, R.C. and Benoit, W.R., 1984, Characteristics of Basin and Range geothermal systems with fluid temperatures of 150ºC to 200ºC: Geothermal Resources Council Transactions, v. 8, p. 417-424.

Evans, C.S., 1986, The geology, geochemistry, and alteration of Red Butte, Oregon: A precious metal-bearing paleo hot-spring system [Master's thesis]: Portland State University, Portland, Oregon, 133 p.

Evans, J.G., 1994, Geologic map of the Hope Butte 7.5' quadrangle, Malheur County, Oregon: unpublished, scale 1:24,000.

Evans, J.G., 1994, Geologic map of the Swede Flat 7.5' quadrangle, Malheur County, Oregon: unpublished, scale 1:24,000.

Faulds, J.E., Garside, L.J., and Opplinger, G.L., 2003, Structural analysis of the Desert Peak-Brady geothermal fields, northwestern, Nevada: Implications for understanding linkages between northeast-trending structures and geothermal reservoirs in the Humboldt structural zone: Geothermal Resources Council Transactions, v. 27, p. 859-864.

Faulds, J.E., Coolbaugh, M., Blewitt, G., and Henry, C.D., 2004, Why is Nevada in hot water? Structural controls and tectonic model of geothermal systems in the northwestern great basin: Geothermal Resources Council Transactions, v. 28, p. 649-654.

Faulds, J.E., Moeck, I., Drakos, P., and Zemach, E., 2010, Structural assessment and 3D geological modeling of the Brady's geothermal area, Churchill county (Nevada, USA): A preliminary report: 35th Workshop on Geothermal Reservoir Engineering, Stanford University, Stanford, California, February 1-3, 2010, 5 p.

Faulds, J.E., Coolbaugh, M.F., Vice, G.S., and Edwards, M.L., 2006, Characterizing structural controls of geothermal fields in the northwestern Great Basin: A progress report: Geothermal Resource Council Transactions, v. 30, p. 69-75.

Faulds, J.E., Coolbaugh, M.F., Hinz, N.H., Cashman, P.H., and Kratt, C., Dering, G., Edwards, J., Mayhew, B., and McLachlan, H., 2011, Assessment of favorable structural settings of geothermal systems in the Great Basin, western USA: Geothermal Resources Council Transactions, v. 35, p. 777-784.

Ferns, M.L. and Ramp, L., 1989, Geology and mineral resources map of the Grassy Mountain Quadrangle, Malheur County, Oregon: Oregon Department of Geology and Mineral Industries Geological Map Series, GMS-57, scale 1:24,000.

Ferns, M.L., 1990, Geology and mineral resources map of the Mitchell Butte Quadrangle, Malheur County, Oregon: Oregon Department of Geology and Mineral Industries Geological Map Series, GMS-61, scale 1:24,000.

Ferns, M.L., Brooks, H.C., Evans, J.G., and Cummings, M.L., 1993, Geologic map of the Vale 30 x 60 minute quadrangle, Malheur County, Oregon, and Owyhee County,

Idaho, Oregon Department of Geology and Mineral Industries Geological Map Series, GMS-77, scale 1:100,000.

Ferns, M.L. and McClaughry, J.D., 2011, Stratigraphy and volcanic evolution of the middle Miocene to Pliocene La Grande – Owyhee eruptive axis in eastern Oregon: unpublished.

Gannett, M.W., 1984, Hydrogeologic assessment of the developed geothermal aquifer near Vale, Oregon: State of Oregon Water Resources Department, Open-File Report No. 88-04.

Gauthier, B., and Angelier, J., 1985, Fault tectonics and deformation: a method of quantification using field data: Earth and Planetary Science Letters, v. 74, p. 137-148.

Gilbert, D., 1988, Geology and geochemistry of the Mahogany hot-springs gold prospect in the Owyhee region of south-eastern Oregon [Master's thesis]: Seattle, University of Washington, 76 p.

Hinz, N.H., Faulds, J.E., and Oppliger, G.L., 2008, Structural controls of Lee-Allen Hot Springs, southern Churchill County, western Nevada: A small pull-apart in the dextral shear zone of the Walker Lane: Geothermal Resources Council Transactions, v. 32, p. 285-290.

Hooper, P.R., Binger, G.G., and Lees, K.R., 2002a, Ages of the Steens and Columbia River flood basalts and their relationship to extension-related calc-alkalic volcanism in eastern Oregon: Geological Society of America Bulletin, v. 114, no.1, p. 43-50.

Idaho National Laboratory, 2006, The future of geothermal energy: Impact of enhanced geothermal systems (EGS) on the United States in the 21st century: Idaho National Laboratory, Idaho Falls, Idaho, DOE/INL Report No. INL/EXT-06-11746.

Kenai Resource, 2013, Hope Butte gold project, east Oregon: http://kenai.ca/wp/?page_id=56 (accessed January 2013).

Kittleman, L.R., Green, A.R., Hagood, A.R., Johnson, A.M., McMurray, J.M., Russell, R.G., and Weeden, D.A., 1965, Cenozoic stratigraphy of Owyhee region, southeastern Oregon: University of Oregon, Museum of Natural History Bulletin, no. 1, 45 p.

Knudsen, K.L., Wong, I.G., Bott, J.D.J., Weber, G.E., Silva, W.J., and Lettis, W.R., 1995, Seismotectonic evaluation, Agency Valley and Bully Creek Dams, Vale Project, east-central Oregon: Oakland Calif., William Lettis and Associates, 1000

Broadway, suite 612, and Woodward-Clyde Federal Services, 500 12th St., suite 100, 181 p., 4 plates.

Layman, E.B., 1984, A simple Basin and Range fault model for the Beowawe geothermal system, Nevada: Geothermal Resources Council Transactions, v. 8, p. 451-456.

Lawrence, R.D., 1976, Strike-slip faulting terminates the Basin and Range province in Oregon: Geological Society of America Bulletin, v. 87, p. 846-850.

Lees, K.R., 1994, Magmatic and tectonic changes through time in the Neogene volcanic rocks of the Vale area, Oregon, northwestern USA [Ph.D. dissertation]: Milton Keynes, UK, Open University, 284 p.

Lillie, R.J. and Couch, R.W., 1979, Geophysical evidence of fault termination of the Basin and Range Province in the vicinity of the Vale, Oregon, geothermal area, *in* Newman, G.W. and Goode, H.D., eds., Basin and Range Symposium and Great Basin Field Conference: Denver, Colorado, Rocky Mountains Association of Geologists and Utah Geological Association, p. 175-184.

Lowell, R.P., and Rona, P.A., 2005, Hydrothermal activity: Encyclopedia of Geology, v. 5, p. 362-372.

Mann, P., Hempton, M.R., Bradley, C., and Burke, K., 1983, Development of pull-apart basins: Journal of Geology, v. 91, p. 529-554.

Mann, G.M., and Meyers, C.E., 1993, Late Cenozoic structures and correlations to seismicity along the Olympic-Wallowa Lineament, northwest United States: Geological Society of America Bulletin, v.105, p. 853-871.

Malde, H.E., and Powers, H.A., 1962, Upper Cenozoic stratigraphy of western Snake River Plain, Idaho: Geological Society of America Bulletin, v. 73, no. 10, p. 1197-1220.

Marrett and Allmendinger, 1990, Kinematic analysis of fault-slip data: Journal of Structural Geology, v. 12, p. 973-986.

McCaffrey, R., Qamar, A.I., King, R.W., Wells, R., Khazaradze, G., Williams, C.A., Stevens, C.W., Vollick, J.J., and Zwick, P.C., 2007, Fault locking, block rotation and crustal deformation in the Pacific Northwest: Geophysical Journal International, v. 169, p. 1315-1340.

McNitt, J.R., 1990, Stratigraphic and structural controls of the occurrence of thermal fluid at the Soda Lakes geothermal field, Nevada: Geothermal Resources Council Transactions, v. 14, p. 1507-1513.

Moore, J.N. and Nielson, D.L., 1994, An overview of the geology and geochemistry of the Roosevelt Hot Springs geothermal system, Utah: Utah Geological Association, no. 23, p. 25- 43.

Payne, S.J., McCaffrey, R., King, R.W., and Kattenhorn, S.A., 2012, A new interpretation of deformation rates in the Snake River Plain and adjacent basin and range regions based on GPS measurements: Geophysical Journal International, v. 189, p. 101-122.

Petit, J.P., 1987, Criteria for the sense of movement on fault surfaces in brittle rocks: Journal of Structural Geology, v. 9, no. 5/6, p. 597-608.

Ramp, L. and Ferns, M.L., 1989, Geology and mineral resources map of the Double Mountain Quadrangle, Malheur County, Oregon: Oregon Department of Geology and Mineral Industries Geological Map Series, GMS-58, scale 1:24,000.

Reiter, F., and Acs, P., 1999, Tectonics FP 1.5: A computer program for structural geology: Universität Innsbruck.

Rhodes, Gregory, T., 2011, Structural controls of the San Emidio geothermal system, northwestern Nevada [M.S. thesis]: University of Nevada, Reno, 72 p.

Russell, I.C., 1903, Preliminary report of artesian basins in southwestern Idaho and southeastern Oregon: U.S. Geological Water Supply and Irrigation Paper, no. 78, 53 p.

Rytuba, J.J., and Vander Meulen D.B., 1991, Hot-spring precious-metal systems in the Lake Owyhee Volcanic Field, Oregon-Idaho, *in* Raines, G.L., Lisle, R.E., Schafer, R.W., and Wilkinson, W.H., eds., Geology and Ore Deposits of the Great Basin: Geological Society of Nevada Symposium Proceedings, v. 2, p. 1085-1096.

Sheriff, S., 2010, Edge detection with hgm, as lwn. http://www.cas.umt.edu/geosciences/faculty/sheriff/495-Applied Magnetics/sources/Edge Detection with USGS_Oasis_Montaj.pdf (accessed July 2012).

Simpson, G.D., Hemphill-Haley, M.A., Wong, I.G., Bott, J.D., Silva, W.J., and Lettis, W.R., 1993, Seismotectonic evaluation, Burnet River Project – Unity Dam, Baker Project – Thief Valley Dam, northeastern Oregon: Oakland, Calif., William Lettis and Associates, Inc., and Woodward-Clyde Federal Services, prepared for U.S. Bureau of Reclamation, 167 p.

Wood, S.H. and Clemens, D.M., 2000, Geologic and tectonic history of the western Snake River Plain, Idaho and Oregon; Tectonic and Magmatic Evolution of the

Snake River Plain Volcanic Province: Idaho Geological Survey Bulletin 30, p. 69-103.

APPENDIX A: DESCRIPTION OF MAP UNITS

Anthropogenic Features and Deposits

Qx Disturbed and modified areas Highly disturbed, modified, and leveled areas including the U.S. Geothermal power plant and facilities.

Ql Bully Creek Reservoir, 1989 level Fluctuations in precipitation and agricultural demand affect reservoir volume and therefore reservoir height by tens of meters annually. Unit Ql is mapped lake level from an August 1989 aerial photo.

Qlf Shallow reservoir sediments (late Anthropocene) Mostly fine-grained, beige to light-tan to gray, poorly to moderately sorted, very weakly indurated gravel, sand, silt, and clay associated with fluctuating Bully Creek Reservoir levels. Moderate soil development with vegetation. Unknown thickness but likely no more than a few meters.

Qlf1 Shallow reworked reservoir sediments (late Anthropocene) Mostly fine-grained, white to beige to light tan, poorly to moderately sorted, weakly indurated and unconsolidated sand, silt, and clay resulting from slight reworking of colluvial and fan material along reservoir margins. Generally little to no soil development and vegetation. Unknown thickness but likely no more than a few meters.

Hillslope Deposits

Qc Colluvium (Holocene to Pleistocene) Colluvial and talus deposits generally along and at the base of steep slopes. Deposits typically consist of poorly sorted, angular, unconsolidated cobbles and boulders with interstitial clays. Because Qc is prevalent throughout the area, it is mapped only where obscuring bedrock.

Qls Landslide deposits (Holocene to Pleistocene) Landslide and slump deposits formed from gravitational and/or weathering bedrock failure. Chiefly composed of disoriented and disjointed volcanic rocks, namely Trcm, Thb, Tav, and Tbar, likely as a result of their greater competency compared with underlying sedimentary rocks, thus resulting in over-steepening and failure.

Alluvial Deposits

Qa Young alluvium, undivided (Holocene to late Pleistocene) Alluvium in recently abandoned (Holocene to late Pleistocene) or annually active drainages generally consisting of poorly to well-sorted, poorly to well-rounded, sands to cobble-pebble gravels; locally contain boulders. Surfaces generally have bar-and-swale morphology. Little to no soil development. Thicknesses vary considerably but range from 0-25 m.

Qfy Young active fan alluvium and recently abandoned active alluvial surfaces (late Holocene) Poorly to well-sorted, pebble to cobble gravel and sand with angular to subangular clasts; locally contain boulders. Surfaces slightly to fully smoothed textures. Deposits are up to 2 m thick.

Qfy1 Young inactive fan alluvium (Holocene to Pleistocene) Poorly to well-sorted, poorly to moderately-rounded, pebble to cobble gravel to clay; locally contain boulders. Surfaces are generally smoothed to slightly smoothed, with bar-and-swale morphology. Little to no soil development. Poorly stratified, matrix-supported deposits. Deposits are up to 3 m thick.

Qfi Intermediate fan alluvium, undivided (late to middle Pleistocene) Cobble to pebble gravel, sand, silt, and clay with isolated boulders. Weakly indurated, poorly to moderately stratified, poorly to moderately sorted, matrix-supported deposits with poorly to moderately rounded clasts. Surfaces are mostly smoothed, well dissected, and incised. Thicknesses are poorly known but likely 1-5 m.

Qfo Old fan alluvium, undivided (middle to early Pleistocene) Poorly to well-sorted pebble to cobble gravel, sand, silt, and clay with isolated boulders; poorly to moderately stratified, matrix-supported deposits with poorly to moderately rounded clasts. Surfaces are well dissected and incised. Thicknesses are poorly known but likely 1-5 m.

Qf Fan alluvium, undivided (Holocene to Pleistocene) Fan surfaces that cover broad, low lying areas; poorly incised, cobble to pebble gravel, sand, silt, and clay; locally contain boulders; mostly matrix supported with poorly to moderately rounded clasts. Variable surface morphology. Surfaces range from rough to smooth. Thicknesses are variable but up to 10 m.

QTg Terrace gravels, undivided (Pleistocene to Pliocene) Poorly sorted and poorly to well-rounded gravels that overlie the Hog Creek Formation along the Bully Creek and Cottonwood Creek drainages. The gravels consist of Hunter Creek Basalt and Cottonwood Mountain Rhyolite. These gravels are found along benches that overlie the Hog Creek Formation.

Spring Deposits (Quaternary to Pliocene)

Qst Subaerial siliceous opaline sinter (Holocene) Siliceous opaline sinter mounds from which hot springs currently or have recently effused. Mounds are broad, low-lying, with silicified reeds and other incorporated biogenic fragments. Thicknesses are poorly constrained but likely up to 5 m.

Qss Opaline silicified alluvium and silicified Bully Creek Formation (Holocene to Pleistocene?) Well-indurated, highly-altered, with variable remnant lithology, derived from Quaternary alluvium and sedimentary rocks of the Bully Creek Formation.

Conspicuous layering suggests remnant bedding. Exposed near Neal Hot Springs and along water canal north of hot springs. Zone of silicification within hanging wall of Neal fault ~100 m thick.

QTss Silicifed rocks, undivided (Pleistocene to Pliocene?) Pervasively silicified sedimentary rocks, exposed throughout study area, extensively at Sugarloaf and Hope Butte, with known gold and mercury mineralization at Hope Butte.

QThbr Hydrothermal volcanic breccia (Pleistocene to Pliocene?) Reddish-brown to beige silicified volcanic breccia. Massive, matrix-supported, subangular, poorly sorted, with clasts up to ~30 cm long, but most less than ~5 cm. Original textures and mineralogy of clasts are replaced, but proximity to Hunter Creek Basalt makes it the likely source. Unit exposed along production fault and hillside north of Neal Hot Springs. Thickness up to 10 m.

Western Snake River Plain Deposits

Tsd Dacite scoria (Pliocene?) Red to reddish-brown scoraceous aphyric to sparsely porphyritic dacite, with spatter cone features. Contains up to 10% plagioclase, <2% quartz, <2% sanidine, and <1% pyroxene phenocrysts. Incorporated blocks of tuffaceous siltstone and tuff throughout, discontinuous flow fabrics, and variable flow thicknesses. Brownish-red iron coating likely responsible for red color. Exposed in two localities, and likely representative of two discrete, evolved, small-volume magmatic pulses. Thickness up to 8 m. Unit local to study area.

Tlm Fossiliferous limestone (Pliocene?) Beige to light gray silty limestone. Small bivalve and gastropod shells are abundant, along with stromatolitic and algal structures. Unit overlies Tbar and is exposed on high ridges ~2 km south of Neal Hot Springs. Thin to medium bedded. Up to 3 m thick.

Tbcu Upper Bully Creek Formation tuffaceous sedimentary rocks and tuff (late Miocene) Mostly interlayered tuffaceous sandstone and lesser tuffaceous siltstone, arkosic sandstone, ash-fall and possibly water-laid tuff, and gravel. Thin veneer (unknown thickness, but likely 0.5-2 m) of white to beige, poorly exposed silty limestone overlies much of this unit, but not mapped separately. Massive, aphyric, ash-fall tuff, ~1-2 m thick, with sparse pumice exposed below north-trending ridge in northeastern portion of study area. Thin lenses of white matrix, with brown and beige organic rich, fibrous fragments exposed locally. Tuffaceous arkosic sandstones vary from yellow, brown, and beige, medium- to coarse-grained, subrounded, and moderately sorted, with thin beds and fluvial sedimentary structures (e.g., planar bedding). Unit has unknown thickness, but in eastern portion of study area, which is adjacent to the 2 km deep Willow Creek sub-basin (Lillie and Couch, 1979), thickness could be hundreds of meters. Stratigraphically correlative to upper Chalk Hills Formation of Malde and Powers (1962) and possibly upper Bully Creek Formation of Kittleman et al. (1965).

Tbn Neal basalt Aphyric to porphyritic, medium to dark gray basaltic andesite flows. Flows are dominantly dense and platy to moderately vesicular. Contains up to ~35% phenocrysts of plagioclase, olivine, and sparse pyroxene. Felty to trachytic groundmass, which contains 60% plagioclase microlites, up to ~15% glass content, and 25% crystallites. Variable weathering of olivine to iddingsite. Vesicules filled with calcite. Vertical columnar jointing exposed locally with up to ~1 m width and ~6-8 m height. Maximum thickness observed in central part of quadrangle, within northwest-trending Rock Cabin Creek drainage ~100 m north of Cottonwood Creek, where up to 25 m thick. Well logs reveal thickness up to 220 m, but likely intersect part of a volcanic neck. Unit local to study area. Whole rock yielded an $^{40}Ar/^{39}Ar$ date of 8.81 ± 0.05 (sample 11026, Plate 1).

Tbcg Bully Creek Formation conglomerate (late Miocene) Matrix-supported, cobble conglomerate with subangular to subrounded clasts up to ~20 cm long and composed almost entirely of Trcm. Moderately indurated, moderately sorted, massive, with silica cement. Thickness ~3 m.

Tbcl Lower Bully Creek Formation tuffaceous sedimentary rocks, ash-flow tuff, and diatomite (late Miocene) Tuffaceous siltstone, diatomite, and ash-fall and ash-flow tuff. The upper portion of this unit largely consists of light gray, brown, pinkish-brown, greenish-gray, and beige poorly bedded to massive tuffaceous siltstone and lesser tuffaceous sandstone and conglomerate. The tuffaceous sandstone consists of glass shards and subrounded grains of feldspar, quartz, and volcanic rock fragments ~2 mm long. Subrounded pebble- and cobble-sized rock fragments occur locally. The lower portion of this unit consists of diatomite, thin partings (1-50 cm) of ash-fall tuff, and a thick bed (6-7 m) of medium to dark gray, aphyric ash-flow tuff. Just north of Cottonwood Creek, this prominent tuff contains entrained, coherent blocks of diatomite cross cut locally by thin bodies of tuff. These lithologic characteristics are similar to the regional ~8.4 Prater Creek tuff (Ferns pers. comm., 2012). The diatomite is white, homogenous, non-resistant, massive to locally fissile. Locally contains minute fossils of leaf impressions and various small organic fragments. Thin partings of gray and brownish-gray, aphyric, ash-fall and locally reworked tuff occur throughout entire diatomite section. Local reverse grading in tuff beds. Yellow to orange vitric alteration common along margins of beds. Exposed unit thickness up to ~250 m. Well log thickness ~30 m. Stratigraphically correlative to lower Chalk Hills Formation of Malde and Powers (1962) and Bully Creek Formation of Kittleman et al. (1965).

Oregon-Idaho Graben Deposits

Tav Vines Hill andesite Aphyric to porphyritic basaltic andesite and andesite flows and flow breccias. Medium to dark gray weathering grayish to reddish brown. Flows are dominantly platy and dense to coarsely vesicular near flow tops. Contains up to 20% phenocrysts of plagioclase, lesser olivine, and sparse pyroxene. Trachytic groundmass

consists of ~80% plagioclase, ~15% glass content, and <5% interstitial mafics. Maximum thickness is observed within Bully Creek drainage, where up to ~40 m. In well logs, thickness is up to ~55 m. Intercalated with thin tuffaceous siltstone. Stratigraphically and chemically correlative to mafic volcanic rocks (Tdmv) of Brooks (1991) and Brooks and O'Brien (1992). Whole rock yielded $^{40}Ar/^{39}Ar$ ages of 11.46 ± 0.17 and 10.87 ± 0.08 Ma (samples 7274 and 7221, Plate 1). Regional $^{40}Ar/^{39}Ar$ age of 10.1 ± 1.4 (Hooper et al., 2002a).

Tbar Reservoir basaltic andesite Dark gray to black, weathering reddish-brown, fine- to medium-grained aphyric basaltic andesite flows. Flows are platy to blocky. Up to 15% plagioclase microphenocrysts. Needle-like, felty groundmass consists of plagioclase (80%), Fe-Ti oxides (10%), and interstitial pyroxene (10%). Flows are thin, from 2-10 m thick, with unit thickness unknown, but likely 5-20 m. Sandstone, siltstone, and limestone beds locally overlie flows. Flows cap mesas and high ridges south of Bully Creek drainage and reservoir. Unit local to study area. Whole rock yielded $^{40}Ar/^{39}Ar$ ages of 12.13 ± 0.02 and 12.29 ± 0.09 Ma (samples 11029 and 110211, Plate 1).

Tds Drip Springs Formation tuffaceous sedimentary rocks, arkosic sandstone, and tuff (middle to late Miocene) Pale brown, yellow-brown, gray, beige, and white tuffaceous siltstone, sandstone, conglomerate and local arkosic sandstone. Sparse interbedded tuff and tuffaceous mudstone. Poorly to moderately sorted, subangular arkosic sandstone exposed along Bully Creek with abundant mica and feldspar components with local cross-bedded sedimentary structures suggesting fluvial input, likely from an Idaho Batholith source. Exposed thickness up to ~300 m. Well log thickness up to ~260 m. Stratigraphically correlative to Drip Springs Formation of Kittleman et al. (1965).

Thcg Hog Creek conglomerate (middle Miocene) Subhorizontal, matrix-supported, moderately sorted cobble conglomerate with subangular to subrounded clasts up to ~20 cm long. Moderately indurated with silica cement. Mostly composed of Cottonwood Mountain Rhyolite clasts. Unit caps Hog Creek Formation sedimentary rocks and forms broad aprons extending outward from Hunter Creek Basalt and Cottonwood Mountain Rhyolite flow margins. Thickness 2-6 m.

Thb Hunter Creek Basalt Dark gray to black to bluish black, dense, aphyric basaltic-andesite to andesite flows with sparse (<1%) plagioclase and olivine phenocrysts. Groundmass contains ~60% plagioclase, ~20% mafics, ~15% crystallites, and 5% Fe-Ti oxides. Sparse illite alteration and calcite filled vesicules. Commonly exhibit subconchoidal fracturing and where weathered, form blocks less than 40 cm across. Field relationships consistently place the Hunter Creek Basalt, up to ~100 m thickness, stratigraphically above the Cottonwood Mountain Rhyolite; however, well-field relationships suggest inter-fingering basalt and rhyolite, with repeated packages of basalt above and below the Cottonwood Mountain Rhyolite, with up to 150 m thickness but variable across well field. Stratigraphically and chemically equivalent to Hunter Creek

Basalt of Kittleman et al. (1965). Regional $^{40}Ar/^{39}Ar$ age of 15.8 ± 0.3 Ma (Hooper et al., 2002a).

Thcs2 Upper Hog Creek Formation tuffaceous sedimentary rocks (middle Miocene) Poorly exposed tuffaceous siltstone, sandstone, and tuff. Locally silicified with textures and mineralogy replaced, chalcedony dominant. Mapped separately where overlying Cottonwood Mountain Rhyolite and underlying Hunter Creek Basalt. Thickness up to ~30 m. Variable well-field thickness up to ~40 m.

Trbr Cottonwood Mountain sedimentary breccia Reddish-brown, angular cobble to pebble sedimentary breccia consisting of clasts of Cottonwood Mountain Rhyolite. Mud matrix, clast supported, poorly sorted breccia wedges that tongue outward from Cottonwood Mountain Rhyolite flows. Interpreted as resulting from talus or small alluvial fans eroded from margins of Cottonwood Mountain Rhyolite flows along east-trending paleovalley south of Hope Butte.

Trcm Cottonwood Mountain Rhyolite Porphyritic, dark reddish-gray lithoidal, platy flows and flow breccias and dark gray to black vitrophyre. Contains up to ~25% phenocrysts of plagioclase (up to 3 cm long and sparsely cumulophyric), with minor sanidine and quartz. Groundmass contains ~40% illite weathering, ~35% plagioclase, ~15% Fe-Ti oxides, and ~10% opaque minerals. Flows locally exhibit columnar jointing, vertical and horizontal, with vertical jointing up to ~2 m across and ~20 m high in Cottonwood Creek canyon. Basal and/or carapace breccia exposed locally, with angular blocks of highly vesicular vitrophyre in a beige to gray ash matrix. Exposed thickness up to ~200 m. Stratigraphically and chemically correlative to Rhyolite of Bully Creek of Brooks and O'Brian (1992) and Cottonwood Mountain Rhyolite of Evans (1994). Regional $^{40}Ar/^{39}Ar$ ages of 14.6 ± 1.0, 15.5 ± 0.7, and 15.7 ± 0.2 Ma (Hooper et al., 2002a).

Tbsc Basalt scoria and lapilli Altered, yellow to yellow-brown basalt scoria and lapilli. Composed of pumice and lithic breccia, with ash to lapilli matrix. Unit is exposed in two localities, both proximal to and stratigraphically below Hunter Creek Basalt and Cottonwood Mountain Rhyolite. Unit is discontinuous, pinching out abruptly in both localities and likely represents parts of cinder cones.

Thcs1 Lower Hog Creek Formation tuffaceous sedimentary rocks Generally pale brown to tan tuffaceous siltstone and sandstone. Mapped separately where below Cottonwood Mountain Rhyolite. Poorly exposed along west-facing slope in footwall of Neal fault, ~4-6 km north of Neal Hot Springs. Exposed thickness ~50 m. Variable well-field thickness up to ~100 m.

Thcs Hog Creek Formation sedimentary rocks, undivided Tuffaceous siltstone, sandstone, conglomerate and tuff. Beige, tan, pale brown to gray rocks mapped undivided where intercalated and interbedded within Cottonwood Mountain Rhyolite and Hunter Creek Basalt. Intercalated ash-fall, ash-flow, and lapilli tuff exposed locally with

thickness up to ~6 m. Mostly exposed in the north part of the study area, proximal to Hope Butte. Variable exposed thickness up to ~80 m. Variable well field thickness up to ~130 m.

Columbia River Basalt Group

Tbcr Birch Creek basalt Encountered in well-field. Medium to dark gray, brown, and/or green, aphyric to porphyritic, with up to 10% phenocrysts of plagioclase. Groundmass contains intergrown plagioclase and pyroxene microlites. Chlorite-calcite alteration, up to 80%, variable hematite staining, variable silica alteration, and variable chalcedony and/or quartz veining. Possibly exposed in one locality on the southern slope of Hope Butte below the Cottonwood Mountain Rhyolite and Hog Creek Formation sedimentary rocks. Mean $^{40}Ar/^{39}Ar$ age of 15.7 ± 0.1 Ma (Hooper et al., 2002a).

Tupc Upper Pole Creek basalt Encountered in well-field. Medium to dark gray, brown, and/or green, with up to 15% phenocrysts of plagioclase and sparse pyroxene. Individual flow tops are possibly marked by red scoraceous horizons. Variable chlorite-calcite alteration, variable hematite staining (up to ~50%), variable silica alteration, sparse chalcedony and/or quartz veining. Intercalated with dark brown tuffaceous mudstone. Mean $^{40}Ar/^{39}Ar$ age of 16.5 ± 0.3 Ma (Hooper et al., 2002a)

Tlpc Lower Pole Creek basalt Encountered in well-field. Medium to dark gray and/or green, with up to 20% plagioclase phenocrysts up to 1-2 cm long. Variable hematite staining up to 80%, variable silica alteration, variable quartz veining and veinlets, and sparse zeolite crystals up to ~2 cm long. Intercalated with dark brown to gray sandy, tuffaceous mudstone and lithic-crystal tuff up to 5 m thick. Mean $^{40}Ar/^{39}Ar$ age of 16.9 ± 0.8 Ma (Hooper et al., 2002a).

Tbm Basalt of Malheur Gorge Sequence, undivided (middle Miocene) Sequence includes Birch Creek (Tbcr), Upper Pole Creek (Tupc), and Lower Pole Creek (Tlpc) basalts. Medium to dark gray/green, gray and brown, aphyric to porphyritic basalt. Flows decrease in phenocryst content upsection. Sequence thickness, constrained by well NHS-11, ~1.6 km. Variable tuffaceous mudstone and tuff intercalated. Correlative to voluminous regional Columbia River Basalt Group.

Blue Mountains Group Basement

Jg Granite, Olds Ferry-Izee Terrane? (Jurassic) Granite body intersected in well NHS-11 at ~2015 m depth. Description here from U.S. Geothermal, 2012 chip logging. Light greenish gray, white, green, brown, and red coarsely granular groundmass with up to 80% phenocrysts of quartz, feldspar and biotite. Variable silicification (up to >95%), quartz-calcite veining, some red-orange hematite staining, and rare hematite breccia seams. Very dark brown to black, coarsely crystalline basalt dike cutting granite, weakly

chlorite altered, moderately calcite altered, and minor calcite and/or quartz veinlets <2 mm wide. Preliminary SHRIMP zircon age: Jurassic (Hoiland, pers. comm., 2012)

APPENDIX B: BULK-ROCK GEOCHEMISTRY

Of the 111 samples collected and submitted for XRF analyses, 99 samples were submitted to the Franklin and Marshall X-ray Laboratory and 13 samples were submitted to the Washington State University GeoAnalytical Lab, with both labs using X-ray flourescene spectrometers (XRF). Samples were analyzed for major and minor elements and are reported as weight percentages (wt %): including, SiO_2, Al_2O_3, CaO, K_2O, P_2O_5, TiO_2, Fe_2O_3, MnO, Na_2O, and MgO. These data are normalized to 100 wt %. Samples were also analyzed for trace elements and are reported as parts per million (ppm): including, Rb, Sr, Y, Zr, Nb, Ni, Ga, Cu, Zn, U, Th, Co, Pb, Sc, Cr, V, La, Ce, and Ba.

Data sampled from well-field are labeled according to well and depth (ft) sampled (e.g. NHS10-480 is from well NHS-10 at 480 ft depth). Samples collected and submitted by Clinton Colwell of Boise State University are denoted by a C in front of sample label. Data from Washington State GeoAnalytical Laboratory are denoted by (W) following sample label. Sample locations and wells are labeled and displayed in Plate 1.

The data are organized according to units and are displayed in two sections. The first section displays major and minor element weight percentages (wt %), and the second section displays trace element parts per million (ppm). The trace element section is displayed over two pages for each sample. The first page displays Rb, Sr, Y, Zr, V, Ni, Cr, Nb, Ga, and Cu (ppm), and the second page displays Zn, Co, Ba, La, Ce, U, Th, Sc, Pb, and Mg# (ppm) for each sample.

Major and Minor Element Oxide weight percentages (wt %)

Name	Rock Unit	SiO_2	TiO_2	Al_2O_3	Fe_2O_3	FeO	MnO	MgO	CaO	Na_2O	K_2O	P_2O_5
NHS10-480	Tbn	53.0	1.2	17.8	9.6	8.6	0.2	5.0	9.3	3.2	1.4	0.4
NHS-10-520	Tbn	53.6	1.2	16.5	10.1	9.1	0.2	5.5	8.9	3.1	1.6	0.4
NHS-12-140	Tbn	54.0	1.2	16.5	9.5	8.6	0.2	5.8	8.6	3.3	1.6	0.3
NHS-12-460	Tbn	54.4	1.2	16.8	9.3	8.3	0.2	4.7	8.6	3.0	1.4	0.4
TG7-80	Tbn	53.8	1.1	17.2	9.5	8.6	0.2	5.1	9.6	3.0	1.2	0.3
11026(W)	Tbn	54.2	1.3	17.0		8.4	0.2	4.0	9.8	3.2	1.6	0.4
TG3-1700	Tbn	53.6	1.2	16.6	9.7	8.8	0.2	5.5	9.2	3.0	1.6	0.4
CNHS-06	Tbn	53.7	1.2	17.2	9.6	8.7	0.2	5.5	8.6	3.3	1.3	0.5
110211(W)	Tbar	56.6	1.4	16.8	9.4	8.2	0.1	3.4	6.7	3.9	1.9	0.8
110210(W)	Tbar	56.8	1.4	16.8	9.4	8.3	0.2	3.4	6.8	3.8	1.8	0.8
11029(W)	Tbar	56.0	1.4	16.6	9.3	8.8	0.2	3.6	6.8	3.9	1.9	0.8
11028(W)	Tbar	55.9	1.4	16.6	9.3	8.8	0.2	3.6	6.7	4.1	1.9	0.8
NHS11-150	?	65.1	0.8	14.7	6.0	5.4	0.2	2.8	5.9	1.4	3.5	0.3
NHS09-110	Tdb	48.9	1.5	17.5	12.3	11.1	0.2	6.9	10.3	2.8	0.5	0.4
NHS9-890	Tdb	50.4	1.6	16.5	11.7	10.6	0.2	6.4	9.7	2.4	0.7	0.4
NHS9-1030	Tdb	48.5	1.5	17.2	11.9	10.7	0.2	6.9	10.2	2.7	0.5	0.4
NHS12-1150	Tdb	48.8	1.4	16.9	11.4	10.3	0.2	8.1	9.9	2.5	0.4	0.4
NHS13-1930	Tdb	48.7	1.6	16.5	11.8	10.6	0.2	6.6	11.3	2.6	0.4	0.4
NHS2-220	Tav	60.1	0.9	17.5	6.9	6.2	0.1	2.7	5.7	4.2	2.3	0.4
NHS08-310	Tav	59.3	0.9	18.1	6.9	6.2	0.1	2.8	5.8	4.2	2.1	0.5
TG-3-160	Tav	60.4	0.9	17.2	6.5	5.9	0.2	2.4	6.3	4.2	2.2	0.4
TG16-240	Tav	59.8	0.9	17.3	7.0	6.3	0.1	2.7	5.9	4.2	2.2	0.5
NHS13-300	Tav	59.8	0.9	17.3	6.7	6.1	0.1	2.6	5.9	4.2	2.0	0.5
CNHS-08	Tav	60.1	0.9	17.8	6.6	5.9	0.1	2.3	5.8	4.3	2.2	0.5
9128(W)	Tav	60.2	0.9	17.2	6.6	6.0	0.1	3.1	6.0	3.8	2.3	0.5
11027(W)	Tav	59.9	0.9	17.2	7.0	6.3	0.1	3.2	5.9	3.9	2.2	0.5
7274(W)	Tav	60.4	0.9	17.1	7.0	6.3	0.1	2.4	5.7	4.2	2.4	0.5
7272(W)	Tav	60.3	0.9	17.6	6.7	6.1	0.1	2.7	5.9	3.7	2.3	0.5
NHS2-100	Tav	55.7	1.0	19.4	8.1	7.3	0.1	4.5	6.8	3.7	1.0	0.5
NHS08-150	Tav	56.9	1.0	19.8	7.1	6.4	0.1	3.8	6.3	3.4	1.6	0.5
NHS05-200	Tav	55.9	0.9	17.5	7.7	7.0	0.1	3.6	8.8	3.3	2.3	0.5
NHS4-100	Tav	59.8	1.5	15.0	9.5	8.6	0.2	2.5	6.1	2.9	2.0	0.6

Name	Rock Unit	SiO_2	TiO_2	Al_2O_3	Fe_2O_3	FeO	MnO	MgO	CaO	Na_2O	K_2O	P_2O_5
NHS-2-1070	Thb	63.3	1.3	13.0	12.6	11.3	0.3	1.2	4.1	1.9	3.1	0.4
NHS03-640	Thb	64.6	1.4	12.5	11.0	9.9	0.2	1.1	3.2	2.6	4.0	0.5
NHS03-880	Thb	59.4	1.7	13.9	13.1	11.8	0.3	1.8	5.6	3.4	1.4	0.6
NHS05-1060	Thb	59.8	1.5	13.3	13.6	12.3	0.3	1.4	5.6	3.4	2.0	0.5
NHS08-1270	Thb	57.4	2.2	13.5	13.6	12.2	0.2	2.6	6.5	2.9	1.9	0.5
NHS-12-1350	Thb	61.5	1.4	12.7	13.3	12.0	0.2	1.0	4.4	3.8	2.5	0.4
TG12-260	Thb	56.0	2.4	14.1	13.8	12.4	0.2	2.6	6.9	3.0	1.8	0.5
CNHS-02	Thb	60.4	1.5	12.9	13.4	12.1	0.3	1.3	5.1	3.2	2.8	0.5
CNHS-05	Thb	56.5	2.3	13.6	13.8	12.4	0.2	2.9	6.5	3.1	2.0	0.5
CNHS-07	Thb	57.0	2.3	13.6	12.9	11.7	0.2	3.0	6.6	3.1	1.9	0.5
NHS13-1240	Thb	59.9	1.5	13.5	13.7	12.3	0.3	1.2	5.2	3.9	1.7	0.5
NHS13-1540	Thb	57.7	2.2	14.3	13.5	12.1	0.2	2.3	5.7	3.2	1.8	0.5
TG16B-1300	Thb	60.6	1.5	12.9	13.2	11.9	0.3	1.3	5.2	3.4	2.4	0.5
TG16B-1540	Thb	56.3	2.3	13.8	13.7	12.3	0.2	3.0	7.3	3.3	0.9	0.5
TG-20-300	Thb	56.5	2.3	13.5	13.8	12.4	0.2	3.0	6.5	3.2	2.0	0.5
TG-20-1060	Thb	58.0	2.2	13.4	13.1	11.8	0.2	2.4	5.9	3.3	2.2	0.6
TG19-80	Thb	56.3	2.3	13.9	13.7	12.3	0.3	2.6	6.2	3.5	2.0	0.5
TG19-580	Thb	55.8	2.4	14.0	13.9	12.5	0.3	2.7	6.3	3.5	2.0	0.5
TG19-880	Thb	58.6	1.9	13.9	12.4	11.2	0.3	2.2	5.6	3.7	2.0	0.7
TG-3-1400	Thb	57.1	2.3	13.7	13.1	11.8	0.2	2.9	6.5	3.2	1.7	0.5
TG-3-1940	Thb	58.8	2.0	13.7	12.7	11.5	0.2	2.5	6.5	3.3	1.0	0.6
NHS-9-1300	Thb	58.1	2.1	13.2	12.9	11.6	0.2	3.0	6.8	3.3	1.1	0.6
NHS09-1420	Thb	57.2	2.2	13.8	12.9	11.6	0.2	2.9	6.5	3.4	1.7	0.5
NHS-10-960	Thb	60.3	1.8	13.8	12.3	11.1	0.2	2.9	7.1	1.0	0.8	0.8
NHS4-600	Thb	61.5	1.6	14.0	10.9	9.9	0.2	1.0	3.3	4.0	2.9	0.6
NHS10-1160	Thb	56.8	2.2	13.5	12.7	11.4	0.2	2.7	6.2	3.5	1.2	0.9
NHS11-900	Thb	62.4	2.2	13.2	12.9	11.6	0.2	1.0	2.1	2.9	2.6	0.5
NHS4-100	Thb	59.8	1.5	15.0	9.5	8.6	0.2	2.5	6.1	2.9	2.0	0.6
10045(W)	Thb	62.1	1.4	12.8	11.8	10.6	0.3	0.8	4.9	3.4	3.3	0.4
9142(W)	Thb	64.0	1.6	13.7	11.1	10.0	0.1	0.5	2.8	3.9	2.9	0.5
NHS03-1580	Thb	57.8	2.0	11.7	18.7	16.9	0.2	3.5	4.3	2.5	0.6	0.6
NHS04-1190	Thb	60.1	1.9	13.8	12.1	10.9	0.2	4.3	5.8	1.1	1.3	0.6
NHS04-1570	Thb	57.7	2.2	13.3	13.7	12.3	0.2	2.6	6.5	3.3	1.1	0.6
NHS02-1940	Thb	59.8	2.2	12.9	12.5	11.3	0.2	2.3	5.4	2.8	2.5	0.6
NHS05-1950	Thb	69.4	1.7	10.7	8.2	7.3	0.2	2.3	4.6	1.7	1.5	0.6

Name	Rock Unit	SiO_2	TiO_2	Al_2O_3	Fe_2O_3	FeO	MnO	MgO	CaO	Na_2O	K_2O	P_2O_5
NHS-2-1270	Trcm	73.7	0.7	12.5	4.5	4.0	0.1	0.6	2.4	2.2	3.6	0.1
NHS03-1000	Trcm	72.5	0.7	13.3	4.7	4.2	0.1	1.4	3.6	3.0	0.9	0.2
NHS04-870	Trcm	73.4	0.7	13.1	4.0	3.6	0.1	0.5	2.5	3.6	2.2	0.2
NHS04-980	Trcm	73.0	0.7	12.1	4.1	3.6	0.1	0.4	2.5	2.7	4.7	0.2
NHS05-1290	Trcm	73.2	0.6	12.7	3.8	3.4	0.1	1.1	3.6	1.9	3.2	0.2
NHS05-1480	Trcm	86.8	0.5	6.2	3.2	2.9	0.1	0.9	0.8	0.2	1.6	0.1
NHS08-1500	Trcm	71.7	0.8	13.1	5.6	5.0	0.1	0.6	4.3	2.8	1.3	0.2
NHS11-1130	Trcm	74.5	0.7	11.9	4.4	4.0	0.1	0.4	0.9	2.1	5.4	0.1
NHS-12-1720	Trcm	73.8	0.7	12.6	3.7	3.4	0.1	0.3	1.3	3.5	4.3	0.1
TG14-600	Trcm	72.3	0.7	13.7	4.0	3.6	0.1	0.8	1.8	3.1	3.7	0.2
CNHS-01	Trcm	72.1	0.8	13.0	4.3	3.9	0.1	0.6	2.5	2.4	4.5	0.2
CNHS-03	Trcm	77.8	0.6	11.0	2.9	2.6	0.0	0.2	1.2	2.9	3.6	0.1
CNHS-04	Trcm	72.7	0.7	13.2	3.9	3.5	0.1	0.7	2.0	2.1	4.9	0.2
10065(W)	Trcm	72.8	0.7	12.7		3.8	0.1	0.4	1.6	2.8	5.1	0.1
9143(W)	Trcm	73.0	0.7	12.8		3.9	0.1	0.5	1.7	2.3	5.0	0.1
NHS-2-3000	Tbcr	55.2	2.9	13.3	14.4	13.0	0.2	3.5	7.5	2.8	1.1	0.4
NHS03-1940	Tbcr	56.7	2.3	14.0	13.1	11.7	0.2	3.8	5.9	3.1	1.8	0.5
NHS04-2260	Tbcr	58.7	2.4	13.7	11.8	10.7	0.2	2.9	6.2	3.0	1.9	0.4
NHS05-2220	Tbcr	60.5	2.4	12.3	11.5	10.4	0.2	2.5	6.5	2.7	2.1	0.4
NHS05-2710	Tbcr	58.7	2.1	12.9	12.5	11.3	0.2	3.4	5.9	3.0	2.0	0.6
NHS08-2230	Tbcr	56.7	2.3	14.2	13.0	11.7	0.2	3.0	6.6	2.6	2.2	0.5
NHS11-1730	Tbcr	57.4	2.2	14.0	12.1	10.9	0.4	2.9	7.0	3.2	1.3	0.5
NHS11-2290	Tbcr	55.2	2.4	13.5	14.1	12.7	0.2	3.7	7.7	3.0	1.1	0.4
NHS-12-2400	Tbcr	54.9	2.4	13.5	14.6	13.1	0.2	3.4	7.0	3.4	1.6	0.4
NHS09-2220	Tbcr	56.7	2.1	13.6	13.1	11.8	0.2	3.3	7.8	2.9	1.2	0.4
NHS09-2880	Tbcr	56.1	2.4	13.4	13.5	12.1	0.2	3.7	7.4	2.7	1.5	0.4
NHS10-1480	Tbcr	57.0	2.3	13.8	13.0	11.7	0.3	3.1	7.1	3.5	0.8	0.5
NHS-10-1520	Tbcr	53.7	2.4	14.6	13.7	12.4	0.3	3.7	8.2	3.2	1.0	0.4
NHS-10-2260	Tbcr	55.2	2.2	13.9	13.9	12.5	0.2	3.8	7.9	3.3	0.7	0.4
NHS13-2240	Tbcr	56.6	2.3	13.6	13.5	12.1	0.2	3.2	7.0	2.8	1.7	0.4
TG-3-2960	Tbcr	57.8	1.9	14.0	12.6	11.3	0.2	2.9	7.3	3.4	1.0	0.3
TG-20-3500	Tbcr	52.5	2.6	13.5	15.1	13.6	0.2	4.4	8.9	3.0	0.9	0.4
NHS08-2770	Tupc	63.4	1.3	13.9	7.3	6.5	0.1	3.2	5.1	2.9	3.2	0.4
NHS03-2250	Tupc	62.6	1.5	13.4	9.3	8.3	0.1	3.8	4.2	3.3	2.4	0.4
NHS04-2750	Tupc	57.4	2.1	14.3	11.8	10.6	0.2	3.6	6.9	3.2	1.6	0.3
NHS-9-3930	Tupc	54.9	2.3	14.0	11.4	10.3	0.2	4.6	9.7	3.1	0.4	0.4
NHS-12-3810	Tlpc	51.2	1.7	15.5	12.2	11.0	0.2	6.5	10.0	2.9	0.7	0.2
NHS-12-4210	Tlpc	49.2	1.5	17.5	11.6	10.4	0.2	6.7	10.9	2.9	0.5	0.2
NHS-12-6170	Tlpc	51.8	2.1	15.7	11.8	10.6	0.2	5.6	9.6	3.2	0.9	0.3
NHS11-7250	Jg	63.2	0.8	15.5	6.4	5.8	0.1	3.2	5.6	3.5	2.2	0.2
NHS11-7520	Jg	64.5	0.8	15.0	5.9	5.4	0.1	3.2	4.6	4.0	2.3	0.2
NHS11-7560	Jg	67.5	0.5	15.6	4.4	4.0	0.1	1.7	3.4	4.4	2.8	0.1
NHS11-7610	Jg	73.0	0.2	14.1	2.2	2.0	0.1	0.8	1.9	4.4	3.5	0.1

Trace Element (parts per million)

Name	Rock Unit	Rb	Sr	Y	Zr	V	Ni	Cr	Nb	Ga	Cu
NHS10-480	Tbn	17	341	31	136	245	59	72	12	16	72
NHS-10-520	Tbn	27	311	30	135	239	63	55	10	16	71
NHS-12-140	Tbn	30	291	30	128	230	65	62	10	16	69
NHS-12-460	Tbn	24	317	33	138	223	62	64	12	16	66
TG7-80	Tbn	16	328	26	126	234	60	60	10	16	67
11026(W)	Tbn	31	378	36	189	337	76	71	17	23	86
TG3-1700	Tbnd	26	307	31	136	227	55	67	11	16	66
CNHS-06	Tbn	15	516	26	137	217	120	100	7	17	71
110211(W)	Tbar	24	697	44	350	237	42	79	36	26	63
110210(W)	Tbar	23	752	73	347	213	41	75	33	26	55
11029(W)	Tbar	23	696	45	349	223	42	81	34	25	66
11028(W)	Tbar	19	700	44	354	223	41	79	35	25	57
NHS11-150	?	104	185	33	189	203	20	45	16	17	34
NHS09-110	Tdb	5	376	28.6	73	285	140	218	4.0	15.5	99
NHS9-890	Tdb	11	353	31	85	275	110	197	7	15	80
NHS9-1030	Tdb	8	375	29	72	282	135	220	5	15	90
NHS12-1150	Tdb	4	357	29	72	262	176	231	5	15	90
NHS13-1930	Tdb	6	393	29	74	292	133	224	5	15	89
NHS2-220	Tav	32	554	27	201	138	43	61	17	18	35
NHS08-310	Tav		612		217	142		67			
TG-3-160	Tav	29	568	26	203	131	37	63	14	18	56
TG16-240	Tav	29	560	26	202	139	30	80	18	18	44
NHS13-300	Tav	28	574	29	204	133	32	66	16	18	46
CNHS-08	Tav	30	605	25	201	132	47	67	17	18	53
9128(W)	Tav	29	697	31	276	177	32	58	22	24	46
11027(W)	Tav	31	686	32	275	173	37	64	23	25	56
7274(W)	Tav	40	669	32	276	187	40	60	25	25	48
7272(W)	Tav	33	696	34	277	177	32	59	22	25	44
NHS2-100	Tav	11	659	31	204	139	29	71	18	18	50
NHS08-150	Tav	23	587	34	213	139	29	71	20	19	48
NHS05-200	Tav	22	538	33	189	128	25	59	16	16	40
NHS4-100	Tav	36	437	58	275	110	12	30	19	20	21

Name	Rock Unit	Zn	Co	Ba	La	Ce	U	Th	Sc	Pb	Mg#
NHS10-480	Tbn	72	40	730	14	39	1	2	31	7	0.37
NHS-10-520	Tbn	77	38	762	15	35	0	0	29	8	0.38
NHS-12-140	Tbn	70	37	692	16	33	2	0	29	12	0.40
NHS-12-460	Tbn	76	36	651	20	43	2	1	29	3	
TG7-80	Tbn	70	39	713	19	38	2	0	29	3	0.37
11026(W)	Tbn	101		887	20	46	0.2	1.8	45	5	
TG3-1700	Tbnd	71	36	654	15	42	0	1	28	4	0.38
CNHS-06	Tbn	82	36	594	20	47	0	0	25	2	0.39
110211(W)	Tbar	140		1259	44	98	0.9	4.2	28	9	
110210(W)	Tbar	136		3099	65	106	1.9	3.0	29	9	
11029(W)	Tbar	138		1255	47	95	1.4	1.9	29	9	
11028(W)	Tbar	140		1309	46	102	3.0	2.6	28	9	
NHS11-150	?	72	14	685	30	66	3	4	17	7	0.34
NHS09-110	Tdb	81	51	482	10	25	0.3	0.3	32	1	0.015
NHS9-890	Tdb	82	43	1387	13	34	<0.5	1	29	11	
NHS9-1030	Tdb	78	49	878	12	28	<0.5	<0.5	30	2	
NHS12-1150	Tdb	82	52	507	11	32	<0.5	1	28	3	
NHS13-1930	Tdb	83	45	181	13	28	<0.5	<0.5	32	<1	
NHS2-220	Tav	74	21	899	25	62	2	0	18	20	0.30
NHS08-310	Tav										0.31
TG-3-160	Tav	76	20	907	28	62	1	0	18	9	0.29
TG16-240	Tav	74	21	907	26	64	2	2	17	6	0.30
NHS13-300	Tav	76	21	929	30	65	1	<0.5	18	9	
CNHS-08	Tav	77	23	1192	31	60	0	0	19	2	0.28
9128(W)	Tav	103		1164	35	77	1.2	2.3	23	9	
11027(W)	Tav	102		1150	31	71	0.3	3.2	23	9	
7274(W)	Tav	109		1060	35	69	1.2	1.9	22	9	
7272(W)	Tav	100		992	31	67	2.6	3.0	24	9	
NHS2-100	Tav	85	24	901	26	78	1	3	20	16	0.38
NHS08-150	Tav	84	23	645	28	66	2	3	21	16	0.37
NHS05-200	Tav	77	21	1091	26	70	1	0	20	3	0.34
NHS4-100	Tav	136	21	820	37	81	2	7	27	1	

Name	Rock Unit	Rb	Sr	Y	Zr	V	Ni	Cr	Nb	Ga	Cu
NHS-2-1070	Thb	315	57	267	52	10	8	19	19	12	157
NHS03-640	Thb	104	50	279	76	4	14	21	20	9	141
NHS03-880	Thb	479	0	304	42	0	17	0	0	0	0
NHS05-1060	Thb	405		285	51		17				
NHS08-1270	Thb	366	41	234	269	4	19	17	19	15	119
NHS-12-1350	Thb	312	53	276	48	14	13	19	20	14	158
TG12-260	Thb	368	40	238	312	3	19	17	19	180	127
CNHS-02	Thb	331	52	274	45	13	6	19	20	14	152
CNHS-05	Thb	317	39	229	291	13	16	16	19	14	131
CNHS-07	Thb	333	38	231	298	14	13	16	20	20	130
NHS13-1240	Thb	466		293	26		16				
NHS13-1540	Thb	354		245	259		29				
TG16B-1300	Thb	337	54	277	49	2	10	20	19	9	147
TG16B-1540	Thb	423	40	229	301	3	19	16	20	13	123
TG-20-300	Thb	325	39	227	294	13	15	16	19	16	125
TG-20-1060	Thb	319	42	235	118	12	32	16	19	18	123
TG19-80	Thb	335	54	230	324	2	26	21	21	11	155
TG19-580	Thb	344	40	343	297	3	22	17	20	18	126
TG19-880	Thb	340	48	249	122	3	16	18	20	12	128
TG-3-1400	Thb	339	40	231	288	14	24	16	19	15	127
TG-3-1940	Thb	438	46	237	157	13	17	15	19	14	133
NHS-9-1300	Thb	426	41	208	144	36	39	14	18	57	140
NHS09-1420	Thb	362	41	221	246	5	32	14	19	36	110
NHS-10-960	Thb	219	63	228	123	15	13	15	17	16	112
NHS4-600	Thb	332	52	312	51	2	19	24	22	10	158
NHS10-1160	Thb	388	45	230	119	3	23	16	19	17	115
NHS11-900	Thb	196	38	228	264	2	25	17	21	15	117
NHS4-100	Thb	437	58	275	110	12	30	19	20	21	136
10045(W)	Thb	402	79	418	20	1	1	33	30	8	227
9142(W)	Thb	375	55	432	28	0	0	33	32	9	192
NHS03-1580	Thb	127	43	176	113	4	38	13	17	24	117
NHS04-1190	Thb	467	55	235	101	3	13	17	19	15	136
NHS04-1570	Thb	500		234	114		11				
NHS02-1940	Thb	442	44	229	121	3	18	17	18	17	123
NHS05-1950	Thb	163	47	188	104	7	18	15	14	14	97

Name	Rock Unit	Zn	Co	Ba	La	Ce	U	Th	Sc	Pb	Mg#
NHS-2-1070	Thb	21	1090	36	92	2	12	29	29	0.1	9.37
NHS03-640	Thb	18	907	33	107	3	8	25	4	0.1	8.88
NHS03-880	Thb	0	0	0	0	0	0	0	0	0.1	6.44
NHS05-1060	Thb									0.1	8.97
NHS08-1270	Thb	33	887	22	56	1	14	29	20	0.2	4.68
NHS-12-1350	Thb	22	927	36	92	3	16	27	11	0.1	11.92
TG12-260	Thb	36	883	24	52	0	13	32	17	0.2	4.79
CNHS-02	Thb	22	925	35	82	1	14	26	17	0.1	9.56
CNHS-05	Thb	38	695	23	48	1	8	29	8	0	4.29
CNHS-07	Thb	34	755	20	48	3	8	29	1	0	3.86
NHS13-1240	Thb									0.1	10.57
NHS13-1540	Thb									0.2	5.20
TG16B-1300	Thb	23	1006	34	87	1	13	24	5	0.1	9.32
TG16B-1540	Thb	36	1031	23	57	2	11	27	8	0.2	4.09
TG-20-300	Thb	37	702	21	50	2	8	29	14	0.2	4.18
TG-20-1060	Thb	32	754	26	51	0	16	28	25	0.2	4.98
TG19-80	Thb	20	1005	38	88	1	12	26	13	0.2	4.70
TG19-580	Thb	36	804	20	45	2	12	29	5	0.2	4.68
TG19-880	Thb	29	801	27	64	2	12	25	13	0.2	5.02
TG-3-1400	Thb	37	769	21	44	1	8	29	12	0.2	4.01
TG-3-1940	Thb	33	768	28	59	3	9	30	15	0.2	4.66
NHS-9-1300	Thb	37	934	23	52	0	12	29	9	0.2	3.90
NHS09-1420	Thb	33	761	24	48	2	9	27	5	0.2	4.00
NHS-10-960	Thb	30	790	33	73	4	12	29	21	0.2	3.76
NHS4-600	Thb	20	1055	37	94	3	9	31	28		10.14
NHS10-1160	Thb	31	861	28	57	<0.5	10	25	1		4.20
NHS11-900	Thb	36	892	21	53	3	15	28	<1		12.22
NHS4-100	Thb	21	820	37	81	2	7	27	1		3.48
10045(W)	Thb		1437	49	112	3.1	9.6	42	13		12.73
9142(W)	Thb		1319	45	103	2.9	10.6	40	15		20.13
NHS03-1580	Thb	41	300	25	102	0	13	24	1	0.2	4.81
NHS04-1190	Thb	29	823	23	65	1	9	29	1	0.3	2.53
NHS04-1570	Thb									0.2	4.69
NHS02-1940	Thb	30	833	22	55	0	7	29	10	0.2	4.85
NHS05-1950	Thb	23	852	26	56	3	10	20	1	0.2	3.18

Name	Rock Unit	Rb	Sr	Y	Zr	V	Ni	Cr	Nb	Ga	Cu
NHS-2-1270	Trcm	655	42	300	29	11	11	19	18	8	78
NHS03-1000	Trcm	605	45	290	33	5	11	20	17	6	82
NHS04-870	Trcm	293		314	31		44				
NHS04-980	Trcm	149		291	27		12				
NHS05-1290	Trcm	285	39	255	29	2	12	17	17	9	71
NHS05-1480	Trcm	47		157	87		42				
NHS08-1500	Trcm	890		308	36		15				
NHS11-1130	Trcm	95	39	287	22	4	16	20	17	11	73
NHS-12-1720	Trcm	163	40	305	27	15	19	20	19	6	80
TG14-600	Trcm	190	46	314	31	4	11	22	20	7	78
CNHS-01	Trcm	267	40	293	39	16	5	19	19	3	82
CNHS-03	Trcm	155	34	260	31	15	6	18	17	2	58
CNHS-04	Trcm	181	42	313	33	14	8	20	19	8	80
10065(W)	Trcm	208	54	397	22	0	4	26	24	4	115
9143(W)	Trcm	194	51	396	19	0	3	26	26	3	113
NHS-2-3000	Tbcr	199	44	203	401	32	50	14	17	135	136
NHS03-1940	Tbcr	302	40	196	308	6	23	13	17	24	120
NHS04-2260	Tbcr	333	38	216	277	11	37	16	19	31	106
NHS05-2220	Tbcr	194	42	210	273	4	21	15	16	19	101
NHS05-2710	Tbcr	357	43	177	228	6	19	13	16	23	116
NHS08-2230	Tbcr	339		222	278		17				
NHS11-1730	Tbcr	433		229	268		25				
NHS11-2290	Tbcr	317	37	174	383	7	32	12	17	26	114
NHS-12-2400	Tbcr	315	36	190	380	21	30	12	19	47	122
NHS09-2220	Tbcr	380	35	180	380	8	32	11	17	36	107
NHS09-2880	Tbcr	324	40	211	375	14	40	14	17	90	115
NHS10-1480	Tbcr	503	38	202	287	5	27	14	19	18	121
NHS-10-1520	Tbcr	469	36	197	365	17	12	12	18	26	124
NHS-10-2260	Tbcr	481	39	199	374	19	23	11	18	39	115
NHS13-2240	Tbcr	300	39	203	364	14	31	14	19	27	115
TG-3-2960	Tbcr	207	35	176	347	21	44	11	17	37	84
TG-20-3500	Tbcr	322	42	206	411	35	67	13	18	112	126
NHS08-2770	Tupc	266	27	148	191	15	56	11	13	26	70
NHS03-2250	Tupc	220	33	145	239	12	47	10	16	35	88
NHS04-2750	Tupc	342	33	199	312	10	44	13	19	27	103
NHS-9-3930	Tupc	387	37	137	310	65	121	9	14	110	85
NHS-12-3810	Tlpc	310	34	111	314	82	155	5	17	108	87
NHS-12-4210	Tlpc	432	27	88	305	110	121	4	17	93	76
NHS-12-6170	Tlpc	434	29	145	323	106	109	9	17	137	94
NHS11-7250	Jg	44	327	39	114	138	17	183	8	15	32
NHS11-7520	Jg	45	226	23	96	116	61	146	6	15	50
NHS11-7560	Jg	67	230	19	111	73	27	78	7	16	40
NHS11-7610	Jg	77	138	22	88	34	15	48	6	15	16

Name	Rock Unit	Zn	Co	Ba	La	Ce	U	Th	Sc	Pb	Mg#
NHS-2-1270	Trcm	7	1619	48	108	7	18	13	17	0.1	
NHS03-1000	Trcm	7	822	50	108	5	15	13	22	0.3	
NHS04-870	Trcm									0.1	
NHS04-980	Trcm									0.1	
NHS05-1290	Trcm	4	1335	42	97	5	16	12	28	0.2	
NHS05-1480	Trcm									0.2	
NHS08-1500	Trcm									0.1	
NHS11-1130	Trcm	6	1167	41	101	5	21	9	16	0.1	
NHS-12-1720	Trcm	5	1341	44	113	5	19	10	21	0.1	
TG14-600	Trcm	4	1450	46	116	6	22	11	26	0.2	
CNHS-01	Trcm	5	2229	51	121	5	19	12	20	0.1	
CNHS-03	Trcm	4	1245	44	98	5	17	9	15	0.1	
CNHS-04	Trcm	2	1275	45	105	6	17	13	16	0.2	
10065(W)	Trcm		1764	52	116	5	19	18	27		
9143(W)	Trcm		1419	54	106	6	19	18	27		
NHS-2-3000	Tbcr	45	388	15	35	0	9	40	5	0.2	3.72
NHS03-1940	Tbcr	40	894	20	53	3	12	31	18	0.2	3.09
NHS04-2260	Tbcr	35	815	19	49	0	11	30	23	0.2	3.71
NHS05-2220	Tbcr	30	774	22	39	2	12	31	1	0.2	4.15
NHS05-2710	Tbcr	35	630	17	43	0	12	33	4	0.2	3.29
NHS08-2230	Tbcr									0.2	3.94
NHS11-1730	Tbcr									0.2	3.80
NHS11-2290	Tbcr	44	499	18	31	2	8	35	6	0.2	3.39
NHS-12-2400	Tbcr	43	537	17	36	2	7	34	9	0.2	3.81
NHS09-2220	Tbcr	40	568	20	39	1	9	34	10	0.2	3.57
NHS09-2880	Tbcr	42	525	18	35	3	9	35	9	0.2	3.24
NHS10-1480	Tbcr	35	879	21	51	3	11	31	17	0.2	3.85
NHS-10-1520	Tbcr	42	803	18	37	3	14	36	19	0.2	3.31
NHS-10-2260	Tbcr	42	535	20	40	1	3	35	13	0.2	3.29
NHS13-2240	Tbcr	40	555	18	38	2	8	31	8	0.2	3.78
TG-3-2960	Tbcr	38	350	16	37	1	11	32	9	0.2	3.97
TG-20-3500	Tbcr	43	379	14	30	0	3	37	11	0.2	3.11
NHS08-2770	Tupc	22	1006	20	42	2	3	22	18	0.3	2.05
NHS03-2250	Tupc	32	606	19	45	0	3	25	2	0.3	2.20
NHS04-2750	Tupc	40	611	17	46	2	7	29	10	0.3	2.99
NHS-9-3930	Tupc	41	189	10	27	0	2	37	1	0.3	2.24
NHS-12-3810	Tlpc	46	231	10	27	1	3	35	3	0.4	1.68
NHS-12-4210	Tlpc	45	196	7	25	1	1	31	2	0.4	1.56
NHS-12-6170	Tlpc	45	224	9	26	2	5	33	4	0.3	1.89
NHS11-7250	Jg	66	19	967	18	27	1.8	0.3	21	0.5	0.356
NHS11-7520	Jg	53	23	883	18	27	0.9	6.4	17	13.1	0.372
NHS11-7560	Jg	59	13	1111	20	36	2.0	2.3	13	4.0	0.301
NHS11-7610	Jg	27	6	1260	22	41	3.7	8.8	7	10.0	0.281

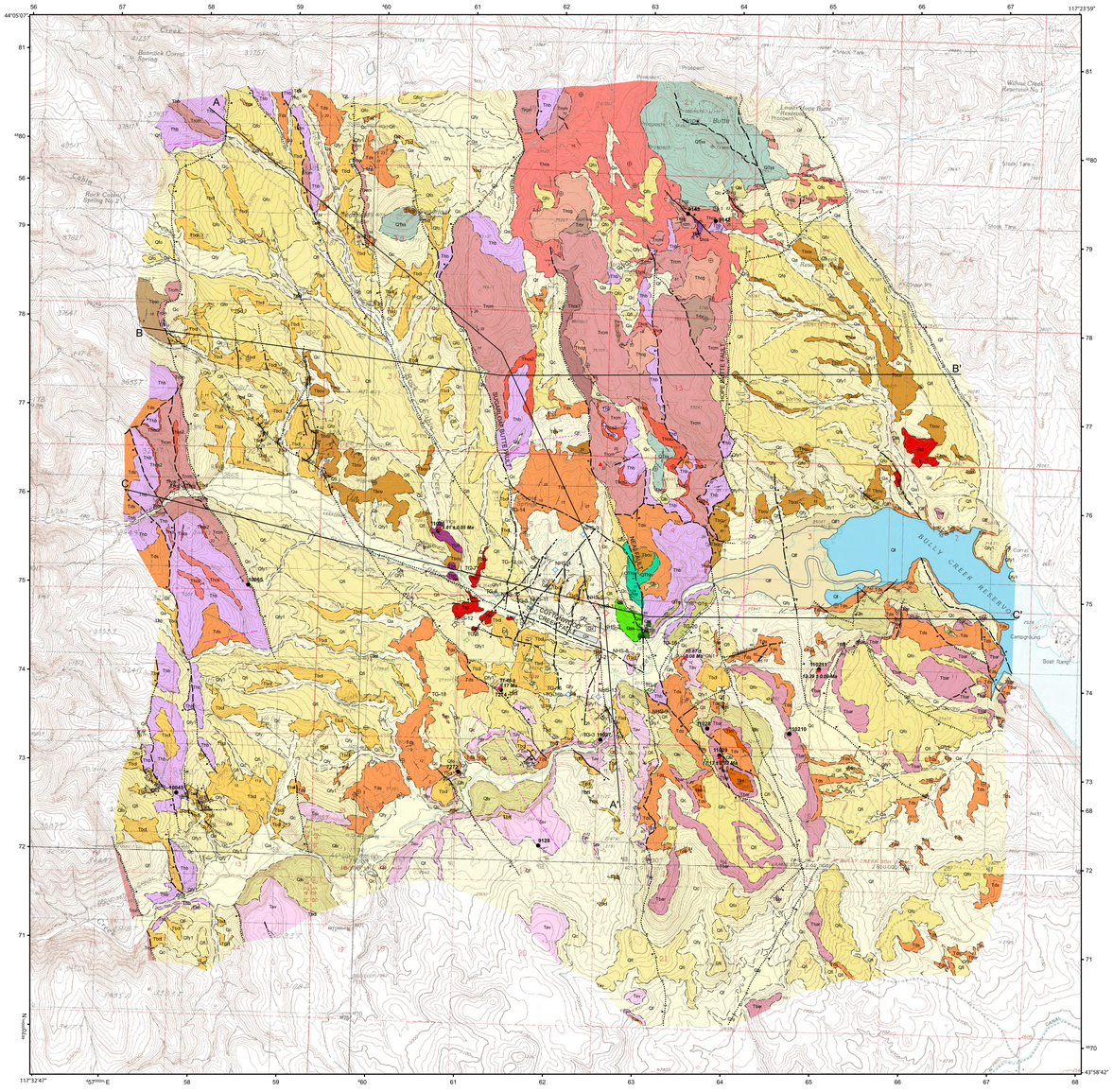

PRELIMINARY GEOLOGIC MAP OF THE NEAL HOT SPRINGS AREA, MALHEUR COUNTY, OREGON

Joel H. Edwards, James E. Faulds, and Mark Ferns
2013

QUATERNARY DEPOSITS

Anthropogenic Features and Deposits

- Qx — **Disturbed and modified areas**

Bully Creek Reservoir Deposits

- Qlf — **Bully Creek Reservoir flood deposits (latest Holocene)**
- Qlf1 — **Bully Creek Reservoir shoreline deposits (latest Holocene)**

Hillslope and Mass-Wasting Deposits

- Qc — **Colluvium (late Holocene to Pleistocene)**
- Qls — **Landslide (Holocene to Pleistocene)**

Alluvial Deposits

- Qa — **Young alluvium, undivided (Holocene to late Pleistocene)**
- Qfy — **Young active fan alluvium and recently abandoned active alluvial surfaces (Holocene)**
- Qfy1 — **Young inactive fan alluvium (late Holocene)**
- Qfi — **Intermediate fan alluvium, undivided (late to middle Pleistocene)**
- Qfo — **Old fan alluvium (middle to early Pleistocene)**
- Qf — **Fan alluvium, undivided (Holocene to early Pleistocene)**
- Qsil — **Siliceous sinter mounds (Holocene to Pleistocene?)**
- Qss — **Silicified sediments, undivided (Holocene to Pleistocene?)**

QUATERNARY AND TERTIARY ROCKS

- QTg — **Gravel deposits (Pleistocene to Pliocene?)**
- QThbr — **Hydrothermally altered breccia (Pleistocene to Pliocene?)**
- QTss — **Silicified rocks, undivided (Pleistocene to Pliocene?)**

PLIOCENE AND MIOCENE ROCKS

Rocks of Western Snake River Plain

- Tbsr — **Dacite scoria (Pliocene?)**
- Tlm — **Fossiliferous limestone (late Miocene?)**
- Tbcu — **Bully Creek Formation sedimentary rocks, upper (late Miocene?)**
- Tbn — **Neal basalt**
- Tbcg — **Bully Creek conglomerate**
- Tbcl — **Bully Creek Formation sedimentary rocks, lower (late Miocene)**

MIOCENE ROCKS

Rocks of Oregon/Idaho Graben

- Tav — **Vines Hill andesite**
- Tbar — **Reservoir basaltic andesite**
- Tds — **Drip Springs Formation, undivided (middle to late Miocene)**
- Tdr — **Rhyolite sedimentary breccia**
- Thcg — **Hog Creek conglomerate**
- Thb — **Hunter Creek Basalt**
- Thcs2 — **Hog Creek Formation tuffaceous rocks, upper**
- Trcm — **Cottonwood Mountain Rhyolite**
- Tbsc — **Basalt scoria and lapilli**
- Thcs1 — **Hog Creek Formation tuffaceous rocks, lower**
- Thcs — **Hog Creek Formation, undivided (middle Miocene)**

Columbia River Basalt

- Tbm — **Malheur Gorge basalt**

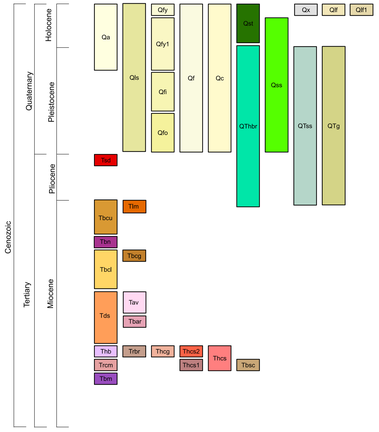

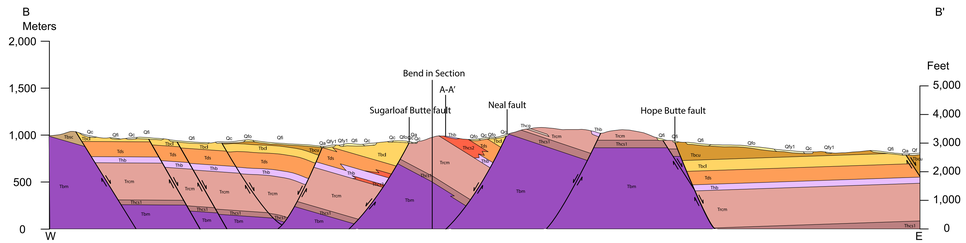

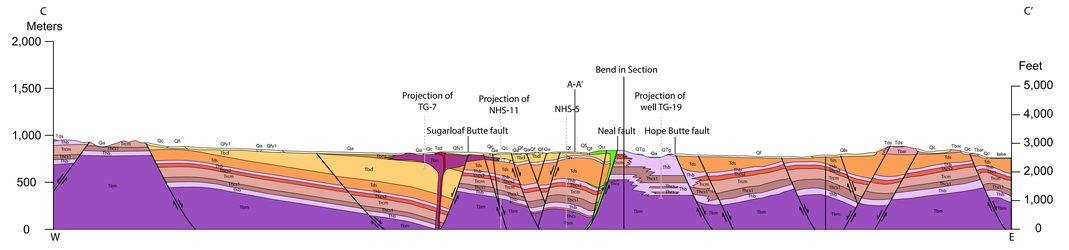

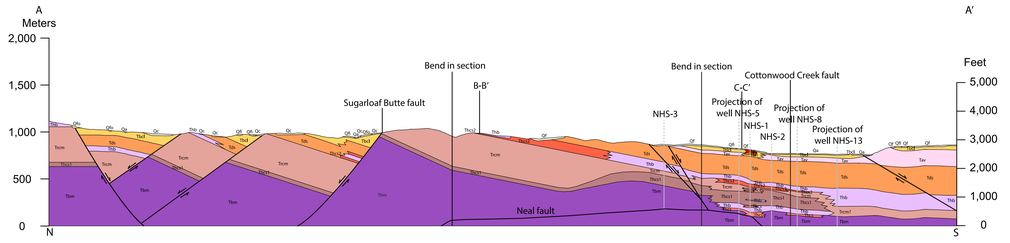

Symbology (per FGDC-STD-013-2006)

Contact Solid where certain and location accurate, long-dashed where approximate, short-dashed where inferred, dotted where concealed.

Normal fault Solid where certain and location accurate, long-dashed where approximate, dotted where concealed; queried if identity or existence uncertain, Ball on downthrown side,

Mainly strike-slip fault Solid where certain and location accurate, long-dashed where approximate, dotted where concealed; queried if identity or existence uncertain, Arrows show relative motion,

Geophysically inferred fault

Anticline Long-dashed where approximate, dotted where concealed,

Monocline Long-dashed where approximate, dotted where concealed, Arrow shows direction of dip,

Syncline Long-dashed where approximate, dotted where concealed,

Strike and dip of bedding

Inclined · Vertical · Horizontal

Strike and dip of flow foliation in volcanic rocks

Inclined · Vertical

A — A' **Line of cross section**

Well-Field

- Exploratory
- Injection
- Production
- Temperature Gradient

- $^{40}Ar/^{39}Ar$ sample locality
- XRF geochemical sample locality showing sample number

GN — MN
0° 07' — 12° 30'
UTM GRID AND 1983 MAGNETIC NORTH DECLINATION AT CENTER OF SHEET

Adjoining 7.5' quadrangle names

1	2	3	4
5	6	7	8
9	10	11	12
13	14	15	16

1 Brady Creek
2 Brogan
3 Jamieson
4 McCarthy Ridge
5 Buckbush Creek
6 Swede Flat
7 Hope Butte
8 Willowcreek
9 Westfall
10 Little Valley
11 Vines Hill
12 Vale West
13 Namorf
14 Harper
15 Kane Spring Gulch
16 Double Mountain

Map location

Scale 1:24,000

0 0.5 1 kilometer
0 0.5 1 mile
0 1000 2000 3000 4000 5000 feet

CONTOUR INTERVAL 20 FEET

Projection: Universal Transverse Mercator, Zone 11, North American Datum 1927 (m)

Base map:
U.S. Geological Survey Swede Flat 7.5' quadrangle (1990)
U.S. Geological Survey Hope Butte 7.5' quadrangle (1990)
U.S. Geological Survey Little Valley 7.5' quadrangle (1990)
U.S. Geological Survey Vines Hill 7.5' quadrangle (1990)

Nevada Bureau of Mines and Geology
Mackay School of Earth Sciences and Engineering
College of Science
University of Nevada, Reno

Field work done in May 2011-June 2012
Supported by the U.S. Department of Energy
(DE-EE0002748)

DRAFT
Preliminary geologic map
Has not undergone office or field review
Will be revised before publication

Edited by XXXXXXXXXXXXXXXX
Compilation by Joel H. Edwards
Cartography and production in ESRI ArcGIS v10.1 (ArcGeology v1.3) by Joel H. Edwards and Matthew Richardson
First Edition, March 2013
Printed by Nevada Bureau of Mines and Geology

This map was printed on an electronic plotter directly from digital files. Dimensional calibration may vary between electronic plotters and X and Y directions on the same plotter, and paper may change size, therefore, scale and proportions may not be exact on copies of this map.

For sale by:
Nevada Bureau of Mines and Geology
2175 Raggio Pkwy.
Reno, Nevada 89512
ph. (775) 682-8766
www.nbmg.unr.edu; nbmg@unr.edu